INSTITUT DES SYSTEMES INTELLIGENTS ET DE ROBOTIQUE
UNIVERSITE PIERRE ET MARIE CURIE

PERCIPIO ROBOTICS

P H D T H E S I S

Tianming LU

Design and Realization of a Desktop Micro-manipulation Cobotic Platform

Thesis Advisors: Stéphane RÉGNIER, David HERIBAN

defended on March 10, 2016

Jury :

Stéphane VIOLLET	-	CNRS Research Director	Reviewer
Philippe FRAISSE	-	Professor at LIRMM / Université Montpellier 2	Reviewer
Michaël GAUTHIER	-	CNRS Research Director	Examinator
David HERIBAN	-	CEO of Percipio Robotics	Co-advisor
Vincent HAYWARD	-	Professor at Université Pierre et Marie Curie	Examinator
Stéphane RÉGNIER	-	Professor at Université Pierre et Marie Curie	Supervisor

Design and Realization of a Desktop Micro-manipulation Cobotic Platform

Abstract: Microrobotics is a fast growing field of research and microsystems are in high demand from across a wide spectrum of our life. Nowadays, mass automation solutions are already available for large batch production of microsystems, while small batch production mainly relies on handmade processes due to the lack of flexible micro-manipulation system. Handmade processes have limited productivity and accuracy, which make it more and more difficult for small and medium-sized enterprises to conquer their place on the international market. Under such circumstances, pioneer microrobotics company Percipio Robotics has proposed a desktop cobotic platform, *Chronogrip*, which aims to handle flexible micro-manipulation. However, the solution is not yet complete and there are three main challenges to resolve:

- the dynamics of the piezoelectric stick-slip actuator is not fully understood, which delays the development of trajectory tracking strategies;
- existing haptic interfaces have limited bandwidth due to their mechanical properties, consequently there is no available option that is able to render high dynamic haptic information from the microworld;
- for tweezers-based micro-manipulation in watchmaking process, no existing haptic interface is able to provide intuitive and effective operation.

The objective of thesis is to address these three issues. The first part of the thesis is dedicated to the development of nonlinear dynamic model of the piezoelectric stick-slip actuator. The result shows that it is the first dynamic model which can describe the actuator dynamics in time and frequency domain, for stepping and scanning mode, and for both forward and backward motion. The second part of the thesis is devoted to develop a method to extend the bandwidth of dual-stage haptic interface by using the signal crossover technique. The result shows that the bandwidth is uniformly extended to 1 kHz, which makes it possible to reproduce high dynamic phenomena from the microworld. The third part of the thesis aims to design an intuitive haptic interface for tweezers-based watchmaking operations. The design is also compatible with conventional tweezers-based usage. It is expected to integrate all of the three research results into the cobotic platform Chronogrip to enhance the productivity and effectiveness of micro-manipulation.

Keywords: Microrobotics; Micro-manipulation; Cobotics; Haptics; Nonlinear Dynamics; Piezoelectric Stick-Slip Actuator; Bandwidth; Signal Crossover; Haptic Tweezers.

Conception et Réalisation d'une Plate-forme de Micro-manipulation Cobotique

Résumé: La microrobotique est un domaine de recherche en croissance rapide et les microsystèmes sont très demandés par un large éventail de notre vie. Aujourd'hui, des solutions d'automatisation massive sont déjà disponibles pour la production en série des microsystèmes, tandis que la production de petites quantités s'appuie principalement sur des processus manuels en l'absence de système de micro-manipulation flexible. Un processus manuel impose des contraintes à la productivité et la précision, ce qui accroît les difficultés pour les petites et moyennes entreprises à conquérir leur place sur le marché international. Dans ce contexte, la société pionnière pour la microrobotique Percipio Robotics a proposé une plate-forme cobotique, *Chronogrip*, qui vise à gérer la micro-manipulation flexible. Toutefois, la solution n'est pas encore complète et il y a trois principaux défis à résoudre:

- la dynamique de l'actionneur piézo-électrique stick-slip n'est pas entièrement comprise, ce qui retarde le développement des stratégies de suivi de trajectoire;
- les interfaces haptiques ont peu de bande passante en raison des propriétés mécaniques, par conséquent il n'y a aucune option disponible qui soit capable de reproduire des informations haptiques de haute dynamique depuis le micromonde;
- pour la micro-manipulation à la pince dans l'horlogerie, aucune interface haptique existante n'est en mesure d'assurer un fonctionnement intuitif et efficace.

L'objectif de la thèse consiste à répondre à ces trois défis. La première partie de la thèse est consacrée à l'élaboration d'un modèle dynamique non-linéaire de l'actionneur piézo-électrique stick-slip. Le résultat montre qu'il est le premier modèle dynamique qui puisse décrire la dynamique de l'actionneur dans des domaines temporels et fréquentiels, pour les fonctionnements en sous-pas et en grand déplacement, et à la fois pour les directions vers l'avant et l'arrière. La deuxième partie de la thèse est consacrée à développer une méthode pour étendre la bande passante d'une interface haptique en double étage en utilisant la technique de signal crossover. Le résultat montre que la bande passante est uniformément étendue à 1 kHz, ce qui rend possible la reproduction des phénomènes de haute dynamique depuis le micromonde. La troisième partie de la thèse vise à concevoir une interface haptique intuitive dédiée aux opérations d'horlogerie à la pince. Le design est également compatible avec l'utilisation conventionnelle d'une pince. Il est prévu d'intégrer tous les résultats de ces trois sujets de recherches dans la plate-forme de cobotique Chronogrip afin d'améliorer la productivité et l'efficacité de la micro-manipulation.

Mots-clés: Microrobotique; Micro-manipulation; Cobotique; Haptique; Dynamique Non-linéaire; Actionneur Piézo-électrique Stick-Slip; Bande Passante; Signal Crossover; Pince Haptique.

Contents

List of Figures

List of Tables

General Introduction

As a recent research domain, micro-robotics deals with the study and application where a robot interacts with microscopic objects. The environment where such an interaction takes place is often mentioned as microworld and it contains objects whose dimension covers from 1 μm to 1 mm [Régnier 2008]. With the rapid progress of science and technology, the industrial integration level becomes much more advanced and the miniature products more popular in our lives [Sun 2002] [Wang 2007] [Sitti 1998] [Romano 2012]. The micro-mechanics, the microsystems, the optics, the micro-electronics, and the biologies are all fast developing industries where efficient and reliable micro-manipulation (especially microassembly) makes a critical difference.

Nowadays, dedicated systems for massive production of microsystems such as MEMS are already available in the market. The extensively adopted method to increase productivity is parallel microassembly: deposit a great amount of micro-components in a predefined matrix pattern on a dedicated pad and then flip it over to align the pad to the other one, which carries the matched micro-components arranged in the same pattern. One example of such technique is flip-chip bonding. Such method is efficient, but restricted to a specific type of product. The blossom of microsystems industry implies a great variety of systems designs and many of them involve small series of complex products. In the case of small batches, adopting product specific parallel microassembly method gives rise to frequent redesign of carrying tools and iteration of all related processes such calibration and alignment. As a result, a more flexible production method must be developed to answer the market window of small series micro-components manufacturing.

Cobotics, a neologism from the combination of the words "cooperation" and "robotics" [Peshkin 2001] [Gillespie 2001] [Chanphat 2006], provides a promising solution to tackle small series of complex production. It refers to a system that establishes collaboration between people and robots. The objective of cobotics is to automate a large range of tasks but keep in close collaboration with operators. Contrary to automation, cobotics emphasizes that people are the source of innovation and should remain central [Vinci-Energies 2014]. Cobotics can be considered as a method to promote flexibility but maintain a high quality of productivity.

Under the collaboration between the MICROB group of the Institute for Intelligent Systems and Robotics (ISIR) of Pierre-and-Marie-Curie University and Percipio Robotics, the objective of this thesis is to design and realize the first desktop cobotic platform dedicated to micro-manipulation. However, it is not to construct a new cobotic system but to build upon the existing cobotic platform Chronogrip, designed and realized by Percipio Robotics. It is focused on the key issues that arise in cobotics during the *interaction* between people and robots as well as the execution of motion command by slave system. A qualified cobotic system must enable desired information flows in mutual directions between operators and robots:

without sophisticated knowledge about how robots work behind, operators can intuitively deliver operation commands via the interface of the cobotic system, and the slave system must be able to realize desired trajectory and convey necessary information via the interface back to operators. That means, in the aspect of slave system, the dynamics of the actuator system must be studied and a sophisticated motion control strategy must be implemented to realize desired trajectory; in the aspect of user interface, the mechatronic design of interface must be intuitive to operators for the dedicated application and a set of algorithms must be designed and implemented to guarantee the quality of information flows. Concretely, three specific research objectives are defined below:

Research objective 1: *Nonlinear dynamic modeling for a class of microrobotic systems using piezoelectric stick-slip actuators.* For a teleoperation task of cobotic platform, velocity control is crucial for fluent operation. This issue concerns the study of positioning actuator. Piezoelectric stick-slip actuator that used in Chronogrip system is promising solution to realize a great range of microrobotic applications, and many innovation companies have commercialized this kind of product with reasonable price. However, none of these companies or any research results is able to propose a complete control strategy for velocity. The main difficulty lies in the complexity of the dynamics of piezoelectric stick-slip actuators. More precisely, no research result has been reported to be able to fully describe the dynamics of such actuator. The first research objective is to develop the dynamic model of the piezoelectric stick-slip actuator, in order to prepare for sophisticated trajectory tracking strategies for the cobotic platform.

Research objective 2: *Developing a method to extend the bandwidth of dual stage haptic interface to render high dynamic haptic information from micro-environment.* The cobotic platform to realize is dedicated to microrobotic applications. In the microworld, surface forces are more dominant due to scale effect. In such situation, thermal agitation and other environmental elements cause the micro-objects to follow high dynamic motions. As a consequence, this will lead to high dynamic interaction forces between target objects and gripper tools. Taking into account the mechanical structure and design of the existing haptic interface, no option has enough bandwidth to render high dynamics arisen from microrobotic applications. The lack of high bandwidth haptic interface causes the interaction with the microworld non-intuitive and inefficient. In this case, the second objective is to develop a method to extend the bandwidth of haptic interface. The haptic interface used in the thesis is based on dual stage design. With this method, the cobotic platform will be able to render high-bandwidth haptic information.

Research objective 3: *Design of an intuitive haptic interface for watchmaking process.* One of the target application fields of our cobotic system is the prestigious watchmaking industry. In this sector, due to its flexibility of models and small batch

production, the manufacturing process can hardly be automated. But handmade process has saturated accuracy and productivity, which makes the watchmaking players more and more difficult to conquer their place in global competition. One most important issue to apply Chronogrip to watchmaking process lies in the design of interface. Actually the general purposed interface installed in Chronogrip is way too different from the conventional tools used by watchmaking experts, and hence they have to be trained very hard to be familiar with the interface. Furthermore, there is no haptic feedback which makes the process nonintuitive. Nowadays, there is not yet a haptic interface based on a tweezers form available in prototype. The combination of realizing haptics and maintaining mechanical properties of tweezers is a challenging task. The third objective of the thesis is to address issue: design an intuitive haptic interface for watchmaking process.

The thesis is organized as follows: Chapter 2 is focused on the dynamic modeling and development of a novel velocity control strategy for a class of nano-robotic systems using stick-slip linear actuators. The dynamic modeling of stick-slip linear actuators is able to describe the dynamics in both frequency and time domain. With the knowledge of the dynamic model, a sophisticated nonlinear control strategy will be developed for complete trajectory tracking; Chapter 3 is dedicated to the development of a novel method which applies signal crossover to extend the frequency bandwidth up to 1 kHz. Within the bandwidth, the haptic display can be rendered uniformly. The method is implemented in a dual-stage haptic interface and finally a haptic optical tweezers application is demonstrated; Chapter 4 is dedicated to the design of an intuitive haptic interface for watchmaker industry. The concept is prototyped, and analyzed in dynamics; The final section concludes the thesis, followed by the bibliography.

Chapter 1

State-of-the-Art

Contents

This chapter will firstly introduce the basic physics of the microworld and the existing observation methods. Then it describes the available technologies of micro-manipulation systems as well as what is still missing. To address the need, some challenges must be handled in terms of actuator and haptic interface for micro-manipulation. The current development of those two aspects will be introduced in the second and third sections. Finally, specific research objectives of the thesis will be summed up in the last section.

1.1 Microrobotics

1.1.1 Microworld

The microworld refers to the environment where typical objects are characterized by dimension ranged from 1 μm to 1 mm [Régnier 2008] (see the figure 1.1). It is dominated by special physics which is different from that in the macroworld where human lives. Such difference causes counter-intuitiveness, which makes the microworld difficult to understand. Though the special physics in the microworld often leads to impediment in research and engineering fields, it can also be the source of innovation for manipulation.

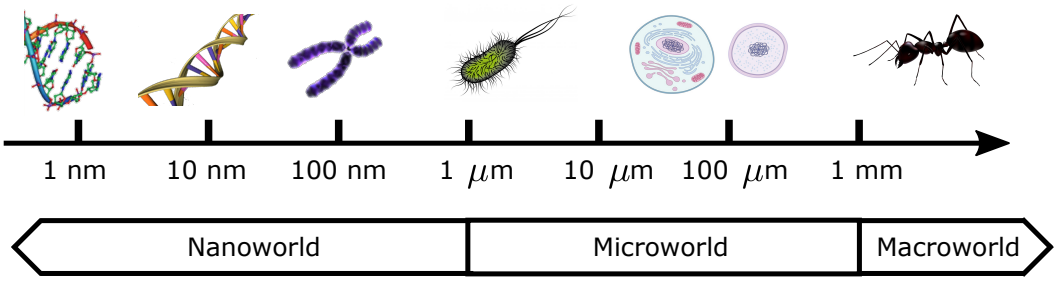

Figure 1.1: Macroworld: beyond 1 mm. Typical biological items are such as ants or tissues; microworld: from 1 μm to 1 mm. Human hair is around 100 micron, red blood cell is about 6 micron, from 1 to 15 microns, typically there are cell nucleus and bacteria; nanoworld: smaller than 1 micron. Chromatin is around 100 nm, DNA helix is about 10 nm, nucleotide is in the order of 1 nm [Nature-Education 2010].

1.1.1.1 Scale Effect

The modification of object's scale can have an impact over a series of physical phenomena, which is referred to as *scale effect* [Régnier 2008] [Régnier 2010] . In the world of macro-scale, the dominant forces are mostly volumetric such as gravity or inertial forces, which means the amplitude is proportional to the volume in question. In the microworld, the surface forces become dominant compared with volumetric forces.

The scale effect can be illustrated by an example of a cube, see the figure 1.2. If the side length is 10 cm, the volume is 1000 cm^3 and the surface area for each is 100 cm^2. Suppose a volumetric force F_{vol} and surface force F_{sur} are proportional to the cube's volume and surface's area respectively, with the same constant factor. When the side length is 10 cm, the force ratio between F_{vol} and F_{sur} is 10, meaning the volumetric force is more dominant. If the cube is scaled down by a factor of 1000 (length is reduced 1000 times smaller), that ratio becomes 0.01, meaning the more miniaturization, the more important the surface force becomes compared to volumetric force.

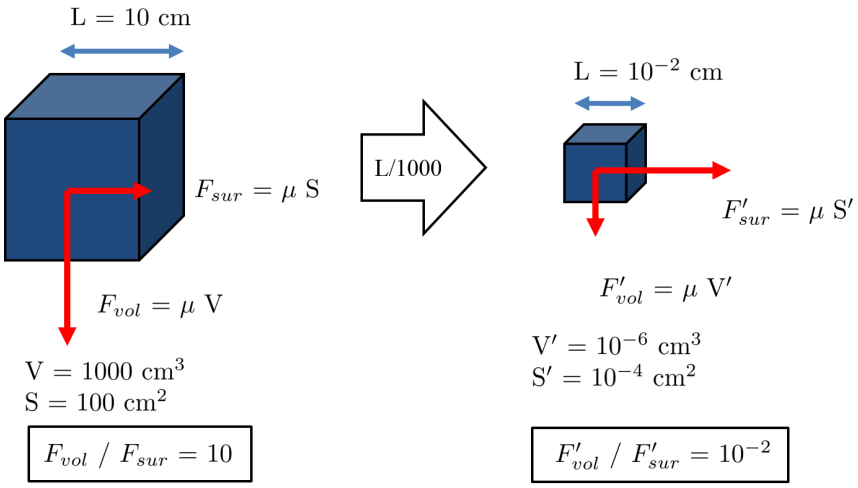

Figure 1.2: Scale effect. Suppose a volumetric force and surface force are proportional to the cube's volume and surface's area respectively. When the side length is 10 cm, the force ratio between F_{vol} and F_{sur} is 10. If the length is reduced 1000 times smaller, the ratio becomes 0.01, meaning the more miniaturization, the more important the surface force becomes compared to volumetric force.

The change of force ratio illustrated in the example above is only one part of physical phenomena due to scale effect. The scale effect not only applies to the volumetric force and surface force, it also affects the dynamics of the fluid and solid, as well as heat transfer.

1.1.1.2 Surface Forces

Surface forces are important phenomena in the microworld. According to [Israelachvili 2011], they can be classified into three large groups which dominate on the microscopic scale:

- *van der Waals forces* are the interaction forces in the molecule level between two adjacent objects [Landragin 1996]. The forces mainly depend on the materials in contact and the interaction distance. Indeed, the computation of the strength of the force involves a wide range of spec data of concerned materials. The van der Waals interaction consists of three interparticle forces: the induction force, the orientation force, and the dispersion force.

- *electrostatic forces* are the interaction phenomena arisen from charged objects. In terms of force action range, it has a limited effect compared to var der Waals forces and can only act in close proximity [Butt 1991].

- *capillary forces* are resultant effect from environmental humidity [Xiao 2000]. It depends on a wide range of parameters, such as the property of the liquid

involved, the volume of the liquid, the property of the material, the distance between two solids and their geometry.

As can be seen from the description above, those forces are highly related to the separation distance. According to the study [Lee 1991], a classification of forces is listed in the table 1.1 as a function of separation distance.

Interaction range	Force type
Infinity	gravity
A few nm to 1 mm	capillary force
$>$ 0.3 nm	electrostatic force
$>$ 0.3 nm	van der Waals force
$<$ 0.3 nm	molecular interactions
0.1 - 0.2 nm	chemical interactions

Table 1.1: A list of forces as a function of distance [Lee 1991].

1.1.2 Observation

The microworld is far beyond human perceptive capabilities. Dedicated tools must be developed to allow observation in this special environment. For research and engineering purpose, position measurement and force sensing are two of the most important perception tasks. They remain, however, difficult to carry out.

1.1.2.1 Position measurement

In recent years, various technologies have been developed to observe microworld. They are based on different physical mechanisms and could lead to different operation principles: one could interact directly with the target object and provide image frame in run time; the other may not ask direct interaction but reconstruct the desired image in an asynchronous manner. The type of equipment to choose depends on the specific application, where requirement of precision, position range, time response vary largely from one to the other.

To date, the most common methods of position measurement in the microworld are visual based. In particular, two methods are widely applied: optical microscope and scanning electron microscope (SEM). Those two methods are both able to visualize micro objects of size between 1 μm and 1 mm.

- *Optical microscope* also referred to as light microscope, is a system built with lenses and mirrors. It provides the user with magnified image of small samples. Typical optical microscope can be very simple to set up, though complex components can be added to improve image resolution or contrast. Figure 1.3 is an example of AmScope optical microscope [AmScope 2015]. In terms of performance, there are several limitations:

  - resolution, which is limited to 0.2 μm for a classical optical microscope;

- field of view, which decreases when resolution is increased;

- depth of field, which degrades the same manner as field of view, and can only cover a very thin layer due to the focus plane.

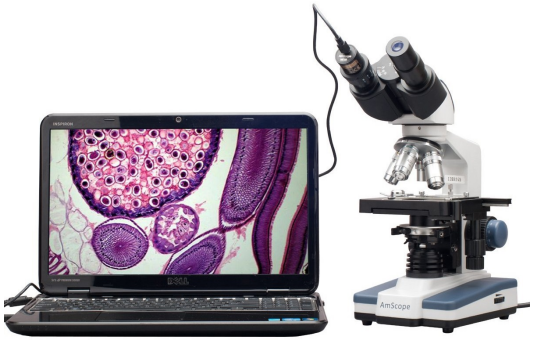

Figure 1.3: AmScope optical microscope B120C-E1 [AmScope 2015].

- *Scanning electron microscope* often abbreviated as SEM, provides an alternative option for position measurement in the microworld. Instead of relying on photons as the working principle of optical microscope, SEM is based on electrons. Briefly, streams of electrons, emitted by an electron emitter gun, are reflected when they come into contact with target objects. During interaction, emissions of back-scattered electrons, X-rays, etc. are resulted. Captured by some specific sensors, an image of the target object's surface can be reconstructed. Figure 1.4 illustrates an example of SEM system designed by FEI [FEI 2015] and a typical image produced by SEM for material science.

  Compared to optical microscope, SEM has infinite depth of field. However, it has a larger response time in the order of 500 ms. Some other limitations must also be taken into account. One major consideration is that the electron beam can also interact with any medium along the space between the target object and the electron emitter gun. The medium includes air molecules. As a consequence, SEM requires the sample be placed in a vacuum chamber. Furthermore, the sample must be conductive so that no electric charge accumulated on them.

1.1.2.2 Force measurement

To fix ideas, the amplitude of generated force in micro-scale is typically in the order of micro-Newton to milli-Newton. This directly gives rise to the requirement that the force sensor must be extremely sensitive and be compatible with the microworld environment, if based on contact approach. Furthermore, the absence of reliable measurement techniques and the lack of multi-axis sensors with required resolution lead to impediment to the measurement force applied to micro objects. In addition to the requirement of force sensor described above, the force measurement system must also be able to comply with several conditions [Régnier 2008]:

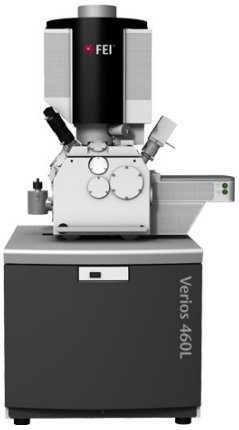

(a)

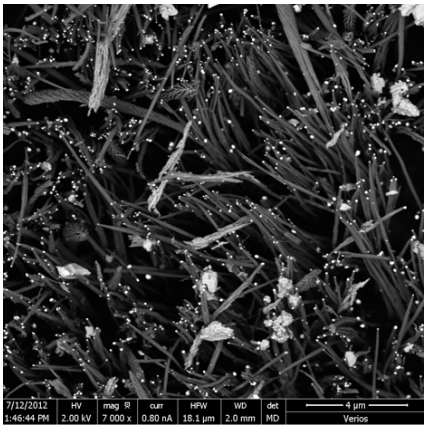

(b)

Figure 1.4: (a) FEI Verios XHR SEM; (b) An image example for material science [FEI 2015].

- it must ensure adequate grip. Particularly too much grip can lead to severe deformation or damage to target objects or even sensor components;

- it may require sophisticated strategy to control insertion strength during assembly process. Position plus force control is a classical challenge in macro environment, which becomes more difficult in the microworld context;

- it can faithfully detect if a contact is made when critical vision information is not available.

The current available force measurement approaches can be classified as indirect and direct methods.

- *Indirect measurement methods*: due the space limitation, a range of indirect approaches have been developed in the literature. Several popular methods are described below:

  - Force measurement by vision system: this kind of method usually requires no physical contact and can deliver force measurement from remote computation. To implement such method, a camera or laser sensor must be equipped, as well as fast and faithful image processing algorithms (e.g. pattern recognition). Research work can be found in the studies [Greminger 2004] [Anis 2006] [Wang 2001]. The working principle relies on the prerequisite knowledge of mechanical property of the tool. Typically, based on the flexion or deformation of the tool detected by image processing, the interaction force can be computed with the knowledge of the tool's mechanical properties [Chang 2009]. This method liberates additional force sensing equipment on the working site, but gives rise to complex vision electronic system. Furthermore, the corresponding algorithm must be able to produce fast and faith processing result, which is still a challenging issue today. The figure 1.5 illustrates the vision method.

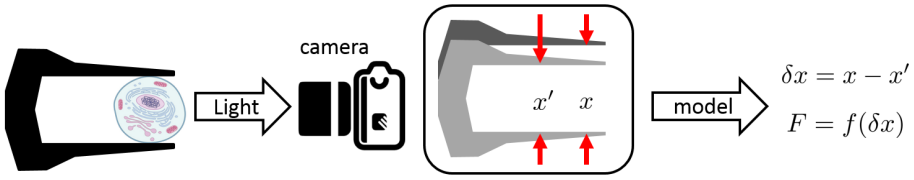

Figure 1.5: By processing image provided from vision system, the force in question can be derived with force model.

- Force transfered from working site to base: the working site is limited in space, but not necessarily the base of manipulation station. this method is established on the assumption that the mechanical structure chain is highly rigid that the force sensed at the tool end can be faithfully transferred along the chain to the base. With necessary force sensor at the base, measurement is achieved. Unfortunately, the micro-manipulation of small objects require the interaction tool (which is in contact with the micro objects) with dimensions comparable to the micro-scale [Régnier 2010]. A direct impact is that the miniaturization significantly reduces the stiffness of the mechanical structure, which consequently violates the assumption and makes the method very difficult to realize. The figure 1.6 illustrates the schematic diagram.

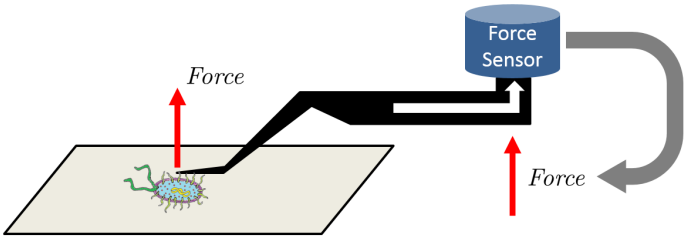

Figure 1.6: Contact force is transformed from working site to base. This method requires the rigidity of the mechanical structure in chain.

- Force measurement based on the model of actuator: such kind of method makes use of a range of smart materials such as piezoelectric materials, shape memory alloy, etc. With load carried, the change of physical properties, e.g. variation in resistivity, charge output, can be used to estimate the applied force [Shi 2012] [Lee 2005] [Goldfarb 1997]. This method typically relies on approximate polynomial model for state estimation. Precautions must be made to applications when dynamics must be considered and nonlinear behavior cannot be ignored, where resolution might be affected. Studies show that the information obtained in this way does not always provide a sufficiently high resolution for the intended applications [Régnier 2010]. Figure 1.7 illustrates an example of such force sensor based on force-charge model.

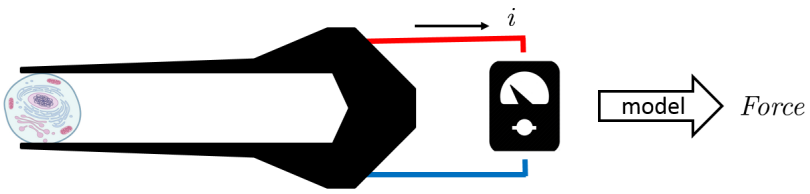

Figure 1.7: Contact force is transformed to electric charge variation. Based on an inverse model, the force can be measured within certain resolution and range.

- *Direct measurement methods*: as suggested by the name, this kind of method integrates directly the force sensor into the interaction device (gripper system). This is considered as the most efficient approach since it brings the sensor closest to the working site to measure the force in question. The difficulty of integration must be the first problem to tackle. Nowadays, the advancement in development of micro-manipulation and micro-fabrication makes this method possible and controls the cost of reproduction into reasonable scale. The available technologies can be categorized by physical process. Two of the most widely used are resistive strain gauges and capacitative sensors.

  - Resistive strain gauges. The sensor is composed of one or more resistive elements which deforms in response to the force acting on it. The figure 1.8 illustrates an example of a thermal microgripper made of polysilicon [Kristian 2005]. During contact with target objects, the flexion of the cantilever structure will lead to variation in resistance, which can be used to measure the gripping force. From the figure, it can be seen that this approach is extremely compact and fully coupled with the gripper design.

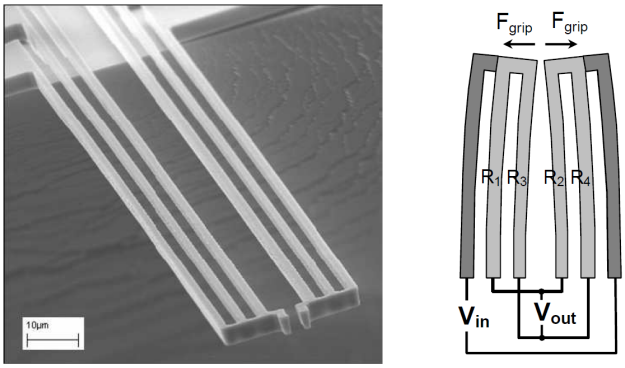

Figure 1.8: Direct force sensor: thermal microgripper [Kristian 2005]. The originality of the design is that it uses the bulk piezoresistive properties of polysilicon to obtain the gripping force.

  - Capacitative force sensors. The basic idea of this approach is to deduce contact force based on variation of capacitance. Typical structure contains

two parallel plates with a dielectric in between. One plate is fixed while the other is subject to the external force and moves accordingly. The dynamics of the movement can be approximated by a simple linear spring model. When subject to external force, the plate moves, the overlapped area is reduced, and the capacitance is changed. By relating all the physics in chain, a linear model can be established to obtain the force in question. In practice, such sensor is commonly composed of interdigitated combs with variable spacings, or double differential capacitors [Enikov 2000] [Sun 2004]. An example is illustrated in the figure 1.9 .

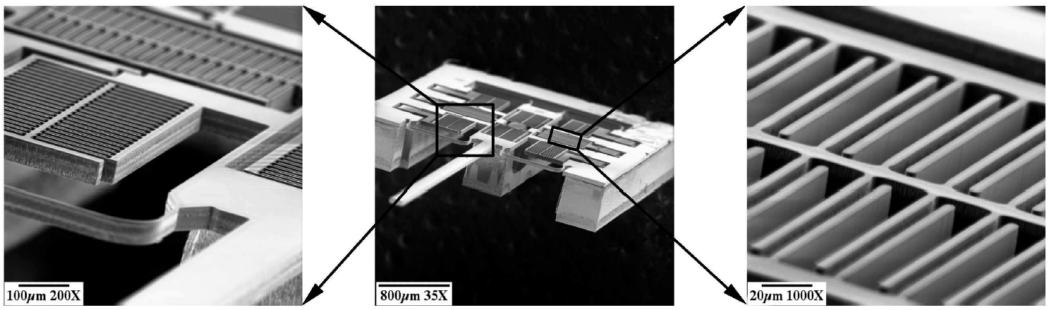

Figure 1.9: Direct force sensor: capacitative force sensor [Sun 2005].

1.1.3 Micro-Manipulation Systems

The previous texts describe the physics of the microworld and the corresponding observation methods. The environmental difference determines that micro-manipulation cannot be handled the same way as the macro-manipulation at our scale. Challenges arise when size becomes smaller. Efforts are required to realize desired micro-manipulation systems. On the other hand, microsystems are highly demanded from across a wide spectrum of our life. The application domains include automotive industry, IT peripherals, telecommunications, biomedical, scientific experiments and etc. For example, production of MEMS (Micro-Electro-Mechanical systems) is a huge market where several million pieces are batch-produced annually. The high demand is pushing the micro-manipulation to be a fast growing field. In this text, several available technologies about micro-manipulation systems are describe in the following.

A typical micro-manipulation system mainly consists of several components such as positioning system, sensor system, control unit and user interface. Positioning system can also be referred to as platform, which is composed of several actuators (see the section 1.2) for multi DOF alignment. Sensor system can involve measurement of force, position and others for control purpose. Control unit consists in a computational system which handles algorithms and manipulation sequence for micro-manipulation. Classical user interface is in graphic form, but more and more researches are dedicated to haptic interface (see the section 1.3) to achieve more intuitive interaction.

In the research field, there are fruitful results about the development of micro-manipulation systems. In the research work [Xie 2011], a flexible robotic system for micro/nano-scale manipulation (e.g. pick-and-place) and assembly is presented, as shown in the figure 1.10(a). The system is based on the principle of atomic force microscopy and comprises two individually functionalized cantilevers. The micromechanical testing and assembly station developed by [FemtoTools 2016] is a versatile micromechanical testing instrument, as shown in the figure 1.10(b). It can be reconfigured for a wide range of mechanical testing and manipulation task in the fields of material science, biomaterials testing , microsystems characterization, etc. The research work of [Ni 2011] [Ni 2013a] developed a micro-manipulation system based on haptic optical tweezers. The working mechanism relies on the force generated from laser's electromagnetic field to trap micro-objects. This technique requires no direct contact with manipulated object and is therefore favored in physics, cell engineering and other fields that need micro-manipulation and micro-scale force measurement.

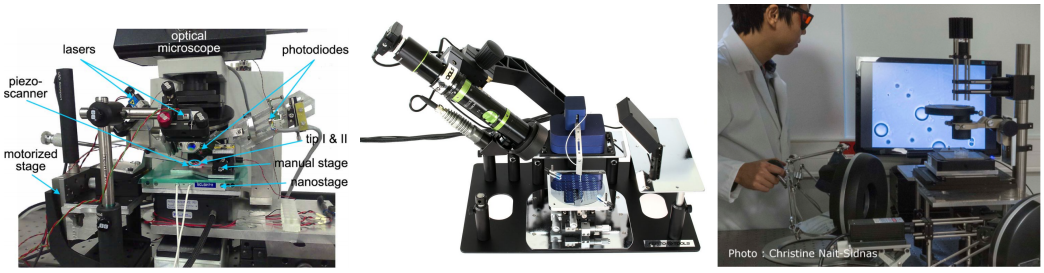

(a) (b) (c)

Figure 1.10: (a) Flexible robotic system for multiscale applications of micro/nano-scale manipulation and assembly [Xie 2011]; (b) The Femto-Tools micromechanical testing and assembly station [FemtoTools 2016]; (c) Haptic optical tweezers system [Ni 2011] [Ni 2013a].

In industry field, large batch automation micro-manipulation systems are already available. International suppliers like Palomar (USA), FineTech (DE/USA), Essemtec (CH) and SET SAS (FR) provide high accuracy automated machines (see the figure 1.11) to address the need. However, assembly is most simplified in packaging design to guarantee the throughput, with techniques such as flip-chip bonding.

In contrast, nowadays the small batch industrial production of complex microsystems is mainly based on handmade process, which requires outstanding human manipulation abilities. For example, the KolibriSensor used as a sensor in scanning probe microscopes (SPMs) (SPMs provide microscopic images of solids with atomic resolution) is produced manually. The handmade process can take up to a full day and is tedious with a high risk of failure. Unfortunately such kind of production cannot be handled by existing large batch automation solutions due to lack of flexibility and high unit price. Therefore, a micro-manipulation system which is suitable for small batch flexible production is urgently in high demand. In the following, a pioneer solution to address this need is presented.

(a) (b)

Figure 1.11: High accuracy machines for large batch microsystem automation: (a) SET FC300R. (b)FINEPLACER pico ama.

1.1.4 Chronogrip System

Created in 2011 in France as a spin-off from the well known Femto-ST Institute (a research team in micro-robotics), Percipio Robotics S.A. is a pioneer in microrobotics and specializes in micro-manipulation. Its activities include robot design, micro-assembly, micro-device fabrication and so on. The company is also involved in research projects with industrial and academic partners to go forward on the path to innovation.

In order to bridge the cap between large batch automation and small batch hand-made process, Percipio Robotics has developed a pioneer semi-automatic solution: a desktop platform called *Chronogrip* (see the figure 1.12). It aims to handle flexible micro-manipulation for small batch production.

Chronogrip is based on the ***cobotics*** principle: collaboration between humans and robots. The main idea is to place human operator at the center of the process and interface with her/him by giving all the tools and information the robotics can provide to master the process. Actually, the need for flexibility and the complexity of the micro-scale environments makes human access an important requirement. With the robotization of accurate and repeat tasks taking place in micro-manipulation, the flexibility is dramatically increased and hence, the productivity is promoted.

Chronogrip is mainly composed of several components: user interface (master device), coupling system, vision, robotic positioning system, and a gripper component (slave device).

- The user interface used in Chronogrip is a joystick. In the context of Chronogrip system, it only conveys motion command to slave device without haptic feedback. For the convenience, we will refer to this kind of unidirectional user interface as a *teleoperation interface* in the thesis. If a user interface can not only convey motion command to slave device, but can also render haptic dis-

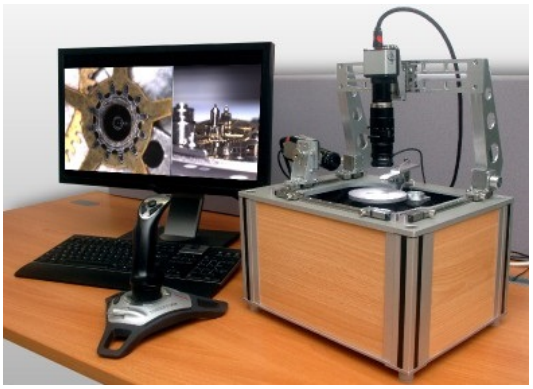

Figure 1.12: Chronogrip system by Percipio Robotics.

play, this kind of user interface will be referred to as a *haptic interface*. For Chronogrip system, a touch screen is provided as an alternative teleoperation interface.

- The coupling system refers to the set of electronic and software components which can enable the bidirectional communication. Concretely, it can convey the motion command (desired position, velocity, or acceleration, etc.) from master device to slave device and send back the information of manipulation (haptic feedback, etc.) from slave device to master device in run time.
- The high resolution vision system zooms viewpoint in the micro-world environment which goes beyond the capability of the human naked eyes.
- The robotic positioning system provides multiple degrees of freedom in both translation and orientation with high resolution and large range. The actuator implemented in Chronogrip is piezoelectric stick-slip actuator.

(a) (b) (c)

Figure 1.13: Chronogrip components: (a) tablet unidirectional interface; (b) vision device; (c) positioning system.

- Percipio Robotics has developed their own gripping device called *PiezoGripper* (see the figure 1.14). It is based on piezoelectric benders, each actuated on two directions (horizontal and vertical). With two benders, it is possible to build

a two fingered gripper, with 4 independent degrees of freedom. Horizontal motion of both fingers is used to the grasping/release of micro-objects, the vertical motion is used to align the fingertips of the gripper.

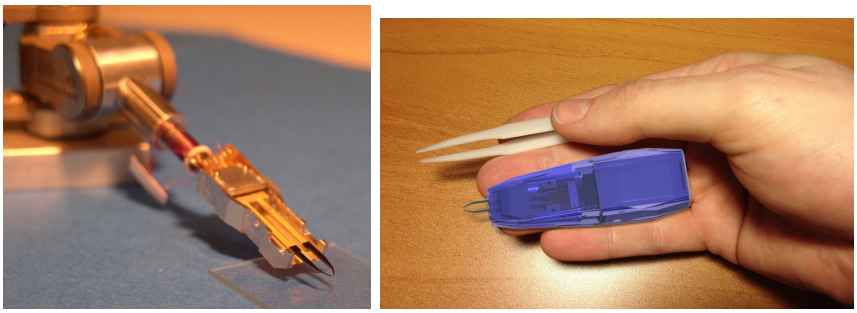

(a) (b)

Figure 1.14: (a) PiezoGripper mounted on a miniature robotic arm; (b) Fully integrated PiezoGripper.

1.1.5 Flexible Micro-Manipulation Solutions

There is currently a market window between large batch automation and small batch handmade process. Flexible micro-manipulation solutions are urgently demanded by small and medium-sized enterprises that want to launch innovative, hybrid and highly miniaturized components as small- to medium-scale production.

As a starting point, the cobotic platform Chronogrip is a promising solution for flexible micro-manipulation, but not yet complete. One missing part is the control algorithm to realize accurate trajectory tracking. Solutions provided today is limited. This topic is challenging and concerns deep study of actuators for the microrobotic system. Another issue concerns human-robot interaction. It is believed that in order to realize intuitive and effective interaction, haptic feedback is indispensable. Haptic functionalities are still absent in Chronogrip platform. More fundamental problem lies in the fact that existing haptic interfaces are general purposed with moderate performance, but they are not able to address the challenges from micro-manipulation. Much more efforts are needed for new design and methods.

In order to understand the challenges, the next two sections will firstly survey available actuators and haptic interfaces for microrobotic applications.

1.2 Actuators for Microrobotic Applications

An actuator is one of the central components of a robotic system. It converts other types of energy, such as electrical, magnetic or thermal energies, to mechanical energy, so as to provide desired force and displacement specified by a control unit. In microrobotics, the demand for the development of reliable and precise actuators of

size compatible with microrobotic applications is urgent and challenging. Potential applications include wide fields such as automotive (airbag, microsensors), biomedical, aeronautical and spatial industries. However, technologies of actuator applied in conventional industries such as hydraulic, pneumatic and electric motor-based are commonly not suitable to be transferred for micro and millimeter scales. Their properties such as resolution, efficiency cannot address challenges in microrobotics when they are miniaturized. Therefore, it is unavoidable to call on different materials and innovative working principles to address the needs in microrobotics.

Nowadays, more and more energies are dedicated to development of actuators for microrobotics. Some popular options are:

- piezoelectric actuators,
- electromagnetic actuators,
- electrostatic actuators,
- thermal actuators,
- shape memory alloys,
- magnetostrictive actuators,
- electro-active polymers,
- electrorheological fluids (ERF) and magnetorheological fluids (MRF).

The criteria for choosing appropriate actuators may depend on the specifications of applications, such as resolution, motion stroke, blocking force, power/weight ratio, cost of fabrication, and dynamics for control aspect (frequency bandwidth, linearity, technical feasibility).

In the following text, some of the most widely used options are surveyed.

1.2.1 Piezoelectric Actuators

Piezoelectric actuators can realize bidirectional conversion between electric energy and mechanical energy. The family of piezoelectric actuators has various working principle but all based on the piezoelectric effect. The physical phenomenon was firstly demonstrated by Pierre and Jacques Curie in 1880, in naturally occurring crystals. The direct effect consists of polarization of the material under the effects of mechanical stress. On the contrary, the inverse effect refers to a mechanical deformation on application of an electric field. Therefore, piezoelectric materials can be characterized by electromechanical coupling. Piezoelectric effect is illustrated by the figure 1.15.

Based on different configurations and aimed for various applications, there are several kinds of actuators as derivatives of piezoelectric materials that are described below:

- *Stack (multilayer) actuators.* This type of actuators consists of multiple layers of piezoelectric materials separated by insulating layers. Power supply of same

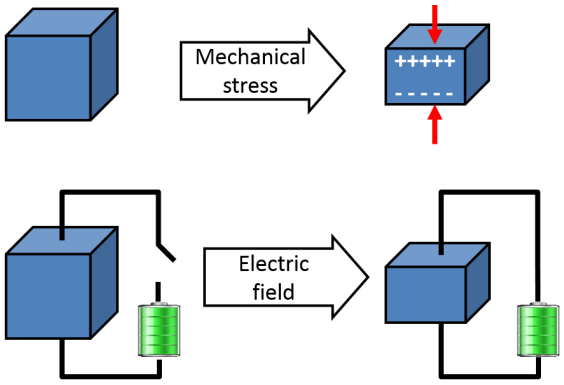

Figure 1.15: Piezoelectric effect. Upper part of figure illustrates direct effect: under mechanical stress, electrical polarization occurs; lower part of figure illustrates inverse effect: under electric field mechanical deformation occurs.

condition is given to each layer to augment inverse effect. The motivation of the design is to maximize the deformation stroke by multiplication of layers number. A schematic diagram of a typical stack actuator is illustrated in the figure 1.16. This kind of technology is already commercialized by company such as Physik Instrumente (PI) [PI 2016].

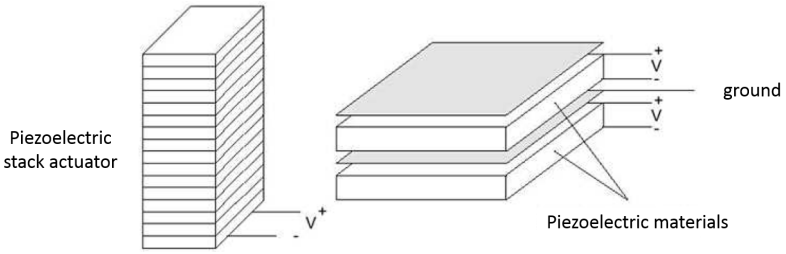

Figure 1.16: Piezoelectric stack (multilayer) actuator [Régnier 2008].

- *Bimorph (bender) actuators.* Similar to stack actuators, bimorph actuators also consist of layers. But the difference is that bimorph layers are not subject to the same power condition. Actually this kind of actuators rely on different mechanical deformation to create flexion. For example, the direction of polarization of the two layers is the same but with the voltage applied to the terminals of the upper layer being opposite to that applied to the lower layer. Since the two layers are glued together, this opposing power condition forces the upper layer to dilate (contract) and the lower layer to contract (dilate). Finally, the tip of bimorph actuator gives rise to net displacement and force. The operating principle is illustrated in the figure 1.17.

- *Stepping motors.* Stack and bimorph actuators take advantage of multiple

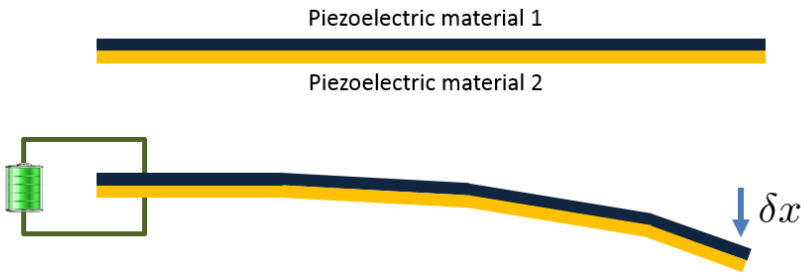

Figure 1.17: Bimorph actuator. With input power conditions being opposite to the upper layer and to the lower layer, one dilate and the other contract. This finally results flexion of the entire structure. The tip can thus give rise to net displacement and output force.

layers to amplify motion stroke. However, the effect is limited. Another group of actuators use the principle of stepping to achieve much larger motion stroke. As suggested by the name, displacement is accumulated by steps. So far, this family of actuators can be mainly classified into three categories ultrasonic actuators, inchworm actuators, and inertial actuators. (i) Ultrasonic actuator relies on the excitation of resonance of the stator. This vibration is generally elliptical. Motion direction can be controlled by shifting phase sign among different piezo components. Such actuators are featured by high speed. (ii) Inchworm actuator has its slider always in contact with alternate preloaded piezo stators. The guided motion mainly depends on the driving frequency and the phase shift among stator groups. Such actuators can provide much higher forces and resolution, but are relatively slow. (iii) Inertial actuator's working principle is based on the competition between the inertial force and friction force. Such actuator provides medium speeds. Typical inertial actuator is composed of only one piezoelectric channel. This simplicity lowers the cost and reduces the complexity in control aspect. As a common characteristic, those three options can generally provide motion stroke up to several millimeters. More details will be described in the section 2.2. An example of each is shown in the figure 1.18, the commercial products from PI [PI 2016].

1.2.2 Electrostatic Actuators

Electrostatics refers to the physical phenomena and properties of stationary electric charges. It has been recognized for centuries and many attempts were devoted to realize electrostatic motorization. However, this field has never reach success comparable to electromagnetic motors. The impediment mainly lies in low energy density of electric field in air and high input voltage.

With the fast development of microrobotics, it has been discovered that electrostatic effect is more favored in the miniature scale. As explained in the text

(a) (b) (c)

Figure 1.18: Commercial piezoelectric-based stepping actuators [PI 2016]. (a) PI-Line ultrasonic actuator; (b) PI NEXLINE inchworm actuator; (c) PI Q-521 inertia actuator.

1.1.1.1, reduction in size promotes surface effects because of scale effect. Thanks to miniaturization, air gap is reduced greatly and required input voltage is much less than that from macro-scale applications. The figure 1.19 illustrates an example of microgripper based on electrostatic principle [Beyeler 2007].

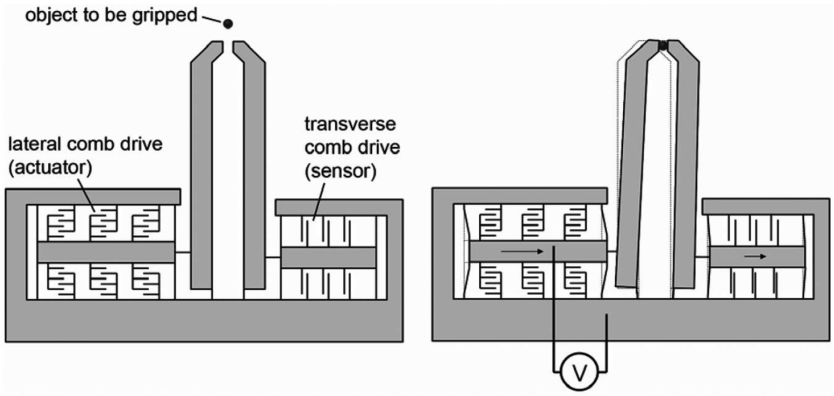

Figure 1.19: Microgripper driven by a comb drive, based on electrostatic principle [Beyeler 2007].

1.2.3 Thermal Actuators

Thermal actuators are based upon two important effects: thermal expansion and phase changes. A typical thermal actuator relies on temperature change to achieve material deformation. As with electrostatic actuator, the scale effect leads to more significant behavior of thermal principle in microworld than in macroworld. One of the first remarkable commercialization of thermal microactuators is the design of thermal inkjet printer heads in around 1970s [Bassous 1977].

Shape memory alloys (SMA), categorized as thermal actuators, is one of the most

active research fields in material science. The working principle of SMA does not simply rely on thermal expansion, but mainly consists in reversible phase change associated with temperature change and applied force. They can, after permanent deformation at low temperature, recover their initial physical state (memorized form) on heating. So far, the physical properties of SMA are still very challenging in control aspect, because of their significant hysteresis, strong nonlinearities, and slow dynamics. An application in micro-manipulation is shown in the figure 1.20, where a miniaturized microgripper is realized using SMA wires [Houston 2007].

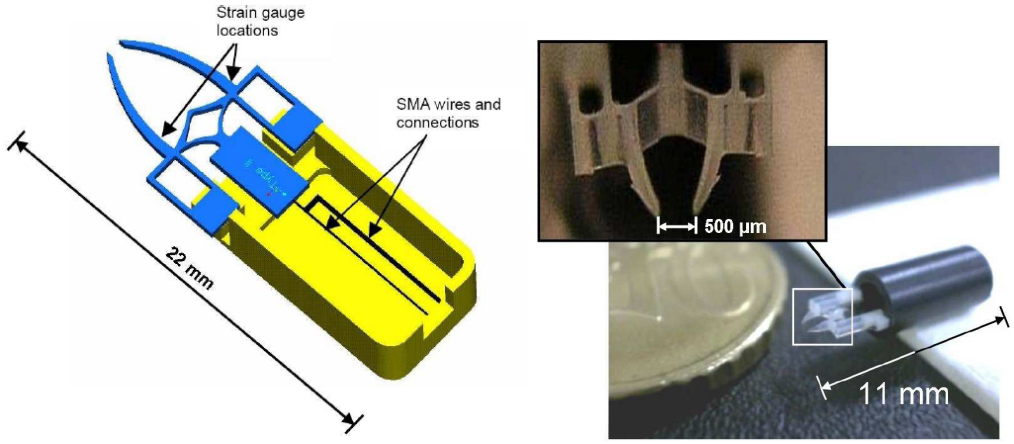

Figure 1.20: Miniaturized microgripper realized using SMA wires [Houston 2007].

1.2.4 Magneto-/Electrorheological Fluids

Magnetorheological fluids (MRF) and electrorheological fluids (ERF) are fluids with microparticles suspensions, whose viscosity changes when subject to magnetic or electric field (see the figure 1.21). In case of applied magnetic/electric field, cluster chains are formed along field lines. The chain effect of this micro-scale phenomenon causes the liquid to become more viscous in macro-scale. This property can be used for energy dissipation. In terms of applications, MRF and ERF can be applied as semi-active dampers or brakes. Though similar in operating principles between MRF and ERF, one significant difference is that MRF typically requires voltages in the order of tens of volts, with currents of a few amps; while ERF needs thousands of volts and currents of a few milli-amps. The maximum stress obtained from MRF is about 20 times higher than that of ERF.

1.2.5 Actuators for Microrobotic Applications

This section has surveyed popular technologies applied for micro-manipulations. The table 1.2 compares various families of micro-actuators [Bellouard 2002]. Most of them remain in low commercialization and efforts are still needed for research and development. The most exploited actuator is piezoelectric material because of high

Figure 1.21: Magnetorheological fluids by LORD Inc.

precision displacement, high force output, large frequency bandwidth, fast dynamics, small footprint, high energy density, etc. Due to the limitation of strain, stepping derivatives are developed for large motion stroke applications. They mainly include ultrasonic, inchworm and inertia actuators (refer to 2.2.1 for details). Among those options, piezoelectric stick-slip actuator (categorized as inertia actuator) is widely applied because of its high speed, high precision, compact size, ease of integration, and affordable price for small and medium-sized enterprises. Considering these advantages, Percipio Robotics has employed this kind of actuator in the cobotic platform Chronogrip to handle flexible micro-manipulations.

1.2.6 Control Algorithm for Piezoelectric Stick-Slip Actuator

Some worldwide companies [PI 2016] [SmarAct 2016] have already commercialized piezoelectric stick-slip actuators and they have reached a fast growing success. However, compared to the counterpart in macro-robotics, the solutions they provide for trajectory tracking are not complete, e.g. they only provide position tracking for most actuators, but no velocity or acceleration tracking. Furthermore, the control schemes they implement are commonly aimed to a limited set of functioning points, e.g. customized dynamics may not be guaranteed with same control performance.

As a consequence, the available trajectory tracking strategies cannot fully satisfy the complex applications demanded by a wide range of micro-manipulations. A more fundamental problem behind is due to the lack of complete study of the actuator dynamics. Therefore, in order to address the need of trajectory tracking for micro-manipulation, a deep study of the piezoelectric stick-slip actuator must be conducted.

	Piezoelectric	Thermal bimorph	SMA
Physical process	piezoelectricity: dipole orientation	difference in thermal expansion coefficients	solid phase transition
Operation principle	electric field	thermal	thermal
Energy density ($J.m^{-3}$)	10^6 (PZT), 10^3 (PMN)	10^5 Ni/Si	10^6 to 10^7
Bandwidth	high (100 kHz)	low, geometry dependent	low, geometry dependent, (10^2) Hz
Mode of operation	depends on orientation of electric field	flexion	flexion, torsion, tension, compression
Deformation	0.12-0.15%	$5.23 \times 10^{-4}/°C$	1-15%

	Conductive polymer	Giant magnetostriction	MRF/ERF
Physical process	oxidation and reduction effect ion diffusion	magnetostriction: orientation of magnetic dipole	particle chains formed along flux lines
Operation principle	voltage	magnetic field	magnetic/electric field
Energy density ($J.m^{-3}$)	10^3	10^4 to 10^5 (Terfenol D)	
Bandwidth	low (10 Hz)	high (100 kHz)	high
Mode of operation	flexion, tension, compression	depends on orientation of magnetic field	viscosity
Deformation	1-5%	0.58-0.81%	–

Table 1.2: Comparison of various materials for micro-actuators [Bellouard 2002].

1.3 Haptic Interface

In the process of human-microworld interaction, operation intuitiveness and effectiveness can be achieved by providing haptic display. Actually, versatile micro-manipulation platforms that have been demonstrated recently often use techniques from haptic feedback teleoperation for micro-manipulation [Bolopion 2013]. The purpose of haptics is to give an illusion that the operator directly worked with the target object without any medium in between. In other words, the haptic interface can serve as an extension of human body for inaccessible working environment. In recent years, tremendous studies are dedicated to the development of haptic interfaces. The available technologies can be mainly characterized by some properties

such as: the degree of freedom (DOF) in motion and in haptic space, the geometry of working space, the maximum rendering forces back to user, the frequency bandwidth of haptic information, and etc. In terms of modeling issue, haptic interface can be efficiently described as an inertia with a damping component [Diolaiti 2006]. In this section, some popular haptic interfaces that employed in micro-manipulation are surveyed in the following.

1.3.1 Series-Structure Interface

Inspired by commercialized industrial robots, a range of haptic interfaces based on series structure can be found, especially in commercial market. Briefly, such kind of haptic interface benefits from large working space, easier integration of orientation. Particular issue arises from the actuator distribution along the mechanical structure in chain. This significantly increases the overall inertia, reduce the resultant stiffness. The dynamics must be considered before using in any haptic application. In the following text, some popular haptic interfaces based on series structure are surveyed.

1.3.1.1 Virtuose

The haptic interface Virtuose is commercialized in 1999 by Haption [Haption 2015], which is the subsidiary of French public government-funded research organization CEA (Commissariat à l'énergie atomique et aux énergies alternatives). The Virtuose 6D35-45 provides haptic feedback in 6 DOF with maximum rendering force as 35 N. The geometry of the working space is a sphere with 450 mm as diameter. The version Virtuose 3D15-25 has 3D haptic rendering with the maximum force as 15 N and the diameter of the working space is 250 mm. The models are shown in the figure 1.22.

(a) (b)

Figure 1.22: (a) Virtuose 3D; (b) Virtuose 6D.

1.3.1.2 PHANToM

The first PHANToM haptic interface is designed in 1994, by the researchers in the laboratory of artificial intelligence in MIT (USA). The motivation was to touch and manipulate virtual 3D objects. The concept was later commercialized by Sensable Technology and the product family was extended to 5 models. The PHANToM Desktop has 3 active DOF and 3 passive DOF. The working space is defined by 16 $\times$ 13 $\times$ 13 cm^3. The model PHANToM 6.0 has 6 active DOF and a working space as 19.5 $\times$ 27 $\times$ 37 cm^3. Two models are shown in the figure 1.23.

(a) (b)

Figure 1.23: (a) PHANToM Desktop; (b) PHANToM Premium.

1.3.1.3 1 DOF Dual-Stage Interface

Electromagnetic drives are subjected to an inherent inertia-torque trade-off that fundamentally limits transparency. A 1 DOF dual-stage haptic interface has been proposed with a small and high dynamic motor coupled with a large and high torque motor by a passive viscous transmission in order to avoid this trade-off and hence improve the transparency for human users [Mohand-Ousaid 2012]. The interface is shown in the figure 1.24.

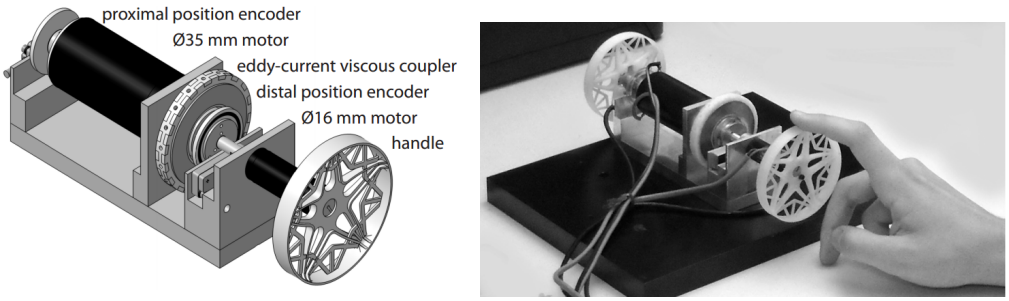

Figure 1.24: 1 DOF Dual-Stage Interface [Mohand-Ousaid 2012].

1.3.2 Parallel-Structure Interface

Though having its working space significantly reduced compared to series structure, the advantage of haptic interface based on parallel structure lies in the fact that the actuators and sensors can be implemented near the base. This design greatly reduces the inertia in mechanical chain and enhances the overall stiffness. As a result, the dynamic performance, e.g. the frequency bandwidth, is greatly promoted compared to its series rivals.

1.3.2.1 Omega 7

Originally developed by Virtual Reality and Active Interface group in EPFL (École Polytechnique Fédérale de Lausanne), the haptic interface Omega is a popular in many research and industrial domains. In 2001, the design is commercialized by Force Dimension (Lausanne Switzerland) [ForceDimension 2016]. The interface is based on parallel structure DELTA and has 3 DOF as translation. The latest version Omega 7 (see the figure 1.25) has 3 DOF for haptic feedback, a working space of 160 ×110 mm as translation and 240 × 140 × 180 deg as rotation. The maximum force it can provide is 12 N.

Figure 1.25: Haptic interface Omega 7 by Force Dimension [ForceDimension 2016].

1.3.2.2 Pantograph

The haptic interface Pantograph (see the figure 1.26) is firstly developed in 1994 by the haptics laboratory in McGill university, Canada [Campion 2005b]. It is based on a planar parallel mechanism, actuated by 2 motors at base. The linkage is optimized to be stiff and light. The working space is about 10 × 16 cm^2 and the maximum output force is 10 N.

1.3.2.3 Cable Interface

Ideal haptic interface based on cable transmission can maximum explored working space with minimum obstacle from mechanical chain. One well known example is

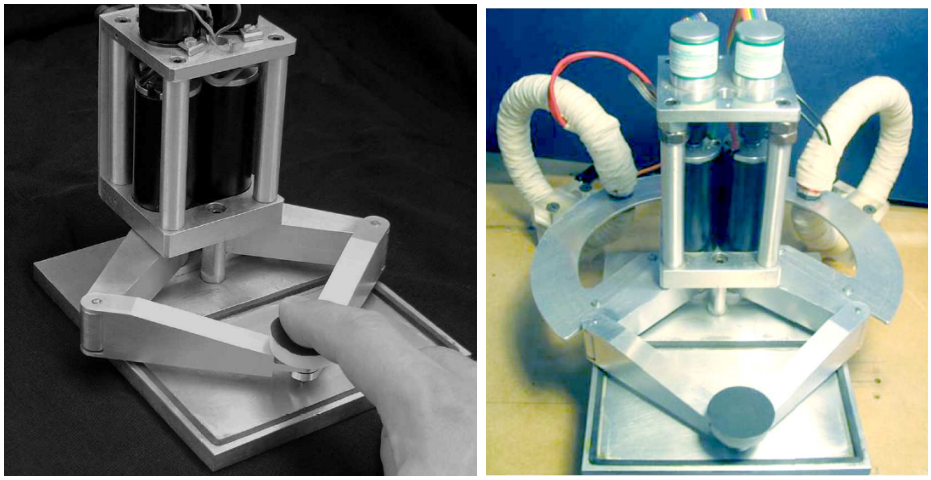

Figure 1.26: Haptic interface Pantograph developed by haptics laboratory in McGill university. The right figure shows a version with brake system.

the haptic interface SPIDAR [Sato 1997] (see the figure 1.27(a)), developed in 1991 by Tokyo Technology Institute, Japan. The handle of the interface is a sphere with position maintained by cable. It has a working space of 3D for translation. The latest version can extend the working space to 6D. Concretely, the SPIDAR I has the working space as $900 \times 600 \times 600$ mm^3 and the maximum force output is 4 N.

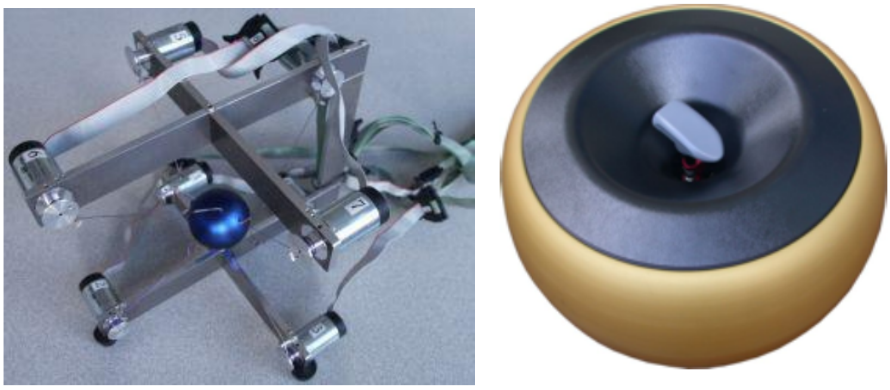

(a) (b)

Figure 1.27: (a)Cable haptic interface SPIDAR; (b)Magnetic suspension haptic interface Maglev.

1.3.2.4 Magnetic Suspension Interface

Different from haptic interface based on mechanical transmission, interface with magnetic suspension is liberated from complex mechanical structure. Maglev (see the figure 1.27(b)) is a such haptic interface. It has 6 DOF and the interface handle

is float due to magnetic field. The position and orientation are measured precisely by optical sensors. This type of interface has very high dynamic performance.

1.3.3 Haptic Interfaces Summary

This section has survey some of the most popular haptic interfaces used in micro-manipulation. They are based on general-purposed design so as to be applied in a wide range of applications. However, being general leads to a compromise among performance properties such as the degree of freedom (DOF) in motion and in haptic space, the range and geometry of working space, the maximum rendering forces back to user, the dynamic range (ration between maximum temporary force and friction; with 1 mN as minimum value as threshold of perception), and etc. A more complete survey is summarized in the table 1.3.

1.3.4 Dedicated Haptic Interfaces for Micro-Manipulation

Nowadays, the available haptic interfaces are still far from being qualified with respect to the need required by micro-manipulation, which may demand a combination of the performance properties described above. For example, some advanced microrobotic applications require large working space and large frequency bandwidth. Typical existing solutions employ cantilever structure to augment working space, however, the frequency bandwidth must be reduced due to the dynamics of cantilever design. Another example is some special micro-manipulation may require dedicated interface design to enhance operation intuitiveness, where general purposed haptic interfaces can hardly fulfill the request.

In summary, available haptic interface solutions cannot fully address the needs from micro-manipulation. Efforts are still needed in haptic interface mechanical design and the development of related algorithms to realize intuitive and effective micro-manipulation.

1.4 Challenges

This chapter has introduced the basics of microrobotics, and the existing technologies for micro-manipulation. As discussed, there is a blank window for small batch production of complex microsystems, which demands flexible solution to address the need. Under such circumstances, Percipio Robotics has proposed its semi-automatic cobotic platform Chronogrip to bridge the cap between prevailing non-flexible mass automation and low-yield handmade process. However, the solution is not yet complete, there is still challenges in terms of trajectory tracking and haptic rendering. Concretely, there are three problems to resolve:

- In the human-robot interaction, control in velocity is crucial. This issue concerns the study of positioning actuator. Piezoelectric stick-slip actuator that used in Chronogrip system is promising solution to realize a great range of microrobotic applications, and many innovation companies have commercialized

this kind of product with reasonable price. However, none of these companies or any research results is able to propose a complete control strategy for velocity, let alone acceleration control. The main difficulty lies in the complexity of the dynamics of piezoelectric stick-slip actuators. More precisely, no research result has been reported to be able to fully describe the dynamics of such actuator. To be more general, no control strategy is available nowadays to address complete trajectory tracking for piezoelectric stick-slip actuator, and its dynamics is not yet fully understood.

- In the microworld, surface forces are more dominant due to scale effect (see the section 1.1.1.1). In such situation, thermal agitation and other environmental elements cause the micro-objects to follow high dynamic motions. As a consequence, this will lead to high dynamic interaction forces between target objects and gripper tools. Taking into account the existing mechanical structure and design of the haptic interface, no option is able to render high dynamics arisen from microrobotic applications. The lack of high bandwidth haptic interface causes the interaction with the microworld non-intuitive and inefficient.

- In prestigious watchmaking industry, due to its flexibility of models and small batch production, the manufacturing process can hardly be automated. But handmade process has saturated accuracy and productivity, which makes the watchmaking players more and more difficult to conquer their place in global competition. To address this challenge, Percipio Robotics proposes Chronogrip to realize cobotic production. However, the most significant issue lies in the interface. A joystick or tablet is way too different from the conventional tools (the tweezers) used by watchmaking experts, and hence they have to be trained very hard to be familiar with the interface. Furthermore, there is no haptic feedback which makes the process nonintuitive. Nowadays, there is not yet a haptic interface based on a tweezers form available in prototype. The combination of realizing haptics and maintaining mechanical properties of tweezers is a challenging task.

The objective of the thesis is not to construct a new cobotic platform for microrobotics, but aimed to address the three challenges described above.

The first challenge concerns the issue of the development of trajectory tracking strategies for piezoelectric stick-slip actuator. Particularly, velocity control is the subset of this general tracking challenge. In order to handle this issue, a thorough study of the actuator dynamics must be conducted. Today, modeling methods have been proposed by various studies, but none of them is able to describe the dynamics completely, meaning the lack of description in time and frequency domain, for stepping and scanning mode and for backward and forward motion. In chapter 2, the study of nonlinear dynamic modeling for a class of microrobotic systems using piezoelectric stick-slip actuators is conducted. It will show that the model can

describe the dynamics for all the three aspects mentioned above. This result paves the way for the next development of trajectory tracking strategies.

The second challenge concerns the study of bandwidth of haptic interface. Large bandwidth is important for the realization of high dynamic interaction for micro-manipulation. In chapter 3, analytical results show that cantilever interface (whatever the material) cannot lead to satisfying bandwidth for micro-manipulation. To handle this issue, a method is proposed to extend the bandwidth of dual stage haptic interface by using signal crossover technique. With the method implemented, experimental results show that the dual stage interface has an extended bandwidth from DC to 1 kHz.

The third challenge concerns design of a novel haptic interface for watchmaking process. The particularity is that the interface must resemble a conventional tweezers to promote intuitiveness. In chapter 4, it will show that difficulties arise when providing haptics and tweezers-based characteristics must be satisfied simultaneously. Realization of actuator system is the most challenging part, where several candidate solutions are proposed and evaluated. A final design will be presented as well as the first prototype. Since it is tweezers-based design and is compatible with conventional usage, the interface is not limited to watchmaking and can be used in a wide range of micro-manipulations.

Supplier	Product	DOF	H-DOF	Work space (cm)	Peak force (N)	Continue force (N)	Friction (N)	Dynamic range	Percep. inertial (g)	Stiffness (N/mm)	Structure
Novint	Falcon	3	3	8	9				> 300	8	P
Force dimension	Omega 3	3	3	11	12	12	0.3-0.5	40		14.5	P
Force dimension	Delta 3	3	3	32	20					14.5	P
Force dimension	Delta 6	6	6	32	20					14.5	P
3D Systems	Phantom Omni	6	3	11	3.3	0.88	0.3-0.5	3	45	1-2.3	S
3D Systems	Phantom Desktop	6	3	23	7.9					1.5-2.3	S
3D Systems	Phantom 1.5	6	3	27	8.5	1.4			75	3.5	S
3D Systems	Phantom 3	6	3	58	22					1	S
Quanser	5-DOF Wand	6	5	38	7-9	2-3				6	H
Quanser	HD^2	6	5	41	14-20	8-11	0.35	40-57	300	3	P
Haption	Virtuose 3D Desktop	6	3	20	10	3				2	S
Haption	Virtuose 6D Desktop	6	6	20	10	3				2	S
Haption	Virtuose 6D	6	6	84	31	8.5				2	S
Haption	Inca 6D	6	6	150	37.5	12.5					C
MPB Technologies	Freedom 6S	6	6	22	2.5	0.6	0.06	42	100-200		S
Butterfly Haptics	Maglev 200	6	6	2.4	40		0	4×10^4	510	50	P
ACROE Laboratory	ERGOS MRK	n	n	2	200	60	0.005	4×10^4	300	40	P
Moog	HapticMaster	3	3	36	250	100			2000	50	S
[Campion 2005b]	Pantograph	2	2	10	10	10			55		P
[Mohand-Ousaid 2012]	dual-stage	1	1		5	5	0.003		6		S

Table 1.3: Comparison of various haptic interfaces. P, S, H and C represent parallel, series, hybrid and cable. H-DOF is DOF for haptics. Phantom Omni and Phantom Desktop are now named as Geomatic Touch and Geomatic Touch X respectively.

Chapter 2

Nonlinear modeling for a class of microrobotic systems using piezoelectric stick-slip actuators

Contents

In order to develop trajectory tracking strategies for microrobotic systems, the dynamics of an elementary actuator must be studied and well modeled. This chapter addresses modeling issues for a class of microrobotic systems using piezoelectric stick-slip actuators. The modeling of this kind of actuators is complex because: (i) several parameters of the system (i.e. dynamics of the piezoelectric material itself, the friction dynamics and the dynamics of the moving slider) are nonlinear and coupled, (ii) there is no systematic methodology for parameters identification and (iii) existing friction models are often limited due to the complexity of the presliding motion. The consequence is that existing models are quite accurate for a small working range (i.e. input voltage and input frequency ranges). This is not

sufficient when the microrobotic systems are involved for both large displacements (e.g. millimeter range) and small displacements (i.e. micrometer range). The main contribution of this chapter is the proposition of an extended dynamic model for microrobotic systems using piezoelectric stick-slip actuators. The main issues that have been addressed are:

- modeling of hysteresis. This is not as simple as for traditional piezoelectric actuators because here both the hysteresis of the piezoelectric element and the friction dynamic are involved.
- improving the single-state elasto-plastic friction model. In this study, we show that several low frequency vibration modes of the stick-slip piezoelectric actuator are not due to the piezoelectric element itself, but it is due to the friction contact. A multi-state elasto-plastic friction model is then used. Moreover, we show for the first time how the break-away displacement can evolve with the amplitude and the frequency of an input sawtooth signal. Results show that this dependence is not the same when the actuator is moving in a forward direction and in a backward direction.
- obtaining a complete coupled nonlinear model being able to describe the dynamics of stick-slip type actuators for both scanning mode and stepping mode in the time and the frequency domains and for backward and forward directions of the motion.

Results of this chapter open new perspectives for cinematic and dynamic models of robotic systems intended to do tasks at the micro scales. Therefore results can be used for the development of dedicated velocity and/or position control.

The model is validated with experimental data. At last, a velocity control strategy is demonstrated.

2.1 Introduction

The positioning system in Chronogrip is built upon piezoelectric stick-slip actuators. This type of actuator is considered as a promising solution for realizing microrobotic applications (see the section 2.2). In order to realize fluent and effective teleoperation via the cobotic platform, the development of sophisticated trajectory tracking strategies is the key. For this purpose, efforts are required from across the full spectrum of research disciplines about the piezoelectric stick-slip actuators, such as mechatronic design, dynamics analysis and control. Nowadays, commercial microrobotic systems using piezoelectric stick-slip actuators are already available [SmarAct 2016] [PI 2016] (e.g. the figure 2.1). However, the solutions they provide are often limited to position control. Typically, if desired velocity or acceleration is specified in microrobotic applications, no commercial control strategy is available. The main difficulty lies in the complex dynamics of the piezoelectric stick-slip actuators, and no research is reported today to achieve a complete dynamic model. In order to develop a sophisticated control strategy to address the trajectory tracking challenges in microrobotics, the dynamics of the piezoelectric stick-slip actuators must be fully studied.

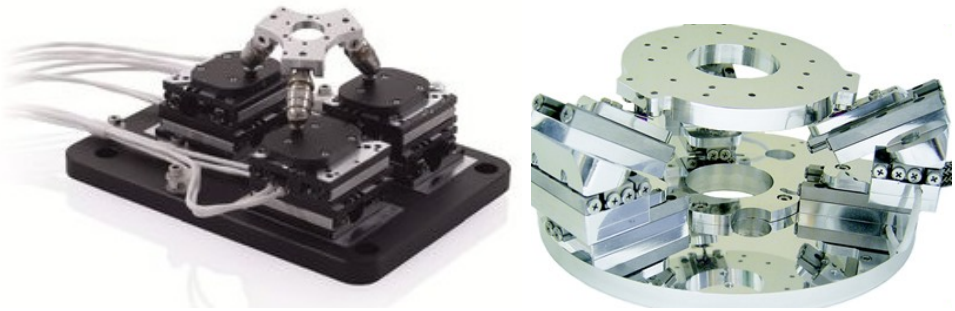

Figure 2.1: Commercial microrobotic platform using piezoelectric stick-slip actuators: (a) PI SF-450 PS SpaceFAB [PI 2016], (b) SmarPod 110.45 [SmarAct 2016].

In this chapter, the dynamic modeling of piezoelectric stick-slip actuators is developed taking into account specifications for microrobotic systems. In particular, the aim is to study the necessary conditions of the model parameters so as to satisfy the following criteria:

- the model must describe the dynamics of a stick-slip actuator, in time and frequency domains, for both scanning mode and stepping mode;
- the model must be able to describe the motion of the slider for both backward and forward drive directions (see the figure 2.3);
- the model must be in agreement with experiments.

It will be shown that the aforementioned criteria can be satisfied only if specific conditions on the model parameters are taken into account. At the end of the

chapter, a velocity control application is demonstrated. The study is based on the theory of the single state elasto-plastic model and on a series of experiments.

In the next section, some popular microrobotic actuators and modeling approaches are surveyed. In the section 2.3, the global architecture of the studied microrobotic system and its main features are presented. The section 2.4 deals with the nonlinear modeling of the system taking into account the friction contact force and the hysteresis nonlinearity. In the section 2.5, the experimental analysis and the model identification are presented. A discussion on the modeling issues is given in the section 2.6. In parallel with the development of complete dynamic model (e.g. inverse modeling), a non-model based velocity control scheme is demonstrated in the section 2.7.

2.2 State-of-the-Art

2.2.1 Microrobotic Actuators

In microrobotics, piezoelectric-based actuators are getting increased market shares because of their desirable properties such as compact size, high resolution, fast response and high power to weight ratio. Increasing the actuation range can be achieved through amplification (bender) or stepping motion [Breguet 2007]. Various solutions using stepping motion are widely used in many applications such as microbiology, neurology, micro-material assembly. So far, piezoelectric-based actuators which are based on stepping motion principle can be mainly classified into three categories [Li 2013] [Breguet 2007]: ultrasonic actuators, inchworm actuators, and inertial actuators. They bear some common characteristics such as their motion are friction based, the travel range depends only on slider's length, and they have a holding force without any power consumption. However, they differ in working principle and performance.

Typical ultrasonic actuator relies on the excitation of resonance of the stator. This vibration is generally elliptical and is used to drive the load by friction [Vasiljev 2007] [Kanda 2006] [Morita 2000]. Motion direction can be controlled by shifting phase sign among different piezo components. Such actuators are featured by high speed (> 100 mm/s). In terms of control, they provide a medium controllability and are sensitive to variations of loads. The control unit can be complex to implement due to the need to track resonance [Cedrat 2015].

Inchworm actuator has its slider (load) always in contact with alternate preloaded piezo stators. The guided motion mainly depends on the driving frequency and the phase shift among stator groups. The accurate synchronization among piezo stators is the key to guarantee desired motion [Lu 2009] [Moon 2006] [Kim 2002]. Such actuators can provide much higher forces and resolution, but are relatively slow (< 10mm/s) with respect to other two options. The corresponding control unit could also be expensive to realize multi-phases based working principle.

Inertial actuator's working principle is based on the competition between the inertial force and friction force. It can be operated in either scanning or stepping

mode depending on the choice between high resolution motion and large range motion [Belly 2012] [Yang 2011] [Špiller 2011] [Fung 2008]. Generally, such actuator provides medium speeds (10-50 mm/s). Instead of multi-phases based design as described from the previous two options, a typical inertial actuator is composed of only one piezoelectric channel. This simplicity lowers the cost, promotes response speed, leads to a better miniaturization potential, and greatly reduces the complexity in control aspect.

Piezoelectric stick-slip actuator is one of the most widely used inertial actuators. Based on the simplicity described above, it is believed that piezoelectric stick-slip actuator is a promising choice for microrobotics and it is chosen to build up our micro-manipulation cobotic system. The comparison among those three actuators is summarized in the table 2.1.

	Ultrasonic	Inchworm	Inertial
Resolution	sub-micron	sub-nm	sub-nm
Velocity	$>$ 100 mm/s	$<$ 10 mm/s	10-50 mm/s
Piezoelectric channel	multiple	multiple	single
Travel range	$<$ slider's length	$<$ slider's length	$<$ slider's length
Force	$<$ 40 N self-locking	$<$ 800 N self-locking	$<$ 10 N self-locking

Table 2.1: Comparison among typical piezoelectric stepping actuators.

2.2.2 Working Principle of Piezoelectric Stick-Slip Actuator

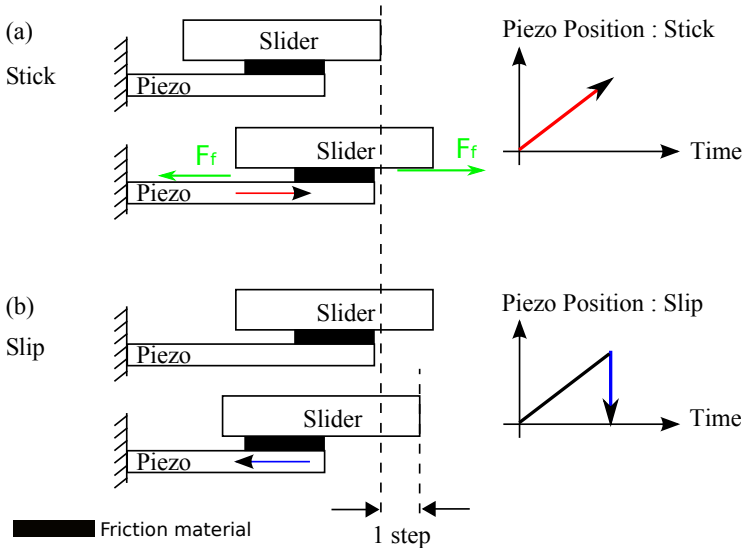

Figure 2.2: The operation principle of the stick-slip actuator. (a) Stick phase; (b) Slip phase.

A piezoelectric stick-slip actuator is made of (figure 2.2) a Piezoelectric Element (PE), a slider moving along a linear axis and a friction material between the PE and the slider. The slider is in charge of carrying a load (e.g. robot axis). It is guided by the deformable PE that converts electrical energy to mechanical energy. During a slow deformation of the PE, the contact friction force F_f drives the slider to a linear motion (figure 2.2(a)). After an abrupt contraction of the PE, the slider slips and cannot fully follow the sudden motion of the PE because the inertia force becomes greater than the contact friction force. The slip phase is illustrated in figure 2.2(b). An alternate stick and slip sequence produces a displacement of the slider relative to the PE. By repeating those operations, large range of motion of the slider can be achieved. This function mode is called *stepping mode*. The input voltage signal applied to the PE is a sawtooth sequence so that alternate slow and abrupt deformations can be realized. If there is only stick motion without any slip, the slider can be driven with higher precision. This function mode is called *scanning mode*. Unlike conventional motors, motion direction cannot be changed by inverting input power. If input sawtooth sequence is given by repeating slow rise and abrupt drop, the actuator goes towards one direction, which will be referred to as *forward direction*; the opposite direction can be produced if sawtooth sequence is given by repeating abrupt rise and slow drop, and this direction will be referred to as *backward direction*, as shown in the figure 2.3.

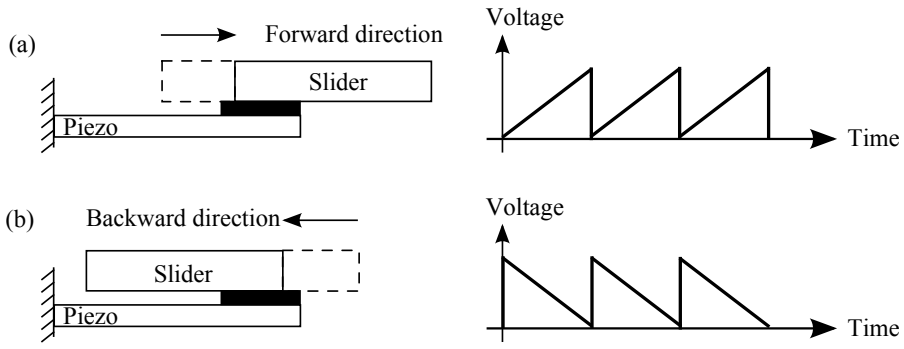

Figure 2.3: Simplified scheme showing that the direction of motion of the slider can be specified by the drive direction of the input sawtooth voltage.

2.2.3 Friction Modeling

Due to the dynamic complexity of the piezoelectric stick-slip actuators, many research and industrial applications employ static models [Breguet 1998] [Bergander 2003] [Rakotondrabe 2009] [Rakotondrabe M 2009]. Such typical solution describes the actuator velocity as a linear function of the input sawtooth frequency and amplitude. It is a simple and efficient approximation. However, such models can only be used for stepping mode within a limited input condition range, and is not suitable for scanning mode. In the research work [Peng 2011], a dynamic model is developed. But the model is only validated in time domain for several input

condition and for only one motion direction. The validation in frequency domain is absent.

As described previously, The phenomenon of stick-slip is determined by the contact friction force in dynamic conditions. As a nonlinear phenomenon, friction is considered as one of the most difficult challenges in mechatronic systems and it can cause control problems such as static errors and limit cycles [Lampaert 2003]. Therefore, friction modeling is considered as the crucial part of the dynamic modeling of piezoelectric stick-slip actuator.

Friction model	Continuity	Presliding	Non-drifting (stiction)	Stribeck	Nb. of states
Regularized Coulomb	√				–
Karnopp			√		–
Dahl	√	√			single
LuGre	√	√		√	single
Single-state elasto-plastic	√	√	√	√	single
GMS	√	√	√	√	multiple

Table 2.2: Comparison among several friction models.

In the literature, various friction force models can be found, but they are not all suitable for microrobotic applications. The Karnopp friction model is a combination between Coulomb and viscous force [Karnopp 1985]. It is a simple approximation and widely used. Nevertheless, the sign function in the model can cause discontinuity in numerical implementation. The regularized Coulomb model [Threlfall 1978] made a compromise between friction properties and numerical continuity. Furthermore, if high precision positioning and low velocity tracking are required, those two models can not give rise to satisfactory results [De Wit 1995]. In order to address the high precision positioning and tracking in microrobotics, a comprehensive friction model must be employed to describe the phenomenon of presliding which is the motion prior the complete slip [Dupont 2002]. The Leuven model [Lampaert 2002] [Swevers 2000] and GMS model [Lampaert 2003] are multi-state complex models established in asperity level. The latter one is the most comprehensive and is able to describe complex behaviors such as presliding regime, Stribeck effect, frictional lag, transition behavior and etc. However, in order to obtain smooth and accurate friction signals, there must be sufficient number of states (asperities). This complexity could be a major impediment for real-time applications where computational time must be strictly controlled. The LuGre model [De Wit 1995] [De Wit 1993], in line with the Dahl model [Dahl 1968], is a single-state friction model which is based on the average behavior of the bristles. This model can describe presliding, Stribeck effect and frictional lag [Zhong 2011]. However, its limitation is that it exhibits undesirable drift behavior [Hayward 2000].

To tackle this issue, Dupont et al. [Dupont 2002] have proposed a single-state elasto-plastic friction model that reduces the drift while it preserves the favorable properties of existing models. This model has been applied in several studies [Serafin 2003] [Buechner 2012] [Han 2011]. In particular, the research work [Peng 2011] [Rakotondrabe 2009] use this friction model to develop dynamic model for piezoelectric stick-slip actuator. However, none of those research work has rigorously investigated how to incorporate this friction model for different motion directions. This seems trivial, but in our study, it will be demonstrated that special condition must be met in order to address motion direction change. Indeed, in the original paper [Dupont 2002] it is suggested that some parameters of the model would be changed in case of direction change. For control purposes, the model must be able to simulate the dynamic motion of the actuator in a wide operating range and for both forward and backward motions.

Based on the simplicity and versatility of the single-state elasto-plastic model, it is chosen as the friction model in our study. As mentioned above, additional condition of the friction model must be specified so as to address different motion directions. The comparison of friction models is summarized in the table 2.2.

2.3 Presentation of the microrobotic system

The microrobotic system is designed by SmarAct company. It is composed of a 6 DOF parallel robot and a 3 DOF Cartesian robot (see the figure 2.4). Each axis of the microrobot is actuated by a piezoelectric stick-slip actuator of the same reference (SLC-1720-S-HV). The maximum stroke of each axis in the Cartesian microrobot is 12 mm, the maximum amplitude of the input driving voltage is 100 V and the scanning resolution is in submicron range. The study is mainly concerned with the dynamic modeling of the stick-slip actuator. The actuator of the Y axis in the Cartesian structure is used for the experimental validation. The motion of this actuator is measured with a laser interferometer sensor (SP-120 SIOS Mebtechnik GmbH).

2.4 Nonlinear dynamic modeling

To define the dynamic model of the complete microrobotic system, the dynamics of each axis must be well modeled. As such, the challenge is to define an accurate dynamic model of an elementary stick-slip actuator.

The major impediment lies in the fact that the internal structure is no public information. As such, hypothesis must be made for the modeling. There are three main assumptions (Fig. 2.5):

(i) the Piezoelectric Element (PE) is attached to the base of the actuator,

(ii) the moving slider is guided by a linear crossed roller guideway and has only one translational DOF,

(iii) there is a friction material between the slider and the PE without lubricant.

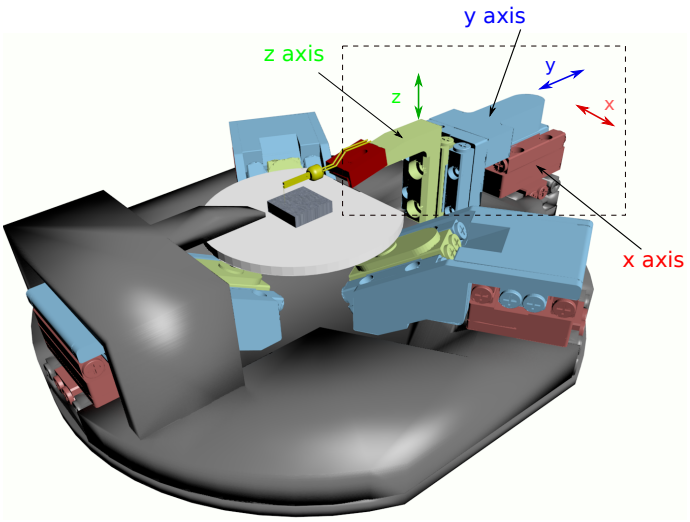

Figure 2.4: CAD view of the microrobotic system. The dashed block shows the Cartesian 3 DOF (XYZ) microrobotic part.

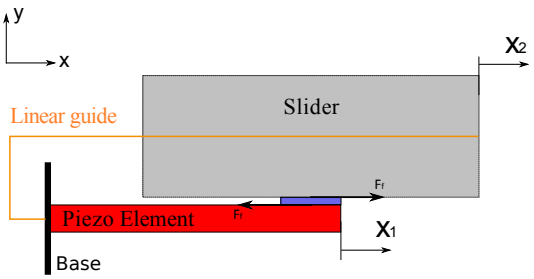

Figure 2.5: Simplified scheme of the piezoelectric stick-slip actuator.

2.4.1 Dynamic Modeling of the PE and the slider

2.4.1.1 Dynamic Modeling of the PE

Experiments (see section 2.5) have shown that the PE has two main vibration modes at 64 kHz and 118 kHz. Let us first consider the linear dynamic equations of each vibration mode as follows:

$$M_p \frac{d^2 x_{1a}}{dt^2} + D_{pa} \frac{dx_{1a}}{dt} + K_{pa} x_{1a} = K_{act1a} U - F_f \tag{2.1}$$

$$M_p \frac{d^2 x_{1b}}{dt^2} + D_{pb} \frac{dx_{1b}}{dt} + K_{pb} x_{1b} = K_{act1b} U - F_f \tag{2.2}$$

$$x_1 = x_{1a} + x_{1b} \tag{2.3}$$

where M_p, D_{pi} (i=(a,b)), K_{pi} (i=(a,b)), K_{act1i} (i=(a,b)) are respectively the mass, the damping, the stiffness and the static gain of each vibration mode a and b.

x_{1i} is the displacement of a vibration mode i. The total displacement of the PE is x_1. U and F_f are respectively the input voltage and the friction force between the slider and the PE.

In static mode (i.e when t$\rightarrow \infty$), x_1 is given as:

$$x_1 = (\frac{K_{act1}}{K_{pa}} + \frac{K_{act2}}{K_{pb}})U - (\frac{K_{pa} + K_{pb}}{K_{pa}K_{pb}})F_f \tag{2.4}$$

Let us now consider the hysteresis nonlinearity $H(U)$. The dynamic equation of the PE becomes:

$$x_1 = H(U)F_h(K_{act1}G_{xa} + K_{act2}G_{xb})U - (G_{xa} + G_{xb})F_f \tag{2.5}$$

where

$$F_h = \frac{K_{pa}K_{pb}}{K_{act1}K_{pb} + K_{act2}K_{pa}} \tag{2.6}$$

$$G_{xa} = \frac{1}{M_p s^2 + D_{pa}s + K_{pa}} \quad G_{xb} = \frac{1}{M_p s^2 + D_{pb}s + K_{pb}} \tag{2.7}$$

The PE is also characterized by the creep [Gu 2014]. The creep is a very slow phenomenon and is therefore not considered in this study. The hysteresis is analyzed in scanning mode. Experimental results (see section 2.5.2.2 for more details) have shown that the shape of the hysteresis depends on the input signal frequency. The hysteresis is therefore rate-dependent (i.e. dynamic hysteresis). However, the hysteresis does not modify the resonance frequencies. This is why in equation 2.5 it has been modeled as a static hysteresis $H(U)$ followed by a linear dynamic part of the PE whose static gain is equal to 1 [Rakotondrabe M 2009].

The Prandtl-Ishlinskii (PI) static Hysteresis model is used to describe $H(U)$. Each element of the PI model is a backlash characterized by a bandwidth $bw_i = 2\times r_i$ and a weighting coefficient ω_i as shown in the figure 2.6. The hysteresis has been modeled in the same way as in [Rakotondrabe 2010]. The number of backlash used in the case of the stick-slip actuator and the identification results are presented in section 2.5.2.2.

2.4.2 Modeling of the Slider

Theoretically, the only external excitation that drives the slider is the friction force F_f. It is due to the relative motion $x_1 - x_2$ between the PE and the slider (see the figure 2.5). The dynamic equation of the slider can be governed by the following equation:

$$M_s \frac{d^2x_2}{dt^2} = F_f \tag{2.8}$$

M_s is the mass of the slider.

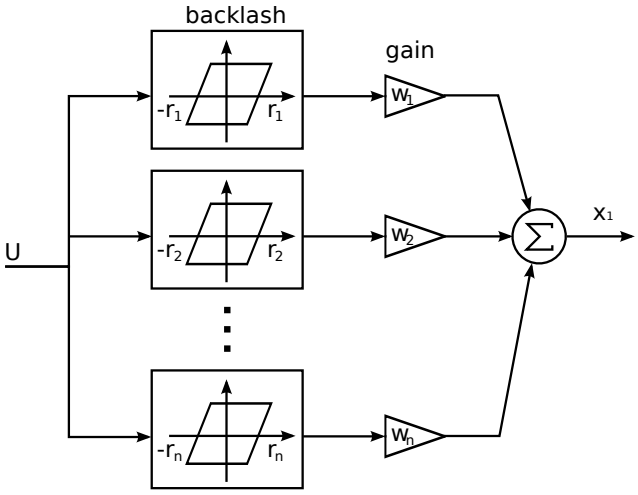

Figure 2.6: Bloc diagram of the Prandtl-Ishlinskii static hysteresis model.

In the sequel, the dynamic equation of the PE and that of the slider will be coupled taking into account the friction force F_f.

2.4.3 Modeling of the Friction

In order to define the dynamic transfer function between the displacement of the slider x_2 and the input voltage U, the friction force F_f must be modeled. The single-state elasto-plastic friction model [Dupont 2002] is used in this work.

The relative motion $x = x_1 - x_2$ between the PE and the slider can be generally decomposed into elastic (reversible) and plastic (irreversible) components, denoted by z and w respectively:

$$x = z + w \tag{2.9}$$

The physical representation is illustrated in the figure 2.7. The black bending bristle stands for the asperity between the slider and the friction material surface. In contrast to multiple random asperities representations in multi-states models, this only one connection stands for the *average* effect and thus gives rise to single state model.

The elasto-plastic friction force F_f is governed by the following equation:

$$F_f = \rho_0 z + \rho_1 \dot{z} + \rho_2 \dot{x} \tag{2.10}$$

ρ_0, ρ_1 and ρ_2 are respectively the contact stiffness, the damping for the tangential compliance and the viscous friction constant. The viscous friction force $\rho_2 \dot{x}$ is considered negligible compared to dry friction. This is the case when the frictional phenomenon is presliding dominant with a small relative velocity $\dot{x}$ [Landolsi 2009].

The elastic component z is governed by:

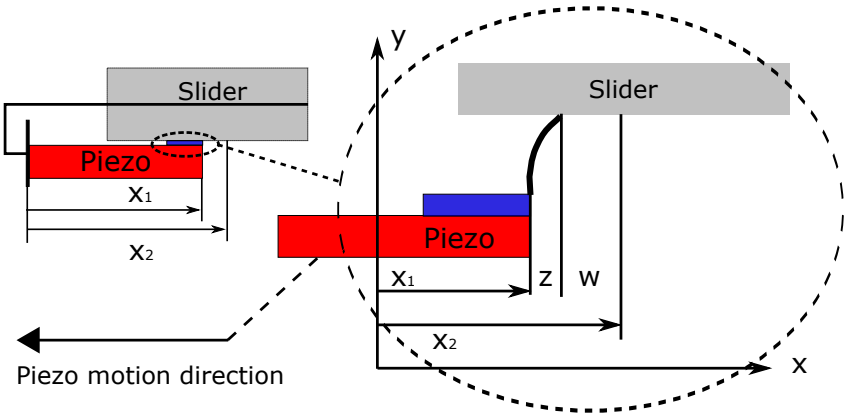

Figure 2.7: Elastic and plastic components of relative motion.

$$\dot{z} = \dot{x}\left[1 - \alpha(z,\dot{x})\frac{z}{z_{ss}}\right] \tag{2.11}$$

z_{ss} is the steady-state elastic strain. This parameter is often considered as a positive constant in the original paper [Dupont 2002] or related applications. As we shall prove later, even without considering Stribeck effect, z_{ss} must change sign with respect to direction change.

The continuous function $\alpha(z,\dot{x})$ is defined by equations (2.13) and (2.12).

$$\alpha\left(.\right) = \frac{1}{2}Sin\left(\pi\frac{|z| - \frac{|z_{ss}|+z_{ba}}{2}}{|z_{ss}| - z_{ba}}\right) + \frac{1}{2} \tag{2.12}$$

$$\alpha\left(z,\dot{x}\right) = \left\{ \begin{array}{ccc} 0 & if & |z| \leqslant z_{ba} \\ 0 < \alpha\left(.\right) < 1 & if & z_{ba} < |z| < |z_{ss}| \\ 1 & if & |z| = |z_{ss}| \end{array} \right\} \begin{array}{ll} if & \mathrm{sgn}\left(\dot{x}\right) = \mathrm{sgn}\left(z\right) \\ & \\ if & \mathrm{sgn}\left(\dot{x}\right) \neq \mathrm{sgn}\left(z\right) \end{array} \tag{2.13}$$
$$0$$

Being different from the original work, z in (2.12) is replaced with its absolute value. This is to guarantee continuity for transition among elastic, mixed and plastic phases when both two motion directions are considered. Here, $z_{ba} > 0$ is the break-away displacement.

The model behaves elastically when $|z| < z_{ba}$. When $|z|$ is between z_{ba} and $|z_{ss}|$, mixed elastic and plastic displacements are produced. Otherwise, $|z|$ is saturated to $|z_{ss}|$, in which case only plastic displacement or sliding occurs.

As briefly mentioned, the parameter z_{ss} is often assigned as a positive constant in the literature. We shall prove in the following that with z_{ss} defined as a constant, the friction model cannot handle different motion directions.

Proof. Consider a general working scenario where x evolves along only one direction from zero initial conditions. Elasto-plastic presliding begins with pure elastic, evolves then to mixed and finally to plastic displacements. In pure elastic regime, $\alpha(z, \dot{x})$ is zero so that $\dot{z} = \dot{x}$. This equality assures that the elastic strain is consistent with the motion direction. Once $|z|$ goes beyond the break-away threshold z_{ba}, mixed displacements occur. If z_{ss} is kept constant, there will be one motion direction so that $\frac{z(t)}{z_{ss}} < 0$, e.g. the motion is driven in the negative direction (backward) while z_{ss} is a positive constant. Given the condition $0 < \alpha(z, \dot{x}) < 1$ from (2.12) in the mixed regime, it leads to (2.14):

$$1 - \alpha(z, \dot{x}) \frac{z(t)}{z_{ss}} > 1, \quad \text{if } \operatorname{sgn}(z(t)) \neq \operatorname{sgn}(z_{ss}) \tag{2.14}$$

Let us denote $C = 1 - \alpha(z, \dot{x}) \frac{z(t)}{z_{ss}}$. By taking the derivative of (2.9) and combining with (2.11), it yields:

$$\dot{z} = \dot{x} - \dot{w} = C\dot{x} \tag{2.15}$$

$$\dot{w} = (1 - C)\dot{x} \tag{2.16}$$

Since $1 - C < 0$, thus:

$$\operatorname{sgn}(\dot{w}) \neq \operatorname{sgn}(\dot{x}) \tag{2.17}$$

According to [Dupont 2002], this inequality occurs only in the case of elastic super relaxation following motion reversal. This is not in accordance with the working scenario where the motion evolves along only one direction. As a result, keeping z_{ss} a constant cannot address the need of modeling backward and forward motions.

□

From the proof above, it can be seen that the issue arises from the sign difference between z and z_{ss}. In our study, a solution is proposed and all z_{ss} mentioned above must be replaced by $z_{ss}(z)$ described as:

$$z_{ss}(z) = z_{ss} \operatorname{sgn}(z) \tag{2.18}$$

In the sequel, z_{ss} only represents a positive constant value. Combined with the condition that $|z|$ is always saturated to $|z_{ss}|$, for any motion direction it yields:

$$0 \leqslant \frac{z}{z_{ss}(z)} \leqslant 1 \tag{2.19}$$

By taking into account the equations (2.11), (2.12) and (2.13), it can be derived that $0 \leqslant dz/dx \leqslant 1$. This conforms to the property the model must preserve as described in the original paper, when super relaxation is precluded and no Stribeck effect is considered.

In the following, it is demonstrated how the condition 2.18 fits into motion of the piezoelectric stick-slip actuator. The scenario is set to backward direction (see the figure 2.8), with a complete period including a stick and slip phase.

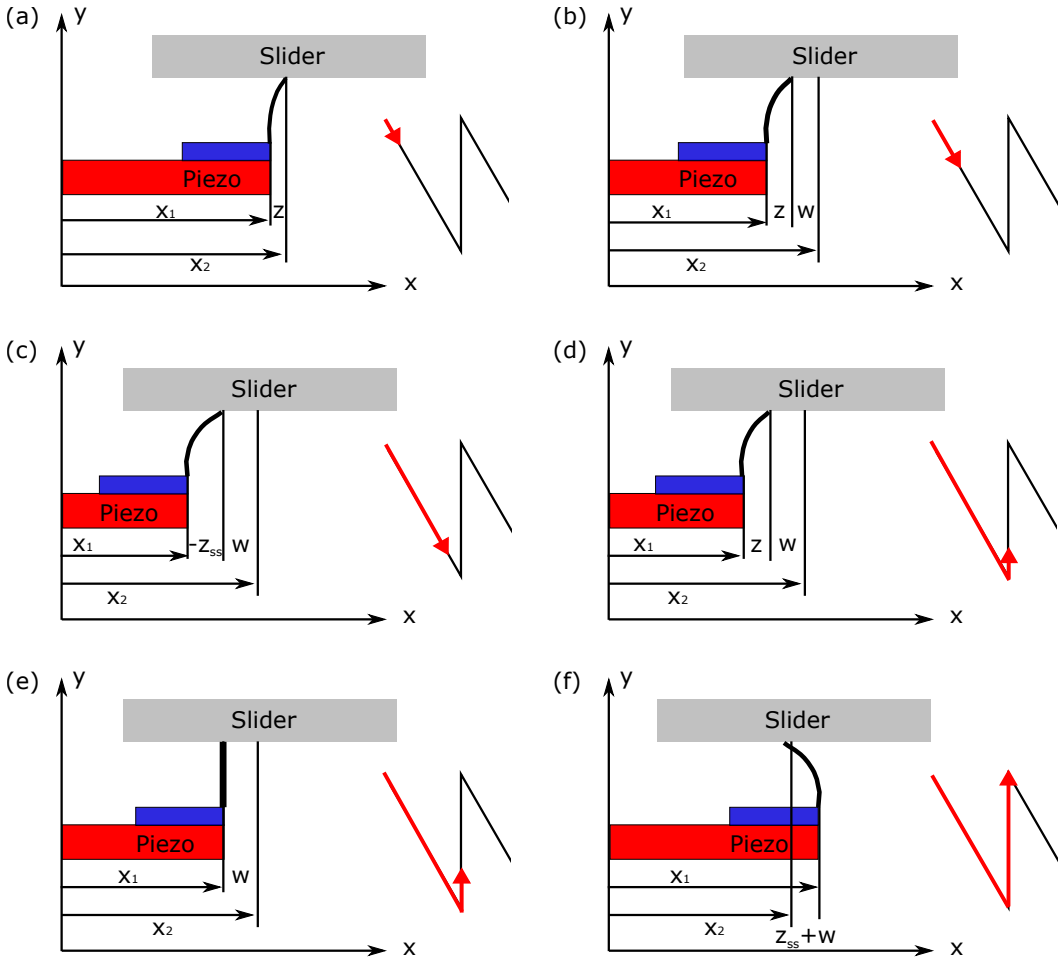

Figure 2.8: Elasto-plastic phases evolution in stick-slip sequence. The corresponding evolution of saw-tooth signal is shown alongside each figure. (a) Elastic phase: start contraction from initial state with $|z| \leqslant z_{ba}$; (b) mixed phase: contraction continues with $z_{ba} < |z| < |z_{ss}(z)|$; (c) plastic phase: contraction continues with $|z|$ saturated to $|z_{ss}(z)|$; (d) motion reversal initiated: z has not fully relaxed to stretch in the opposite direction, thus $\text{sgn}(\dot{x}) \neq \text{sgn}(z)$; (e) z fully relaxed: elongation continues, (a) - (c) will be repeated; (f) PE fully stretched: a net displacement of slider is produced.

- **Elastic phase:** contraction starts from zero initial state (figure 2.8 (a)), with conditions $|z| \leqslant z_{ba}$ and $\alpha(z, \dot{x}) = 0$. The condition (2.18) has no effect on friction model (see table 2.3 for related variables).
- **Mixed phase:** contraction continues (figure 2.8 (b)), with conditions $z_{ba} <$

$x < 0$	$\dot{x} < 0$	$\dot{x} = \dot{z}$
$z < 0$	$\dot{z} < 0$	$\lvert z \rvert \leqslant z_{ba}$
$\omega = 0$	$\dot{\omega} = 0$	$\alpha(z, \dot{x}) = 0$

Table 2.3: Model variables in elastic phase.

$|z| < |z_{ss}(z)|$ and $0 < \alpha(z, \dot{x}) < 1$. Since z is negative and in order to preserve the property $0 \leqslant dz/dx \leqslant 1$, $z_{ss}(z)$ must be negative (see equation (2.11)). This is consistent with the proposed condition (2.18), (see table 2.4 for related variables).

$x < 0$	$\dot{x} < 0$	$\dot{x} = \dot{z} + \dot{\omega}$
$z < 0$	$\dot{z} < 0$	$z_{ba} < \lvert z \rvert < \lvert z_{ss}(z) \rvert$
$\omega < 0$	$\dot{\omega} < 0$	$0 < \alpha(z, \dot{x}) < 1$

Table 2.4: Model variables in mixed phase.

- **Plastic phase:** contraction continues (figure 2.8 (c)), with conditions $z = -z_{ss}$ and $\alpha(z, \dot{x}) = 1$. Since z stops evolving, it must satisfy $z_{ss}(z) = -z_{ss}$ to keep $\dot{z} = 0$. This is consistent with the proposed condition (2.18), (see table 2.5 for related variables).

$x < 0$	$\dot{x} < 0$	$\dot{x} = \dot{\omega}$
$z < 0$	$\dot{z} = 0$	$z = -z_{ss}$
$\omega < 0$	$\dot{\omega} < 0$	$\alpha(z, \dot{x}) = 1$

Table 2.5: Model variables in plastic phase.

- **Motion reversal initiated:** elongation starts (figure 2.8 (d)), with z not fully relaxed. Since $\text{sgn}(\dot{x}) \neq \text{sgn}(z)$ and $\alpha(z, \dot{x}) = 0$, The condition (2.18) has no effect on friction model, (see table 2.6 for related variables).

$x < 0$	$\dot{x} > 0$	$\dot{x} = \dot{z}$
$z < 0$	$\dot{z} > 0$	$\text{sgn}(\dot{x}) \neq \text{sgn}(z)$
$\omega < 0$	$\dot{\omega} = 0$	$\alpha(z, \dot{x}) = 0$

Table 2.6: Model variables in initial motion reversal.

- **Elastic displacement fully relaxed:** back to relaxed contact undergoing elongation (figure 2.8 (e)). z starts to stretch in the opposite direction. Procedures (a) - (c) of the figure 2.8 will be repeated (see table 2.7 for related variables).

- **PE fully stretched:** the friction is in plastic phase (figure 2.8 (f)). Aforementioned steps will be repeated for subsequent motion.

$x < 0$	$\dot{x} > 0$	$\dot{x} = \dot{z}$
$z = 0$	$\dot{z} > 0$	$\lvert z \rvert \leqslant z_{ba}$
$\omega < 0$	$\dot{\omega} = 0$	$\alpha(z, \dot{x}) = 0$

Table 2.7: Model variables in initial motion reversal.

Forward motion can be analyzed in the same logic. From the analysis above, it can be seen that the proposed condition 2.18 preserves the critical property of the single-state elasto-plastic friction model and is consistent with the piezoelectric stick-slip motion. An alternative solution is to relate z_{ss} with relative velocity $\dot{x}$. It can be actually reduced to the proposed condition 2.18. However, in real implementation $\dot{x}$ is obtained by discrete derivation which could cause numerical errors. Therefore condition 2.18 is a more robust choice.

The complete form of single-state elasto-plastic friction force F_f can be expressed by equations (2.9), (2.10), (2.11), (2.12), (2.13) and (2.18).

In the following section of identification, it will be shown that the two dominant dynamic modes of the stick-slip actuator do not come from the dynamics of the PE. But the single-state friction coupled with slider can only give rise to one dynamic mode. In order to deal with this situation, we propose two asperities for describing friction in our study. Concretely that means:

$$F_{fa} = \rho_{0a} z_a + \rho_{1a} \dot{z_a} \tag{2.20}$$

$$F_{fb} = \rho_{0b} z_b + \rho_{1b} \dot{z_b} \tag{2.21}$$

The dynamic models of the PE and the slider, namely equations (2.5) and (2.8) can therefore be coupled taking into account the friction model. In scanning mode, the actuator behaves like a coupled oscillator.

2.5 Experimental analysis and identification

2.5.1 Description of the experimental setup

For the model identification, an experimental platform is set up. It is composed of: (i) the microrobotic system, (ii) the laser interferometer sensor (resolution: 0.1 nm) for position measurement, (iii) a vibration isolation table and (iv) a controller board (dSPACE DS1104) with a Real Time Interface (RTI).

The interferometer sensor and the microrobot are set in two different vibration isolation tables to avoid exciting the laser sensor by the actuator vibrations. The laser of interferometer is aligned to measure the displacement of the Y axis of the Cartesian structure, as shown in Fig. 2.9. In our study, measurements are performed with sampling frequency as 25 kHz and 1 mHz. Megahertz sampling frequency is applied when dominant dynamic modes lie in high frequency band (such

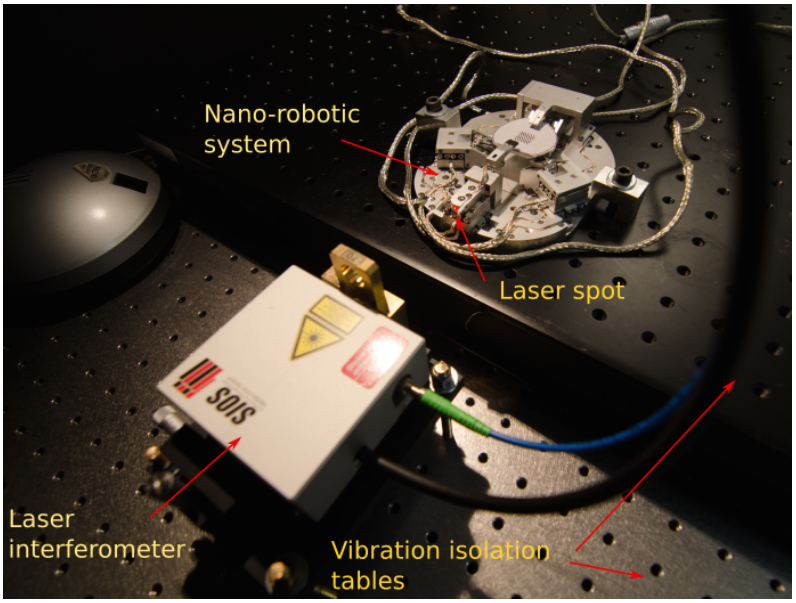

Figure 2.9: Experimental setup for model identification. The interferometer laser is aligned to perform measurements of the position of the Y axis.

as the identification for the PE without slider) while kilohertz is applied when dominant dynamic modes are in low frequency band (such as the identification for the whole actuator). The microrobotic system is interfaced to a host computer via the controller board. The RTI allows applying different kind of input voltages to the stick-slip actuators.

2.5.2 Parameters identification

The input voltage amplitude determines in which mode the stick-slip actuator works: scanning mode or stepping mode. Below a threshold of the input voltage amplitude, there is no stepping phenomenon between the PE and the slider, no matter what is the input voltage frequency. In this case, a step signal with controlled amplitude can be supplied to the actuator in order to characterize the dynamic parameters of the PE and the slider. Beyond the voltage amplitude threshold, slip occurs and a large stroke can be produced. The experiments have shown that this amplitude threshold is around 40 V.

The identification of the parameters has been performed in three steps:

2.5.2.1 Step1 - identification of the dynamic parameters in scanning mode

In order to study the dynamics of the PE, the slider is carefully removed and we managed to align the interferometer with respect to the deformation axis of the PE. A 90 V step voltage is applied to the PE. The measurements from laser sensor are

performed with 1 mHz sampling frequency, see the figure 2.10. It can be observed that the PE has two dominant dynamic modes at 64 kHz and 118 kHz. This process allows decoupling the system and identifies the parameters for the PE only. The identification result is shown in the table 2.8.

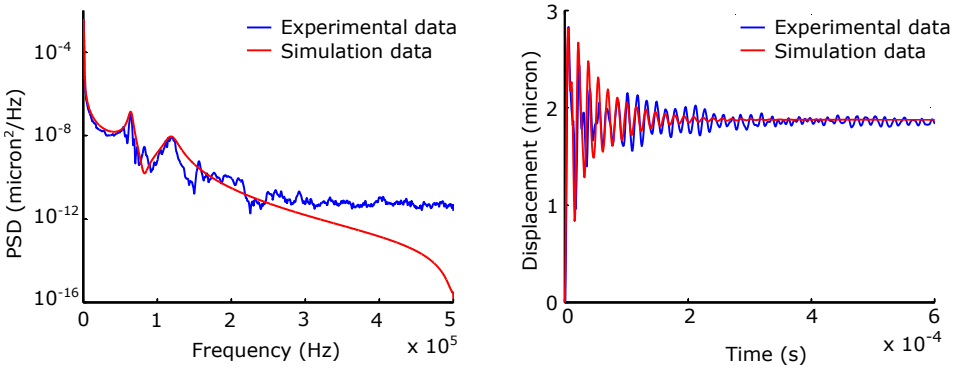

Figure 2.10: Step response of the PE (stick-slip actuator without slider) using a 90 V step excitation. Left: PSD of step response; right: simulation and experimental results in time domain.

A similar identification process is applied to the stick-slip actuator (with slider), the Y axis of the robot. A 40 V step voltage is applied and the measurements are performed with 25 kHz sampling frequency. The measured displacement in time domain and its Power Spectral Density (PSD) are shown in the figure 2.11. The PSD shows two resonant frequencies at 595 Hz and 1633 Hz. They, however, do not result from the dynamics of the PE (as shown from the identification results of the PE). This situation can be handled if the friction model possesses two asperities (ρ_{0a}, ρ_{1a}) and (ρ_{0b}, ρ_{1b}), with each gives rise to one dynamic mode. The identification result is shown in the table 2.8.

2.5.2.2 Step2 - identification of the hysteresis in scanning mode

The PI hysteresis model has been identified as follows: (i) A sine input voltage is applied to the actuator. The amplitude and the frequency of the sine signal are 40 V and 50 Hz respectively. The position of the slider in response to the sine voltage is measured experimentally. (ii) The experimental hysteresis curve is shifted in the positive section of the $[U, x_2]$ plane. (iii) $n = 35$ elementary backlashes are defined. (iv) The input U is split into $n+1$ non uniform partitions. The bandwidth $bw_i = 2 \times r_i$ of each elementary backlash is therefore defined. (v) The weighting coefficient ω_i (see Fig. 2.6) of each backlash is then identified.

See [Rakotondrabe 2010] for more details about the PI identification method.

Taking into account the dynamic model of the stick-slip actuator and the PI hysteresis model, the hysteresis curve of the system x_2/U has been simulated. Results have been compared with experimental measurements as shown in Fig. 2.12.

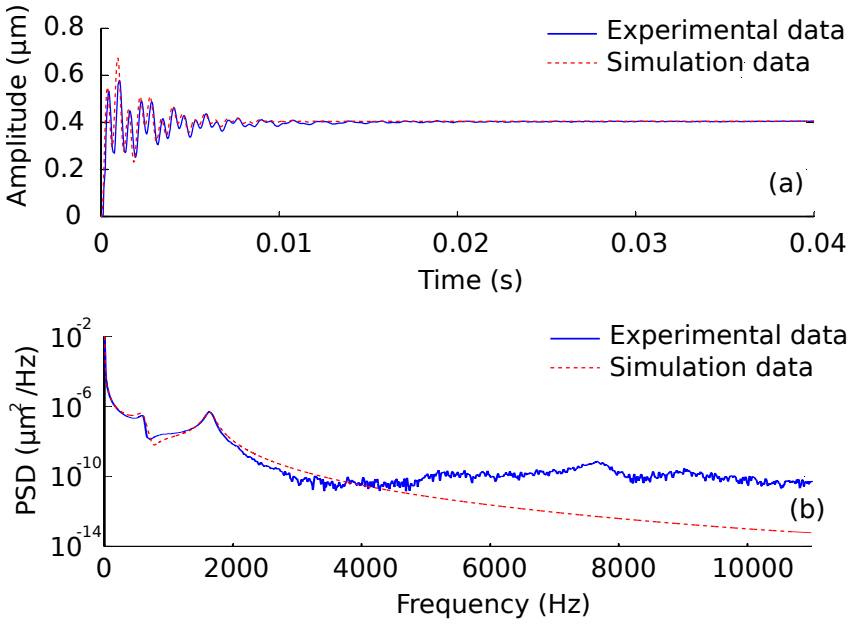

Figure 2.11: Step response of the stick-slip actuator using a 40 V step excitation. Up: simulation and experimental results in time domain; down: PSD of step response.

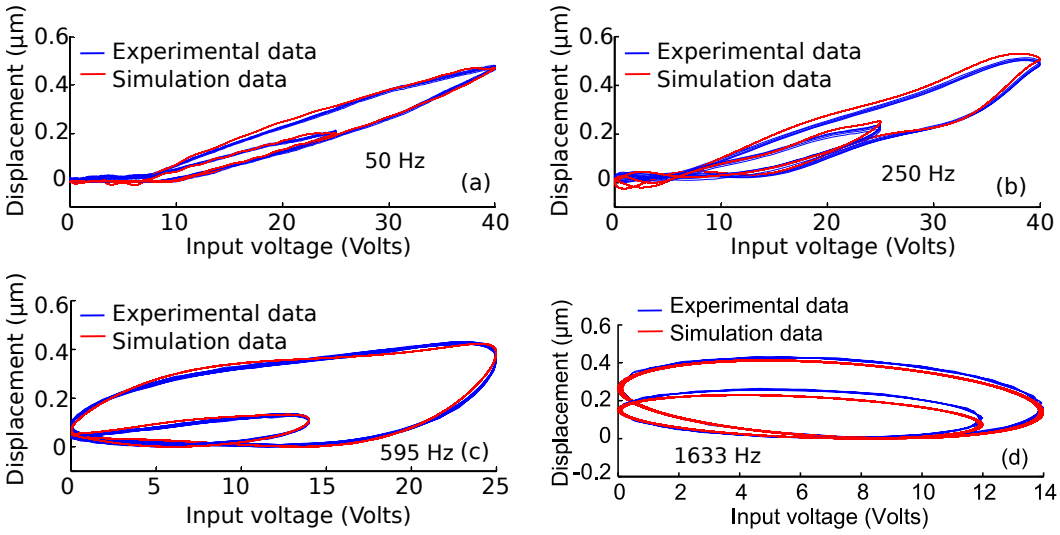

Figure 2.12: Experimental and simulation results of the identified PI model. The frequency and the amplitude of the input sine signal are: (a) 50 Hz, 40 V (OutL), 25 V (InL), (b) 250 Hz, 40 V (OutL), 25 V (InL), (c) 595 Hz, 25 V (OutL), 14 V (InL) and (d)1633 Hz, 14 V (OutL), 12 V (InL). InL: inner loop, OutL: outer loop.

Parameter [unit]	Identified Values
ρ_{0a} $[N/m]$	3.517×10^5
ρ_{0b} $[N/m]$	2.62×10^6
ρ_{1a} $[Ns/m]$	64.9651
ρ_{1b} $[Ns/m]$	15.6125
$z_{ba}/\lvert z_{ss}(z)\rvert$	0.667
M_p $[Kg]$	0.00075
M_s $[Kg]$	0.0247
D_{pa} $[Ns/\mu m]$	25.86
D_{pb} $[Ns/\mu m]$	82.17
K_{pa} $[N/\mu m]$	1.23×10^8
K_{pb} $[N/\mu m]$	4.24×10^8

Table 2.8: Identified parameters of the dynamic modeling.

2.5.2.3 Step3 - identification of the break-away elastic strain and the steady-state elastic strain in stepping mode

The stick-slip actuator is driven by sawtooth signals. The velocity $\dot{x_2}$ (slope of the displacement) can be measured given a sequence of sawtooth with varying frequencies and amplitudes in both drive directions. This measurement is used to identify the break-away elastic strain z_{ba} and the steady-state elastic strain $|z_{ss}(z)|$ so that the velocity matches between the model and experimental data.

In the original work, the mixed phase of friction model with sinus implementation is proposed to ensure continuous transition. The physical motivation about the ratio between z_{ba} and $|z_{ss}(z)|$ still needs further investigation. It is suggested by the authors that the mixed phase should be relatively narrow with respect to the elastic phase. In our study, the ratio has been kept constant as $z_{ba}/|z_{ss}(z)| = 0.667$. Under this condition, it will be shown in the following part how the break-away elastic strain z_{ba} evolves with respect to various input conditions (amplitude and frequency of the sawtooth signal).

The figure 2.13 illustrates the evolution of the identified z_{ba} versus the amplitude of an input sawtooth signal of 50 Hz frequency. In the figure, $z_{ba}(-)$ and $z_{ba}(+)$ denote respectively the identified value for backward and forward motion directions of the slider (see Fig. 2.3) . The fitted curves are shown for both backward and forward motion directions.

The fitting result gives rise to a dynamic model for stepping mode with limited input conditions (fixed frequency as shown in the example). At the time of writing, we are still working on the identification process to derive a complete fitting, i.e. a

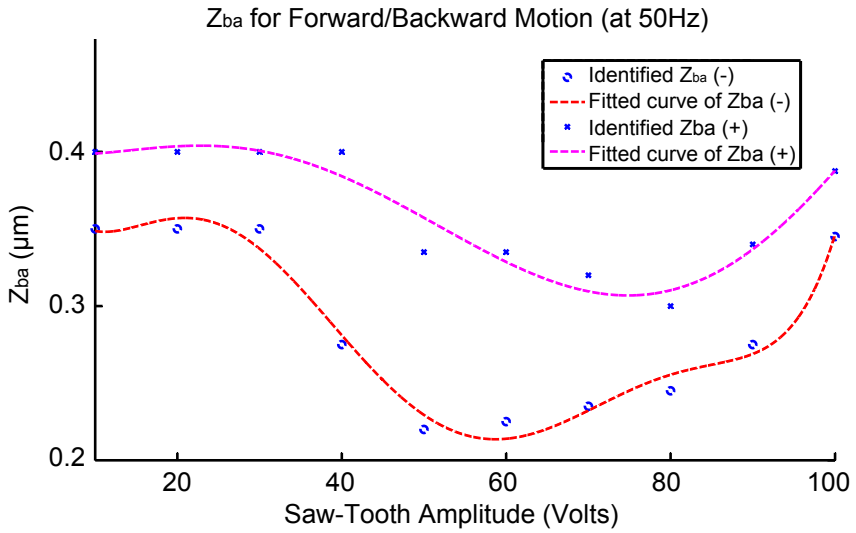

Figure 2.13: Characteristic of the break-away elastic strain versus input saw-tooth amplitude. The value of z_{ba} is identified for input conditions: 10, 20, 30, 40, 50, 60, 70, 80, 90 and 100 V, where the sawtooth frequency is fixed at 50 Hz.

fitting surface of z_{ba} with respect to all combination of frequency and amplitude.

2.5.3 Model Validation

The model describing the dynamic transfer x_2/U is validated with experiments for both scanning mode and stepping mode. For each mode, the input voltage is a sawtooth signal. Three input frequencies are used for the validation: 50, 100 and 500 Hz.

In scanning mode, the input sawtooth amplitude is equal to 20 V. Results of Fig. 2.14 show that the output x_2 of the dynamic model returns back at its initial position after the abrupt drop of the voltage. In other words, there is no accumulated stepping. For different frequencies of the input sawtooth voltage, the model works in scanning mode. This is in agreement with experimental data.

In stepping mode, the model is validated for both forward and backward motions of the slider (Fig. 2.3). For each case, two input sawtooth voltages of 40 and 60 V in amplitude are used. The aim is to study the effect of the amplitude voltage on the velocity of the slider and to show the agreement between experimental data and simulations. The model is validated in the time domain and in the frequency domain.

Results of the figure 2.15 show that for an input voltage of 40 V, the actuator behaves in a stick and slip operating mode (stepping mode). The velocity of the slider motion increases with increasing the amplitude of the input voltage. This can be observed by comparing Fig. 2.15 (a) with Fig. 2.16 (a), Fig. 2.15 (b) with Fig. 2.16 (b) and Fig. 2.15 (c) with Fig. 2.16 (c). Moreover, experiments show that the velocity of the slider (slope of the position curve) is different in forward

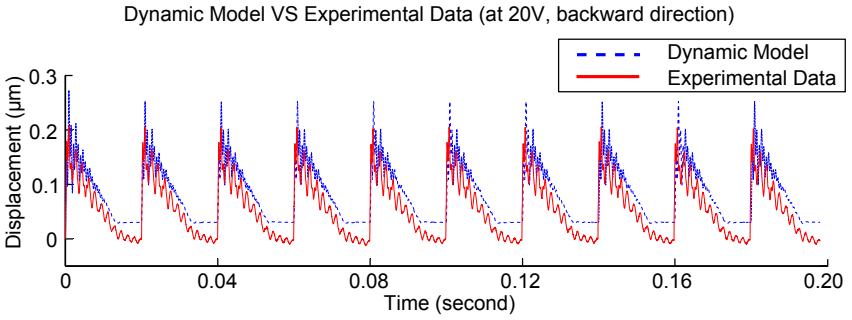

(a) $20V$ 50Hz

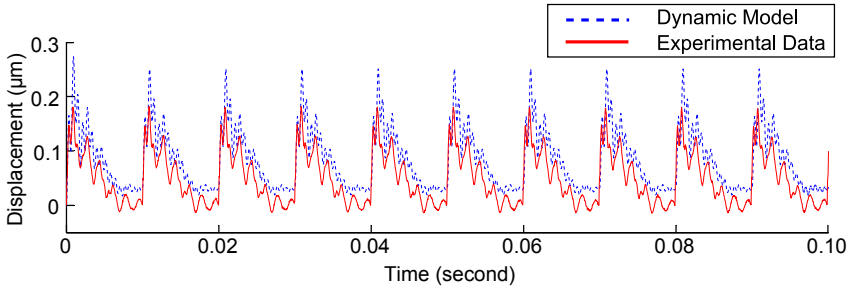

(b) $20V$ 100Hz

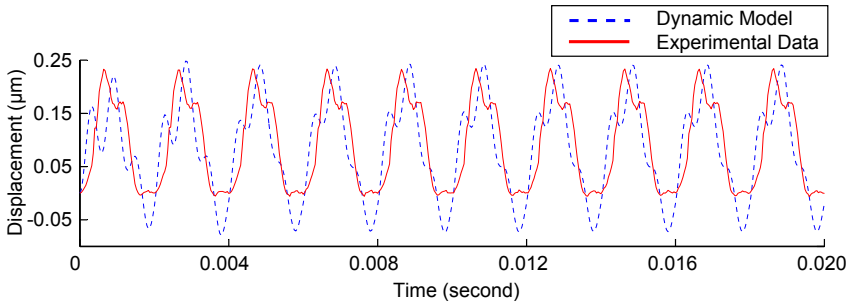

(c) $20V$ 500Hz

Figure 2.14: Comparison in the time domain between experimental and simulation data for different input sawtooth condition (a) [$20V$ 50Hz], (b) [$20V$ 100Hz] and (c) [$20V$ 500Hz].

and backward operating modes. The model describes accurately this “asymmetric" behavior.

In order to validate the dynamic model in the frequency domain for both scanning mode and stepping mode, the PSD of the model output is computed for two different input sawtooth signals. The first one with an amplitude of 20 V and a frequency of 500 Hz and the second one with an amplitude of 40 V and a frequency of 50 Hz. From the figure 2.17, it can be seen that the dynamic model provides a comparable match to experimental results in frequency domain.

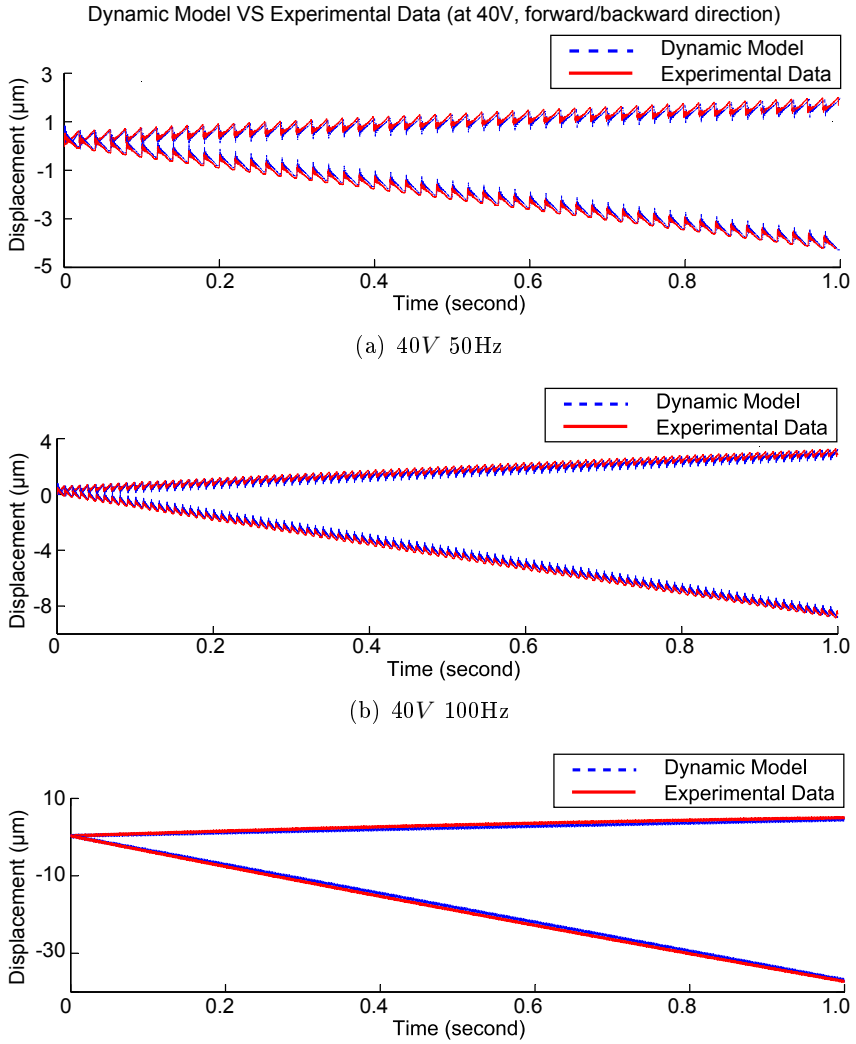

(a) $40V$ 50Hz

(b) $40V$ 100Hz

(c) $40V$ 500Hz

Figure 2.15: Comparison in the time domain between experimental and simulation data for different input sawtooth condition (a) [$40V$ 50Hz], (b) [$40V$ 100Hz] and (c) [$40V$ 500Hz].

2.6 Discussion

In the dynamic modeling, the Stribeck effect [De Wit 1995] is not considered since no lubricant film is assumed to exist between friction surfaces. In the literature, the steady-state elastic strain is often kept as a positive constant. In this paper, it has been shown that such an assumption cannot fulfill the condition to simulate the motion of the slider subject to direction change. The steady-state elastic strain must vary to accommodate the specific drive direction. The experiments have shown the asymmetric behavior of the slider in backward and forward directions. This observation highlights the need of performing a model identification for both drive

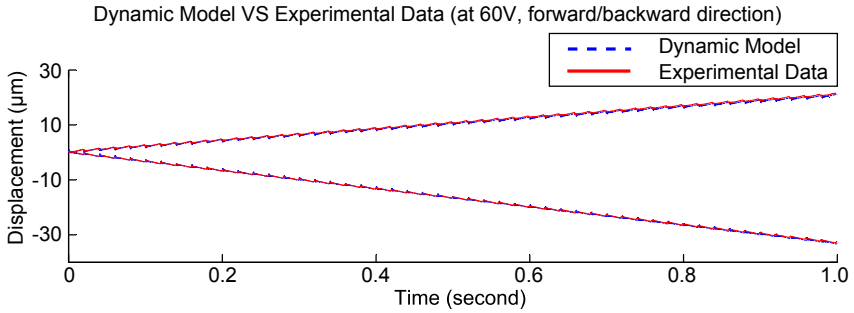

(a) $60V$ 50Hz

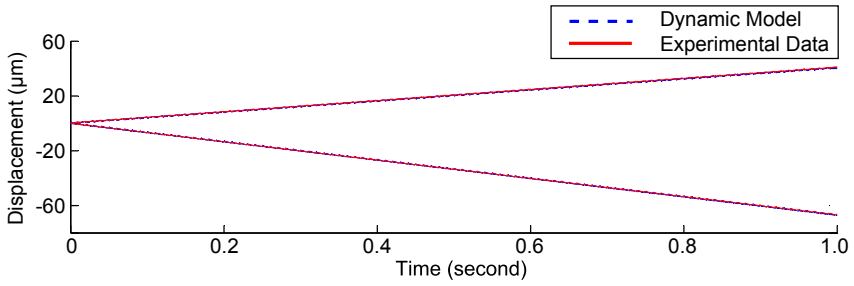

(b) $60V$ 100Hz

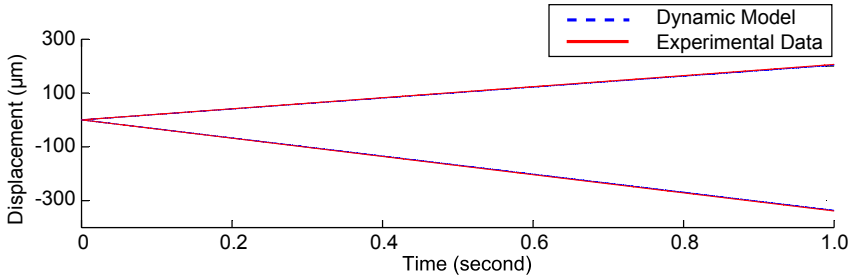

(c) $60V$ 500Hz

Figure 2.16: Comparison in the time domain between experimental and simulation data for different input sawtooth condition (a) [$60V$ 50Hz], (b) [$60V$ 100Hz] and (c) [$60V$ 500Hz].

directions.

Our study applied step response for dynamic identification. In a step sequence, the actuator will firstly experience abrupt elongation/contraction, then vibrate until decayed to final state. The identification is based on the assumption that the vibration after applying step signal does not give rise to sliding between slider and friction material. If the abrupt voltage would cause sliding, static gain of the model will be affected. But this will be compensated by hysteresis identification.

The break-away elastic strain z_{ba} must be identified for different amplitudes and frequencies of the input sawtooth signal. This is due to the fact that the friction force varies with respect to operating conditions, and ρ_0, ρ_1 must be kept constant to comply with dynamic response in frequency domain. The evolution of z_{ba} versus

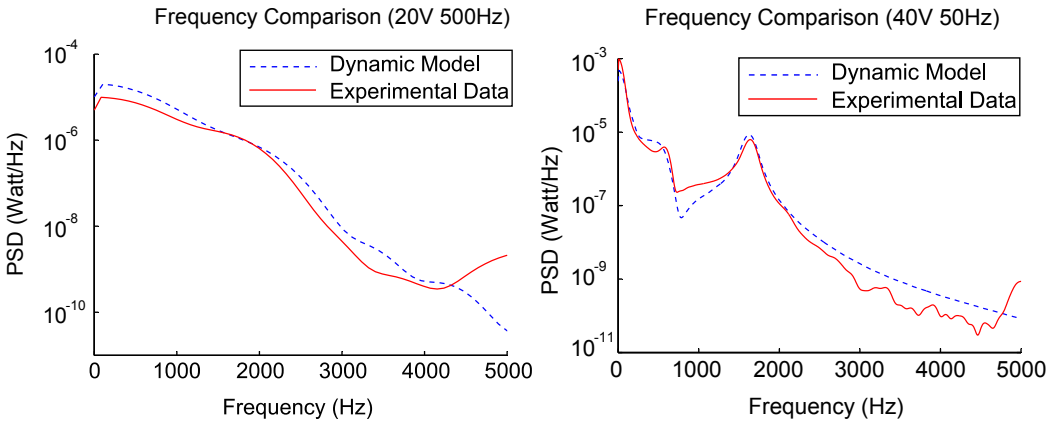

(a) $20V$ 500Hz (b) $40V$ 50Hz

Figure 2.17: Comparison in the frequency domain between experimental and simulation data for different input sawtooth condition (a) [$20V$ 500Hz] and (b) [$40V$ 50Hz].

the amplitude of the input signal has been identified through experiments (figure 2.13) for a fixed frequency. In order to control in closed loop the position of the slider in stepping mode, the PE can be actuated by a sawtooth signal with controlled amplitude and frequency. New control strategies can be developed in the future if the identification of z_{ba} is performed in the workspace including the frequency and the voltage amplitude of the driving signal and the motion direction. This will lead to the extension of the result of the figure 2.13 into a surface fitting.

2.7 Velocity Control

As an important subset of trajectory tracking problems, velocity control is indispensable for micro-manipulation cobotic platform to realize tasks such as fast switch between distant-workspaces, smooth transportation of fragile micro-objects, or other microrobotic applications where desired velocity must be achieved. From the dynamic analysis and model validation of the study, it can be seen that with different input conditions, response in time domain varies greatly. The difference will directly impact the quality of velocity (amplitude, vibration, etc.) For example, to obtain smooth velocity for large motion distance, one can tend to employ stepping mode with increased sawtooth frequency to have a reduced level of vibration. This actually requires the knowledge of frequency domain analysis of the model. If application requires to realize desired velocity within distance that is smaller than a step, control in scanning mode is an obvious choice. In this case, the actuator is reduced to a classical continuous coupled system. If the knowledge of inverse dynamics is known, one can apply strategies such as inverse dynamics or computed torques control in order to obtain desired velocity. If the motion distance in which velocity control is required falls in-between, an intelligent control strategy must be derived

to make on-line switch between hybrid states: stepping mode and scanning mode. This particularly requires the knowledge of friction. In our study, it is shown how the break-away elastic strain z_{ba} evolves with respect to various input conditions, which lead to different output velocity. To sum up, the development of velocity control strategy for piezoelectric stick-slip actuator must be based on the knowledge of its dynamic model. It also explains that the lack of knowledge of dynamics results the current situation that no commercial products or research results are yet able to propose velocity control strategies for piezoelectric stick-slip actuator.

At the time of writing, the development of complete dynamic model is still on the way, i.e. the surface fitting of the break-away elastic strain as a function of sawtooth amplitude and frequency (for both forward and backward motion) still needs effort. With current partial model, we are able to derive a velocity control simulation in case of large motion distance by applying PID control to sawtooth amplitude.

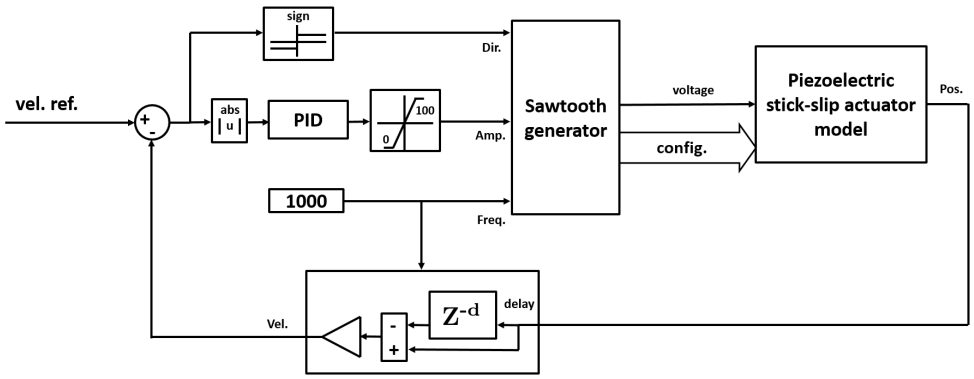

Figure 2.18: Velocity control scheme.

The control scheme is illustrated in the figure 2.18. The input sawtooth frequency is fixed to 1 kHz. In the actuator dynamic model, a fitting function of z_{ba} for 1 kHz is implemented for both forward and backward motion. For this purpose, sawtooth generator passes its current configuration to the dynamic model. Velocity estimation is obtained from the subtraction of position signals. However, if used position signals are adjacent sampled points, the position oscillation within one step will result unstable control result. To deal with this issue, it is proposed to take points separated by several integer times of sawtooth period. Concretely, the delay operator holds state for several integer times of 0.001 second.

The figure 2.19 shows the result of velocity control for both forward and backward motion. The reference speed is set to 100 micron/s.

In this section, a preliminary velocity control strategy for large motion distance is demonstrated. It is based on the current partial dynamic model of piezoelectric stick-slip actuator. In the next step, with the knowledge of a complete dynamic model, we aim to develop a velocity control scheme for more general and complete

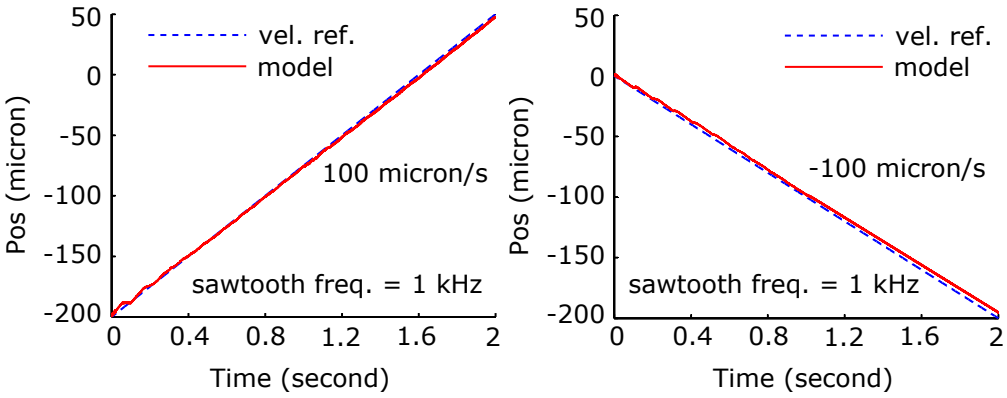

Figure 2.19: Velocity control simulation with partial dynamic model. The sawtooth frequency is set to 1 kHz. The speed reference is set to 100 micron/s for both forward and backward motion.

cases.

2.8 Conclusions

Piezoelectric stick-slip is one of the most promising actuation principles for microrobotic systems. It allows positioning the microrobotic axis in the millimeter range with a submicron resolution. This chapter has dealt with dynamic modeling challenges for this kind of actuator. The result shows that the model is able to describe the behavior for both scanning mode and stepping mode in the time and the frequency domains, and for backward and forward motion. The dynamic model is based on a multi-state elasto-plastic friction model. Identification shows how the break-away elastic strain varies with respect to different input conditions. Results of ongoing research show that the break-away displacement mainly depends on the voltage amplitude and less on the voltage frequency. The proposed modeling approach has been validated with a series of experiments. In our best knowledge, the validation of stick-slip actuator model in such operating conditions has never been demonstrated in the literature.

At the end of the chapter, a velocity control strategy for large motion distance is demonstrated by using partial dynamic model. In the next step, we aim to develop trajectory tracking strategies for more general microrobotic applications. In the future, the complete set of modeling and control algorithms is expected to be implemented in Chronogrip to realize various microrobotic applications.

Chapter 3

Extending the Bandwidth of Dual Stage Haptic Interface by Signal Crossover

Contents

The microworld can be characterized by high dynamics, but existing cantilever based haptic interfaces are not capable of rendering high frequency bandwidth. This chapter presents an approach to extending the frequency bandwidth of haptic interfaces so that interface can have a uniform response over the entire human tactile frequency range. Structural mechanics makes it very difficult to implement articulated mechanical systems that can transmit high frequency signals. Here, we separated the desired frequency range into two bands, where the lower one can be covered within the first structural mode of one mechanism and the higher one can be transmitted accurately by a fast actuator operating from conservation of momentum, that is, without reaction forces to the ground. To couple the two systems, we adopted a channel separation approach akin to that employed in the design of acoustic reproduction systems. The two channels are recombined at the tip of the device to give a uniform frequency response from DC to one kilohertz. In terms of mechanical design, the high-frequency transducer was embedded inside

the tip of the main stage so that during operation, the human operator has only to interact with a single finger interface. In order to exemplify the type of application that would benefit from this kind of interface, we applied it to the haptic exploration with microscopic scales objects which are known to behave with very fast dynamics. Specifically, the novel haptic interface was employed in an optical tweezers scenario to demonstrate its capabilities. Operators could feel interaction forces arising from contact as well as resulting from Brownian motion.

3.1 Introduction

In order to realize intuitive and effective teleoperation for microrobotic applications, a cobotic platform must be equipped with a high-bandwidth haptic interface. The current Chronogrip user interfaces (joystick, tablet) do not yet integrate haptics functionality. Actually a more fundamental problem is that all existing cantilever-based haptic interfaces have limited bandwidth, which is far from the bandwidth of the physical activities in the microworld [Romano 2012] [Sitti 2004] [Finio 2011]. By using existing haptic interfaces, the spectrum of the communication like force fed back to the user is significantly truncated from that taking place in the microworld. As a typical consequence, high frequency vibration is filtered out.

In fact, vibration transmission is a classical problem in mechanics. Any mechanical architectures and materials have their limits of transmission due to their intrinsic physical properties. The transmission of vibration implies the competition between elastic recovery and inertia in the material or the structure. The spectral response can be characterized by their mechanical modes directly deduced from the elastic and inertial parameters of the system. The mechanical modes implies resonances phenomena which are undesirable for accurate transmission. The range of vibration transmission are then limited by the intrinsic frequency response of the materials and structures. Researchers and engineers restrict functional range of transmission from static to a safety zone before the fundamental mode. In practice, typical haptic interfaces might be limited in bandwidth using appropriate low-pass filters [Campion 2005a]. To fix ideas, the popular interface Sensable PHANTOM 1.0A device has a useful mechanical bandwidth of only 30 Hz. In the section 3.2, more recent haptic interfaces are surveyed and analyzed.

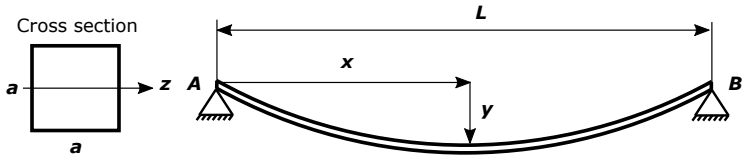

Figure 3.1: The cantilever beam has uniform distributed mass and square cross section. Both ends are fixed. At the position x, the deflection is denoted as y.

In a simple experiment of a fixed beam, it is straight-forward to analytically evaluate the ultimate physical limits of mechanical transmission. The figure 3.1 illustrates the typical scenario. The beam has uniform distributed mass and square cross section. Each end is fixed to ground. At the position x, the deflection of the beam is denoted as y. The general equation for the transverse vibration is:

$$\frac{\partial^4 y}{\partial x^4} + \left(\frac{\rho A}{E I_z}\right)\frac{\partial^2 y}{\partial t^2} = 0 \tag{3.1}$$

where ρ is the mass density, A as the cross sectional area, E as the Young's modulus, and I_z as the area moment of inertia with respect to axis z. By using

points A and B as boundary conditions, the general equation 3.1 can be solved with all the natural angular frequencies expressed as:

$$\omega = \left(\frac{n\pi}{L}\right)^2 \sqrt{\frac{EI_z}{\rho A}} \qquad n = 1, 2, ... \tag{3.2}$$

Using the ideal material, with the highest ratio elasticity/inertia, for example carbon fiber composite, the fundamental mode is just around 611 Hz for a 20 cm-long beam with $5 \times 5\ mm^2$ square cross section. The table 3.1 surveys several widely applied materials' properties and lists their first natural frequency for the same beam model defined above. Parallel structures such as a pantograph helps to rigidify the transmission with less expansive materials and low increase of inertia. However, measurements show that it is comparatively difficult to have bandwidth higher than 300Hz [Campion 2005b] for a few centimeter deported handle. This means that it is impossible to transmit faithfully a vibrations over 300 Hz on a distance of 15 cm through materials, architectures or passive transmissions.

Material type	Young's modulus (GPa)	Density (Mg/m^3)	1st natural frequency (Hz)
Cast Irons	170	7.15	276
Stainless steel	200	7.85	286
Aluminum alloy (7075-T6)	70	2.7	288
Carbon fiber	200	1.72	611

Table 3.1: Lowest natural frequencies of a beam for various materials. The geometry of the beam model is 20 cm-long with $5 \times 5\ mm^2$ square cross section. Assume all mechanical properties are evenly distributed. The Young's modulus and density data in this table are referred from Materials Data Book [Cambridge 2003].

To overcome this problem, in this chapter, an bandwidth-extending method for a dual-stage architecture is proposed. Since cantilever structure precludes high frequency information, high frequency vibrations are not transmitted through an architecture with several degrees of freedom, but directly through a small vibration transducer in the end effector, see the figure 3.2. Using a rigorous coupling of mechanical interaction by crossover techniques, this chapter addresses the problem of mechanical bandwidth of haptic devices that need at least to reproduce stimuli from 0 to 1 kHz in order to fulfill human proprioceptive capacities [Gescheider 1988].

One revolutionary research field in microrobotics which demands 1 kHz haptic bandwidth is optical tweezers [Ni 2013a]. This technique requires no direct contact with manipulated object and is therefore favored in physics, cell engineering and other fields that need micro-manipulation and micro-scale force measurement [Neuman 2004] [Ni 2013b]. The working mechanism is that under a tightly focused

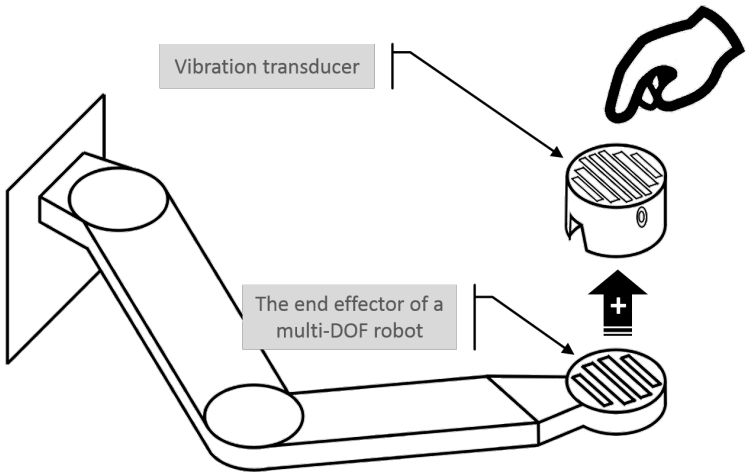

Figure 3.2: Dual-stage mechanical architecture: a multi-DOF cantilever kind of robot with a stand-alone vibration transducer installed on the top of its end effector.

laser beam, a micron-sized object, typically a bead, can be trapped by the force generated from laser's electromagnetic field. The trapped object can then be served as a controlled probe so as to interact with target objects. In order to compute contact force, a linear spring model is often applied to describe the microscopic force exerted by the laser. A schematic diagram of optical tweezers is shown in the figure 3.3. Due to scale effect, the surface forces (van der Waals, electrostatic forces) or thermal agitation can drive micro-objects to high dynamic motions. Brownian motion is a typical consequence in such case. In this context, using cantilever-based haptic interface in the cobotic platform cannot render high dynamic interaction force. The mechanics of cantilevered structures preclude any device in this category to achieve a bandwidth large enough to transmit the signals arising from the micro-scale. That is the reason why a high bandwidth haptic interface is urgently required to address the need from optical tweezers application.

In this chapter, we will firstly survey several most recent and popular haptic interfaces and then describe the signal crossover method and the dual-stage interface setup. Afterwards, the study is extended to dynamic modeling, identification and compensation for control aspect. At the end, the bandwidth of the dual-stage haptic interface will be evaluated and the interface will be applied in optical tweezers application in order to demonstrate the versatility and efficiency of the proposed method.

3.2 State of the art

The literature on the design of haptic devices is abundant [Hayward 2004]. Several actuators and mechanical transmission have been proposed to achieved large

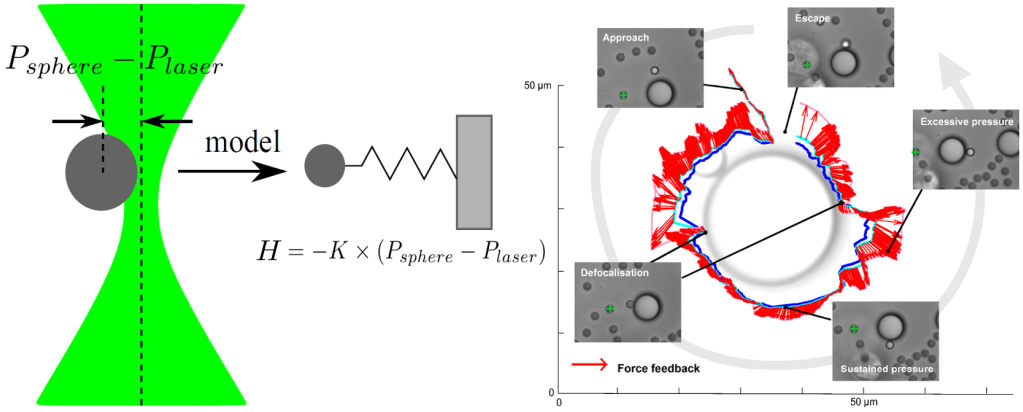

Figure 3.3: In an optical tweezers application, micron-sized bead can be trapped by tightly focused laser, which is displayed as the green part in the figure. The bead can then be controlled as a probe to interact with target objects. For haptic rendering purpose, a spring model is often used to describe the position-force relationship of the trapped bead [Ni 2013b]. The force H represents the general interaction force which covers rich frequency information. Right part of the figure shows the distribution of interaction force H (red flash) when a probe is circling around a big sphere.

number of degrees of freedom (DOF), high magnitudes of forces or good display quality of textures. However, there is a trade-off between all performances and the mechanical frequency bandwidth. Researchers discuss this bandwidth parameter as the efficiency of the whole system is impacted [Hayward 2007].

There is little information about the actual bandwidth of commercial devices [Laycock 2003] and researcher measure it themselves [McJunkin 2005, Berkelman 1997, Stocco 1996] (see Table 3.2). Other laboratories propose their own designs to obtain high bandwidth haptic interface [Berkelman 1997, Florens 2004], but their workspace is limited and the displacement range is inferior to 5 cm.

Several papers propose to augment commercial devices with vibrotactile display [Wall 2001]. So far we know, design and test have been performed only on the vibrotactile part [Wall 2001] and never on the full dual-stage. A 1 DOF dual-stage device has been proposed with a small and high dynamic motor coupled with a large and high torque motor by a passive viscous transmission in order to improve the 1 DOF interface [Mohand-Ousaid 2012]. But the problem reappears if one tries to extend it to dual-stage architecture, the lever arms induce irreducible inertia and lost of bandwidth [Mohand-Ousaid 2014b].

3.3 System description

To apply the method described in this chapter, the dual-stage interface must consist of two haptic interfaces with one responding to low frequency band and the other

Model	Developer	Reference	DOF	Resolution	Workspace	Max Force /Torque	Mech. bandwidth	Identification Sensors
Pantograph	McGill University	[Campion 2005b]	2	10 μm	100 × 160 mm		200 - 300 Hz	Accelerometer
Freedom 6S	MPB Technologies	[J.-G. S. Demers 1998]	6	2 μm - 0.02 mrad	170 × 220 × 330 mm	2.5 N /370 mN.m		
Phantom Desktop	Sensable		3	23 μm	160 × 120 × 120 mm	7.9 N		
Omega.3	Force Dimension		3	10 μm	160 × 160 × 110 mm	12 N		
Delta.3			3	20 μm	200 × 200 × 260 mm	20 N		
Falcon	Novint	[Martin 2009]	3		100 × 100 × 100 mm	8 N	5 Hz	
Two finger grasp	Technical University of Madrid	[López 2012]	6		100 × 160 mm	3 N	8 Hz	Encoders
Maglev	Butterfly Haptics, LLC	[Berkelman 1997]	6	2 μm	⌀ 24 mm	40 N	75 Hz	
ERGOS	Ergos Technologies	[Florens 2004]	3	1 μm	50×50×20 mm	60 N	20 kHz	

Table 3.2: Comparison of desktop haptic devices performances.

to high frequency band. For the high frequency part, the candidate device cannot be based on cantilever structure (as analyzed in the introduction) and must be small enough to be embedded in the other device's handle. Based on this reason, a vibration transducer such as a voice coil actuator is a natural choice. For the low frequency part, the candidate device must have frequency bandwidth high enough to overlap with that of the high frequency component (explained in the crossover method). Furthermore, large bandwidth allows us to have more flexibility to apply crossover technique. The next important criteria must be associated with desired application. In optical tweezers application, the motion and haptics are mostly studied in plane with translation motion, those along the direction of depth or orientation have limited range and dynamics [Ni 2013b]. This condition indicates the application can be realized with a 2D haptic interface. Combined with the requirement of bandwidth, the Pantograph [Campion 2005b] is the best choice for the low frequency component of the dual stage method. Each component of the dual stage interface will be described in the following.

3.3.1 Material description

The first stage the Pantograph haptic interface [Hayward 1994, Campion 2005b] is a planar parallel mechanism of two actuated DOF. It provides a stiff and light set of linkages as shown in the figure 3.4 (a). It has desirable features such as light inertia, high stiffness, compact design and large operating workspace. It is one of the most efficient 2D haptic devices to our knowledge. Our prototype's haptic bandwidth is up to about 200 Hz (see the figure 3.10), but is still not sufficient to cover the full human perception range and our objective up to 1 kHz mechanical bandwidth. This first stage will be responsible in our crossover method of the low frequency haptic sensations.

The second stage is a vibration transducer called Haptuator [Yao 2010] (see the figure 3.4 (b)) developed by TactileLabs. This device is a voice-coil type linear actuator with a moving magnet. The cylinder magnet is designed to move axially as a result of the Laplace force relative to the enclosure. The Haptuator is designed to work at high frequency, it cannot render static forces but it is very efficient for texture haptic feedback [Yao 2010] (see the figure 3.11). This second stage will be responsible in our crossover method of the high frequency tactile sensations.

In order to have the two stages in parallel and mechanically coupled, Haptuator is integrated inside the Pantograph handle, as shown in the figure 3.4 (c). In the context of our research work, only one Haptuator is installed. The first objective is to validate the dual-stage combination by crossover method in one dimension, i.e., the y axis as shown in the dynamic modeling section and the figure 3.9.

In terms of sensors, a pair of relative angular encoders (Gurley Precision Instruments Inc.) is embedded inside the Pantograph for each motor. They are used to track run time handle's positions in the joint space based on the kinematics of the Pantograph. Additionally, inside the handle of the Pantograph, a three-axis analog accelerometer (Freescale MMA7361) is incorporated to measure the resulting

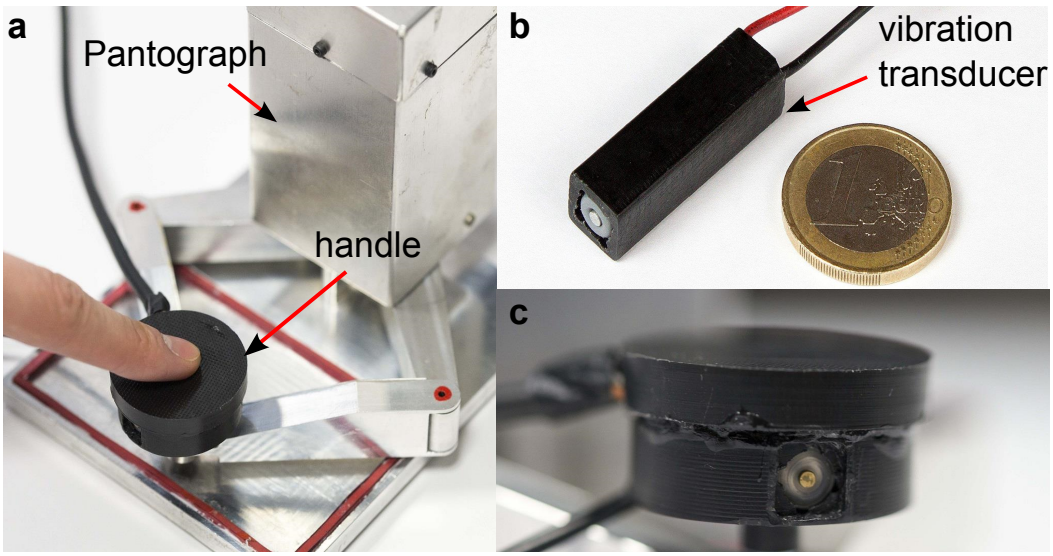

Figure 3.4: Dual-stage haptic interface components. (a) The planar parallel mechanism, the Pantograph, has uniform magnitude in the bandwidth until 200 Hz. (b) The tactile device or Haptuator. This vibration transducer is suitable to work in a high and large frequency region until 1 kHz. (c) The interface handle, inside which the Haptuator and the accelerometer are embedded.

acceleration at the handle. This sensor will be used as the source for our system identification and is essential for evaluating the performance of the whole interface.

In terms of software deployment, the whole haptic device is interfaced to a host computer via a NI (National Instruments [NI 2014]) DAQmx PCIe 6259 card. The host computer provides a soft real-time Linux (RTAI) environment. A real-time application is implemented in this environment to process all algorithms (kinematics, signal crossover, compensation, and other utilities) and to handle user commands. The real-time application runs at 10 kHz as sampling rate to guarantee the quality of signals within demanded bandwidth.

3.3.2 Crossover method

In order to create a large bandwidth haptic system, our idea is to couple two stages of mechanical systems, one which responds well to low frequency signals and one to high frequency signals. The idea is inspired by the techniques used in high fidelity sound management to couple loudspeakers with different frequency responses. This coupling is realized with a method called signal crossover that can be fully adapted to haptic frequency coupling as it is demonstrated later in the section 3.5.

Signal crossover is a class of analog/numerical filters implemented to split signals (audio, haptic, etc.) into separated frequency bands [Harris 2013]. It routes them to corresponding signal transmitters (loudspeakers, haptic interface, etc.) that has been optimized for those frequency bands. In a typical 2-way audio crossover net-

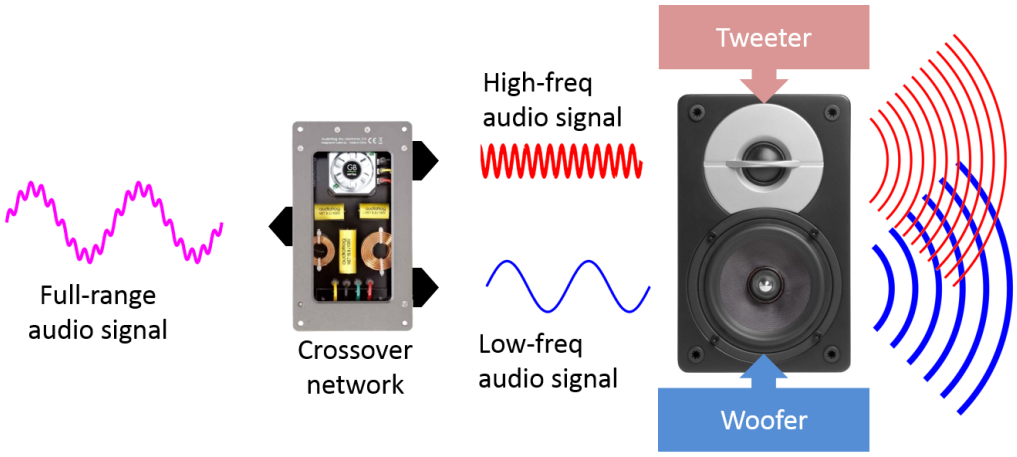

Figure 3.5: Application of signal crossover in audio domain: a sequence of full frequency range audio signal is sent to a 2-way signal crossover network and is then split into 2 frequency channels. The tweeter is responsible for high frequency acoustic output while the woofer is for low frequency acoustic output.

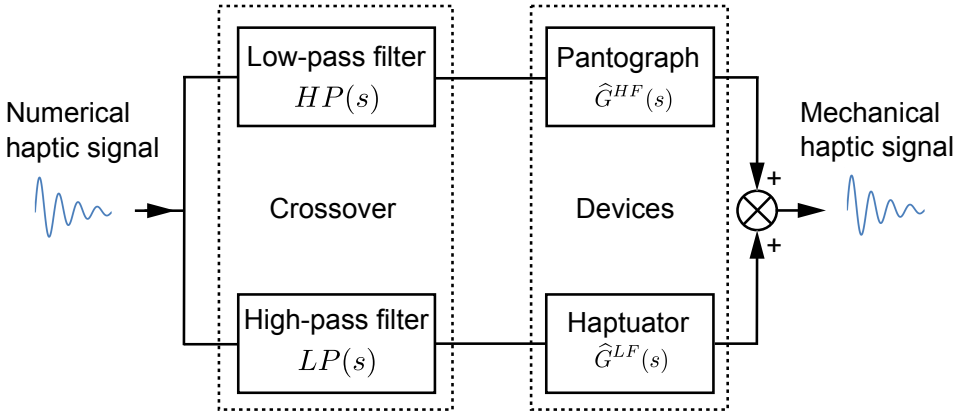

Figure 3.6: The bloc diagram shows how each device of the dual-stage interface connects with a 2-way signal crossover: The low-pass filter is branched to the Pantograph while the high-pass one is connected to the Haptuator.

work as illustrated in the figure 3.5, a full frequency range audio signal is spit by the signal crossover into two channels: a low frequency band and a high frequency band. Then they are sent to a tweeter and a woofer, which are dedicated to high frequency and low frequency acoustic output respectively.

For our haptic example, a 2-way signal crossover is sufficient as we have only two mechanical signal transmitters : it will be composed of a low-pass and high-pass filters in parallel. The bloc diagram 3.6 shows how each device of the dual-stage interface connects with a 2-way signal crossover. The crossover separates the signal in two pathways with different frequency contents. Two mechanical components

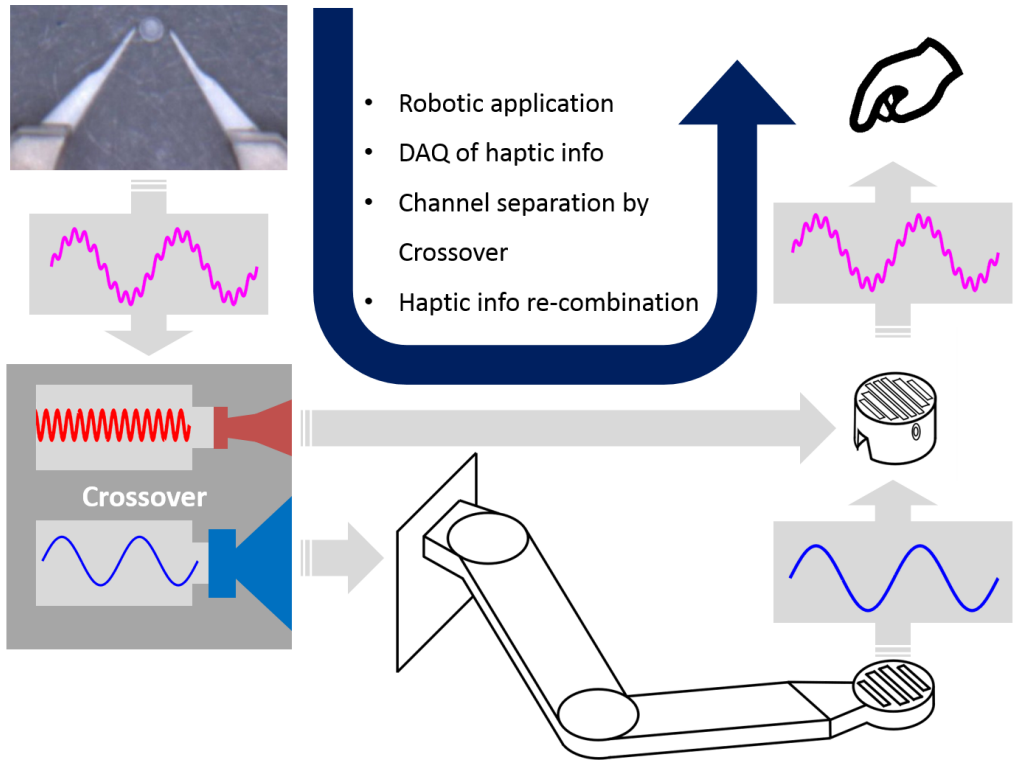

Figure 3.7: The system scheme with crossover illustrates the complete flow logics about haptic information.

receive a part of the signal and transmit mechanical forces on the interface handle. The user's finger on the handle perceives the interaction dynamics. The figure 3.7 illustrates the complete flow logics about haptic information. The selected crossover should be tuned to behave like all-pass filter [Harris 2013] , i.e. the magnitude of the force display on the handle must be faithful to that of the original haptic signal. To address this need, one standard crossover approach widely applied to perform spectral partition is the Linkwitz-Riley (LR) Filters [Linkwitz 1978]. In our study, fourth order of such filters (80 dB/decade as slope) are used for better filtering quality. The figure 3.8 demonstrates the magnitude response of the Linkwitz-Riley fourth order crossover (LR-4), and its low-pass and high-pass component.

In terms of cut-off frequency, a common value must be chosen to satisfy all-pass filter requirement. By means of dynamic modeling and identification, the cut-off frequency can be determined. In case of sharing overlapped frequency band between two devices, the criterion of defining the cut-off frequency is to maximize the overall performance. More concretely speaking, if the Pantograph and the Haptuator share some overlapped frequency band, the cut-off frequency should be chosen the highest that the Pantograph allows to minimize the phase delay introduced by the filters.

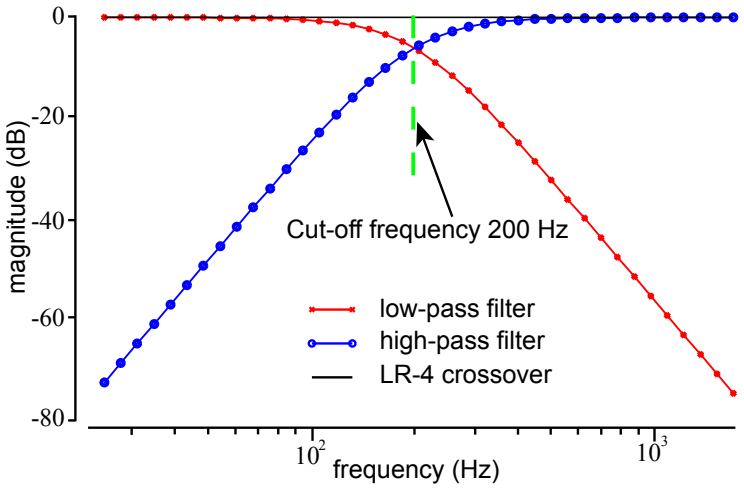

Figure 3.8: Magnitude plot of the LR-4 crossover. The blue, green and red curves represent the LR-4 low-pass filter LP, the LR-4 high-pass filter HP as well as the sum of LP and HP respectively.

3.4 Model and control

3.4.1 Dynamic modeling

To have a better overview of the mechanical interaction, a model of the whole system is proposed in this section. The figure 3.9 explicits the mathematical model. This model highlights the complexity of our mechanical coupling, more complex than a network of independent loudspeakers. The system is composed of three components : the vibration transmitter or the Haptuator, the force transmitter or the Pantograph and the user pressing finger.

Before proceeding with the mathematic analysis, the modeling scenario must be presented. During operations, the human operator places one finger on the surface of the interface handle as shown in the figure 3.9(a). She/he applies a light pressure to assure the contact at all time with the handle. A sequence of numerical haptic signals are sent to both of the haptic channels : the Pantograph and the Haptuator. The numerical haptic signal is transformed to the voltage command U_F by the overall computational system.

The dynamic modeling is studied in one axis around a local position, because apparent masses slightly depend on the Pantograph configuration. The Haptuator axis is aligned with the finger axis in this model. The haptic handle is in the middle of the Pantograph workspace and the input haptic signal is a one directional force in the same considered direction, i.e. the y-axis of the world frame. The complete system is presented in the figure 3.9 and the overall parameters are listed in Table 3.3.

The principle of operation of the Haptuator is the production a Laplace force, denoted by f_v in Fig. 3.9(a), thanks to the interaction of a electromagnetic circuit

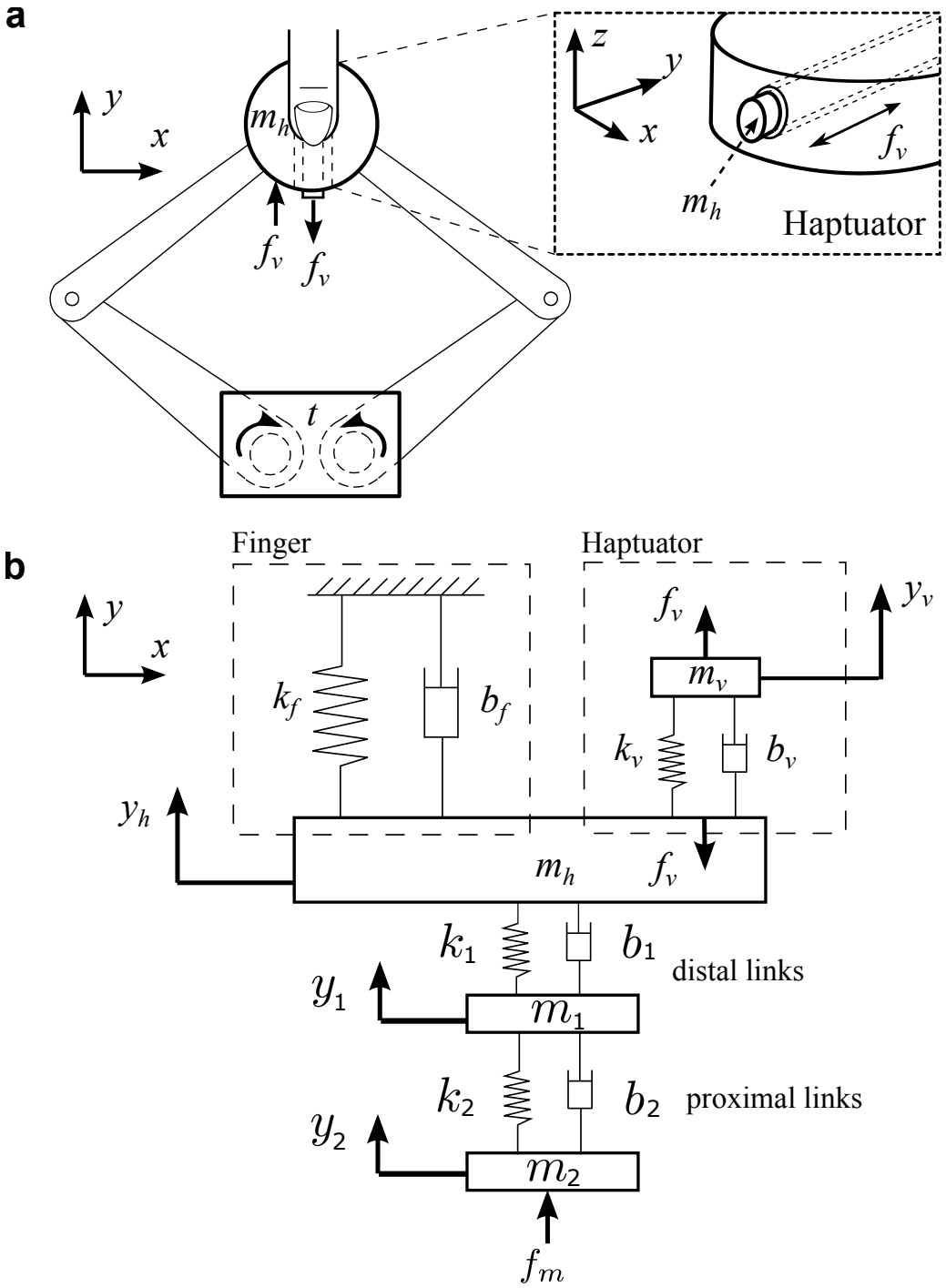

Figure 3.9: System dynamic modeling. (a) Interface top view. (b) Equivalent mechanical system studied in the y axis of the world frame. The impedance parameters of the distal and proximal links are apparent parameters.

Parameters	Description
m_v	mass of the Haptuator's moving magnet.
m_h	mass of the terminal assembly.
m_1	apparent mass of links of Pantograph.
m_2	combined mass of motor windings
k_f, b_f	stiffness and the damping of finger.
k_v, b_v	stiffness and the damping of the Haptuator.
k_1, b_1	combined stiffness and damping of distal links
k_2, b_2	combined stiffness and damping of proximal links
y_h	displacement of the terminal assembly
y_v	displacement of the moving magnet
y_l	equivalent displacements of links
y_2	displacement of motors
f_m	equivalent force acted at motor windings
f_v	interaction pair force due to the haptic signal and the relative motion between the moving magnet and handle
U_F	command voltage (the numerical haptic signal)

Table 3.3: Parameters of dynamic modeling.

and mobile magnet (where m_v and y_v are its mass and its displacement). The vibration of the magnet is transmitted to the structure by an viscous-elastic membrane, where k_v and b_v denote its spring-damper properties. The transmitted force f_v is a complex function of the electrical input signal U_F, the position of magnet y_v compared to the position of holding structure y_h, as described in equation 3.3.

$$f_v = F(U_F, y_h, y_v) \tag{3.3}$$

As the transmission structures of the distal and proximal links are not fully rigid in case of high frequency excitations, their contributions in the mechanical model induce a equivalent system of mass-spring-dampers : k_1, b_1, m_1, k_2, and b_2 (see Fig. 3.9(b)).

The variable m_h stands for the mass of the terminal assembly which enclosed the Pantograph end-effector, the Haptuator structure, the accelerometer, as well as the finger mass. Its displacement is noted as y_h. The equivalent force acted at motor windings f_m is a function of U_F.

The mechanical behavior of the human finger has nonlinear complexity but can be efficiently approximated by a second order system whose spring stiffness and

viscosity factor are k_f and b_f respectively [Wiertlewski 2012].

Based upon the above analysis, the system dynamic model can be derived in the y axis of the world frame , as shown in the equation 3.4:

$$\mathbf{M}\ddot{\mathbf{Y}} + \mathbf{C}\dot{\mathbf{Y}} + \mathbf{K}\mathbf{Y} = \mathbf{F} \tag{3.4}$$

where:

$$\mathbf{M} = \begin{bmatrix} m_h & 0 & 0 & 0 \\ 0 & m_v & 0 & 0 \\ 0 & 0 & m_1 & 0 \\ 0 & 0 & 0 & m_2 \end{bmatrix} \quad \mathbf{Y} = \begin{bmatrix} y_h \\ y_v \\ y_1 \\ y_2 \end{bmatrix} \quad \mathbf{F} = \begin{bmatrix} -f_v \\ f_v \\ 0 \\ f_m \end{bmatrix}$$

$$\mathbf{C} = \begin{bmatrix} b_1 + b_v + b_f & -b_v & -b_1 & 0 \\ -b_v & b_v & 0 & 0 \\ -b_1 & 0 & b_1 + b_2 & -b_2 \\ 0 & 0 & -b_2 & b_2 \end{bmatrix}$$

$$\mathbf{K} = \begin{bmatrix} k_1 + k_v + k_f & -k_v & -k_1 & 0 \\ -k_v & k_v & 0 & 0 \\ -k_1 & 0 & k_1 + k_2 & -k_2 \\ 0 & 0 & -k_2 & k_2 \end{bmatrix}$$

The system input is the electric image U_F and the output of the system is the acceleration of the terminal assembly, $\ddot{y_h}$, or equivalently, the fingers' superficial skin layers.

From the above analysis, it can be deduced that the system has four dynamic modes resulting from the independent masses m_h, m_v, m_1 and m_2 and therefore gives rise to an eighth order system. The distribution of the dynamic modes in the frequency domain, and how they intersect with the demanded working bandwidth (from DC to 1 kHz) depend on all related physical parameters.

3.4.2 Identification

As mentioned in the description section, our objective is to design a crossover method that separates the low and high frequency regions of a haptic image to be displayed. In order to obtain higher quality of the display, the signal is then sent to two mechanical channels optimized for their frequency response regions : the Pantograph and Haptuator respectively (see the figure 3.6). The identification approach adopted in our work is to carry out for each channel independently. This means that, without changing the mechanical coupling presented before, the input signal is sent to only one device each time for identification purpose.

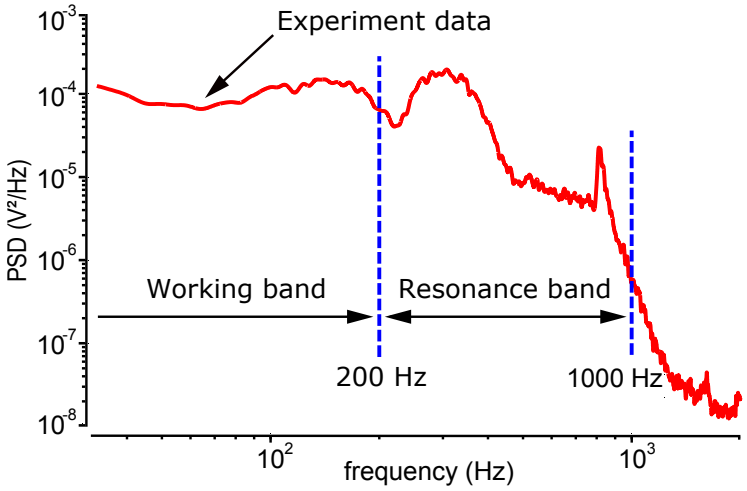

Figure 3.10: PSD analysis (Welch) for the low frequency channel. Identification signals are only sent to the Pantograph. In the frequency band from DC to 200 Hz, the Pantograph has a uniform magnitude response. Beyond 200 Hz, resonance occurs and the low-pass component of the crossover must be applied to the Pantograph to eliminate undesirable magnitude response.

Starting with the identification of low frequency channel, the Pantograph receives the signal while the Haptuator is electrically disconnected and passive. No crossover filter is applied. The model representation in figure 3.9 remains valid and the Haptuator receive no force: $f_v = 0$. The power spectral density (PSD) response to pseudo-random binary sequence input is plotted in the figure 3.10. A first, nicely damped antiresonance is clearly seen slightly after 200 Hz accompanied by a damped resonance at 300 Hz. Another resonance-antiresonance pair is seen around 800 Hz, but this time with a sharp peak. This behavior is explained by the model 3.9 with three masses connected by two damped springs [Campion 2005a].

Within 200 Hz, the Pantograph can be considered to have a uniform magnitude response. Therefore, the maximum working frequency band can be extended to 200 Hz. This also indicates that the cut-off frequency must be chosen within the range of [0, 200] Hz for the signal crossover. Within the frequency band from DC to 200 Hz, the Pantograph can be identified as static gain. Its transfer function is then approximated by :

$$\widehat{G}^{LF}(s) = G_0^{LF} \tag{3.5}$$

For the high frequency region, identification is processed with input signals only provided to the Haptuator. A PSD curve is obtained with the same method for the high frequency channel (see the figure 3.11). Below 100 Hz, the magnitude response quality is degraded by the nonlinearity of the Haptuator. It is due to the intrinsic saturation of the motion stroke in low frequency band. Based on this observation, the cut-off frequency must be set greater than 100 Hz to avoid the nonlinear band of

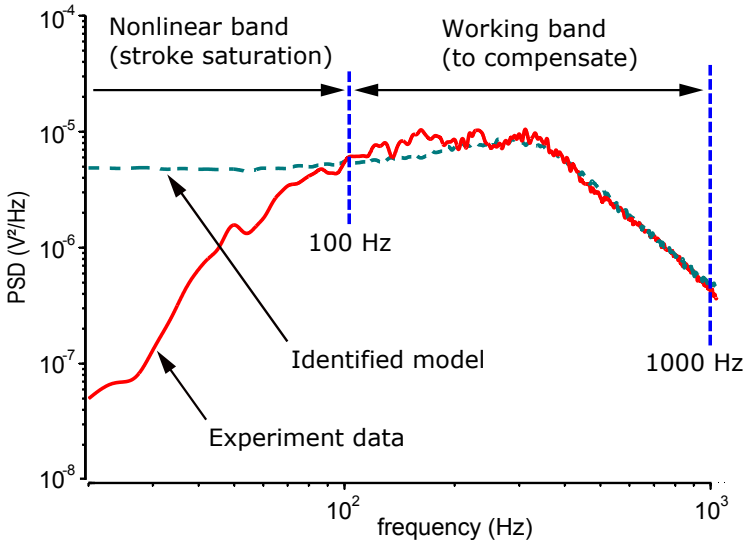

Figure 3.11: PSD analysis (Welch) of the high frequency channel. Identification signals are only sent to the Haptuator. The full curve stands for the measured experimental data and the dashed curve represents the identified model. Below 100 Hz, the Haptuator has intrinsic nonlinearity due to stroke saturation.

the Haptuator. As for identification, the model is only supposed to cover the band between 100 Hz and 1 kHz. The identified model is shown in equation 3.6.

$$\widehat{G}^{HF}(s) = \frac{250s + 6.406 \times 10^5}{s^2 + 2135s + 4.559 \times 10^6} \tag{3.6}$$

In the previous modeling section, it has been shown that the theoretical model gives rise to an eighth order model but the consideration of a limited frequency band in the low frequency channel made it possible to ignore the high frequency modes, reducing the model complexity to a second order system.

After identification for both channels, it has been observed that they have overlapped frequency band between 100 and 200 Hz. As described in the crossover section, the cut-off frequency must be set to maximize the Pantograph's band to minimize the phase delays. Therefore, the cut-off frequency is set to be 200 Hz.

It can be observed from the figure 3.11 that because of the interplay of masses and elasticities, the high frequency channel begins to roll-off at 300 Hz. Thus, in order to achieve a dual-stage haptic interface with 1 kHz bandwidth this channel must be compensated to achieve uniform magnitude.

3.4.3 Compensation

For fidelity of the haptic display, the magnitude of the transmission should not depend on the frequency. The deployment of the signal crossover ensures how to route signals to the corresponding haptic channel in frequency domain. The Pantograph works in the frequency band from DC to 200 Hz while the Haptuator is responsible

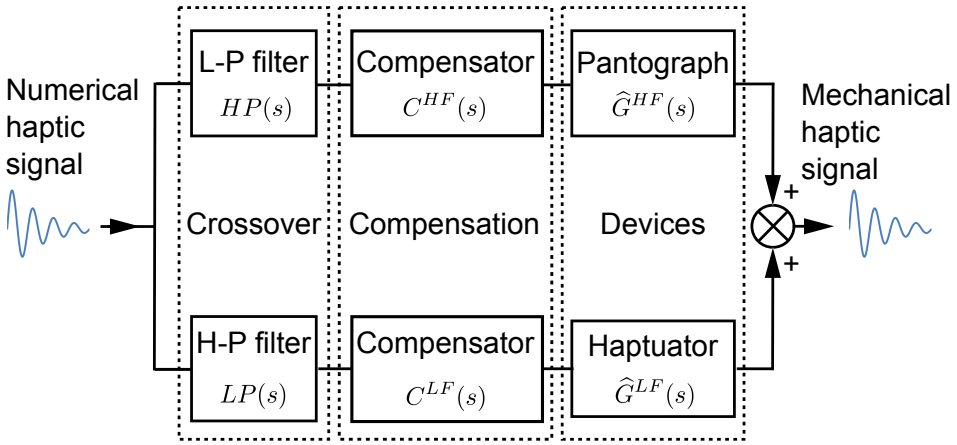

Figure 3.12: System bloc diagram with compensation and crossover. LP and HP stand for low-pass and high-pass respectively.

for the band from 200 Hz to 1 kHz. In the working band of each channel, the haptic device must be compensated to have normalized and flat magnitude response.

From the figure 3.10, it can be determined that the device has uniform magnitude from DC to 200 Hz. Hence, the only compensation is to regulate the gain.

$$C^{LF}(s) = \frac{K_{sys}}{\widehat{G}^{LF}(s)} \tag{3.7}$$

In the equation 3.7, K_{sys} stands for the desired interface gain in the overall frequency band.

Unlike the low frequency channel, the high frequency channel has non-uniform magnitude response from 200 Hz to 1 kHz. Compensation for this channel could in principle be achieved by inversion of the identified model 3.6. Unfortunately, straightforward inversion would have resulted in a physically non-realizable filter with ever increasing magnitude in the high-frequencies. A simple solution was to perform a band-limited inversion according to:

$$C^{HF}(s) = \frac{K_{sys}}{\widehat{G}^{HF}(s)} \times F(f_{max}) \tag{3.8}$$

In the equation 3.8, a candidate of $F(f_{max})$ can be a second order low-pass filter with normalized gain. The argument f_{max} determines the cut-off frequency of the filter, which is equal to the maximum system bandwidth, i.e. 1 kHz. The introduced $F(f_{max})$ can be tuned to make the $C^{HF}(s)$ causal and will not alter any system performance within the considered frequency band.

By adding compensation into the overall system, the block diagram is shown in the figure 3.12.

3.5 Experimental evaluation

3.5.1 Performances of the haptic crossover method

The previous steps provide a method for a high performance device which is built with two haptic channels for the low and high frequency transmitters (see the figure 3.12). They are composed each of three steps:

- a pass filter to increase the selection of the frequency domain and the quality of the crossover;
- a compensator that correct the imperfections in the transmitter's frequency response;
- a mechanical haptic transmitter specialized for a frequency domain.

The two channels sum up on the handle of the haptic device, thanks to a complex mechanical coupling (see the figure 3.9 (a)).

In this section, an experiment is conducted with the complete device to test and verify the fidelity and uniform performances of the crossover method in the desired working frequency band: from DC to 1 kHz. It is important to note that a real-time data processing is essential to guarantee the deterministic performance especially in high frequency band. The real-time sampling rate is setup to be 10 kHz.

The experiment consists of the interface frequency response of several functioning points covering the whole working frequency band. As several sinusoid responses are tested, a logarithmic frequency progression of one third octave-band type has been chosen from 63 to 1250 Hz (see TABLE 3.4).

Band Type	Center frequencies (Hz)				
1/3 Octave-Band	63	80	100	125	160
	200	250	315	400	500
	630	800	1k	1.25k	

Table 3.4: 1/3 Octave-Band.

The mean magnitude responses at each center frequency are plotted in the figure 3.13. The high frequency and the low frequency channels have been tested separately by disconnecting the corresponding opposite channel's signal input. The figure 3.13 shows that the two channel respond like two complementary low and high pass-filters. This results in a impressing flat response when they are both activated. The complete haptic device has a remarkable uniform frequency response on all the DC to 1 kHz bandwidth. A special attention is given to the cut-off frequency where the two haptic channels contribute evenly to the overall magnitude response. The analytical filter and the real-time implementation must be carefully considered so that the two haptic devices work in phase. The experimental result shows that

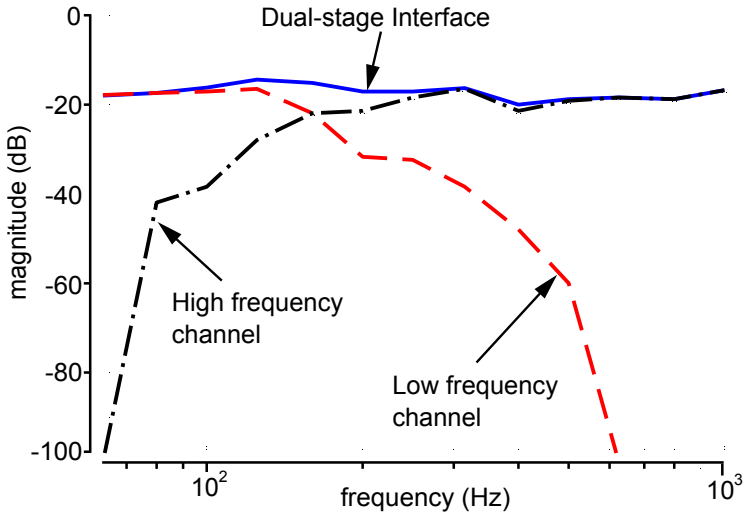

Figure 3.13: Magnitude response of the haptic interface. The interface has a flat response over the bandwidth.

there is then an obvious increase of the haptic performances in frequency bandwidth with the signal crossover method.

3.5.2 Optical tweezers application

In order to illustrate the type of application of this extended system, we propose a challenging experiment. For research and educational purpose, it can be desirable to explore microscopic phenomena. Under microscope, the motion of microscopic particles can be observed and their dynamics is in general very fast.

Using of the available installation in the lab facilities for micromanipulation, a set of phenomena has been recorded using a optical tweezers setup. The recored data consists in using a trapped micron bead to explore the microscopic world by simultaneously recording the force interaction in the medium. The controlled probe records contacts and vibrations like thermal agitations, which are both high frequency mechanical interactions. Integrating an haptic device to teleoperated those tasks has been achieved in previous works [Pacoret 2009, Ni 2013a, Pacoret 2013]. This kind of application benefits directly from higher performance haptic devices.

For the purpose of the present demonstration, recorded data of microscopic forces have been used with the corresponding videos of the scene. The new haptic device displays an offline recording of the forces at the same time that the video recalls the performed task under microscope (see the figure 3.14).

The figure 3.14(a) shows the demonstrator. It includes the haptic interface and a computer running a recorded scenario from the optical tweezers application. The figure 3.14(b) is a captured image frame during a replay where a microsphere levitates thanks to the optical tweezers technique.

In the first tested case, the probe is far from an obstacles and it is only subjected

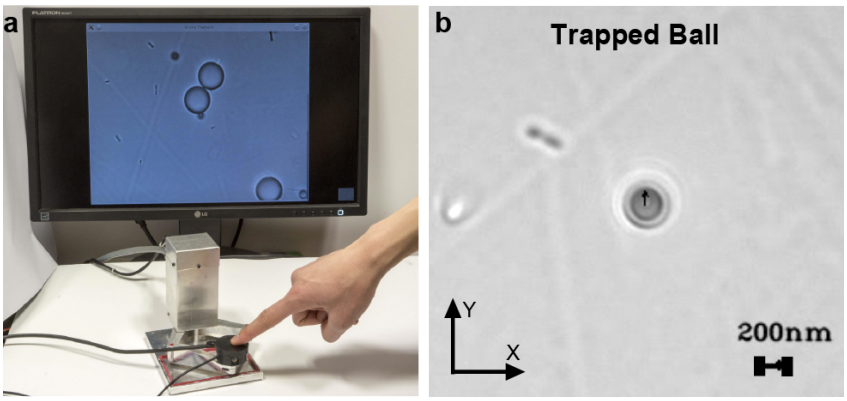

Figure 3.14: Optical Tweezers manipulation scenario. (a) A human operator experiences haptic sensations via the interface. The operation is based upon a virtual scenario recorded from a micromanipulation application. (b) A 3 micrometer bead trapped by optical tweezers is under Brownian motion, i.e. thermal agitation. The human operator feels high frequencies oscillations via the haptic interface. The black arrow on the bead center indicates the instantaneous force fed back to the user.

to Brownian motion, thermal agitations (see [Ni 2011] for more details). The black arrow gives a visual indication of the instantaneous force applying on the bead and recorded by the microscope force sensors. In the optical tweezers application, this force is computed based on linear spring model as a function of displacement. The Brownian motion energy produces force and then displacement of few 100 nm in the optical trap confinement. During the operation, the user with their finger on the handle is able to feel the oscillations of this phenomena. The frequency excited by this energy is equivalent to a white Gaussian noise, so it is theoretically a infinite frequency domain. The practical case show that there is attenuation coming from the experimental conditions and the optical tweezer properties. The force sensors have a limited bandwidth too. A haptic device with 1 kHz bandwidth is fully adapted for this application. The figure 3.15 shows data obtained from the accelerometer on the haptic handle while the Brownian motion is displayed. Since the force model applied is based on a linear spring model, the acceleration data can directly give rise to the distribution of Brownian motion displacement. It is clearly observed the characteristic Gaussian shape of the Brownian noise.

The second proposed scenario involves a contact situation between the probe and a bigger target bead which is stuck on the Petri dish surface. Before contact occurs (see the figure 3.16 (a)), the human operator only perceives Brownian motion as explained in the previous scenario. At the moment of impact between the tool and the target obstacle, the operator is able to experience a significant force feedback in the direction indicated as the red arrow in the figure 3.16 (b) and an acceleration peak is measured by the accelerometer and observed on the curve (right bottom corner).

This demonstrator is available at our lab and several visitors have already ex-

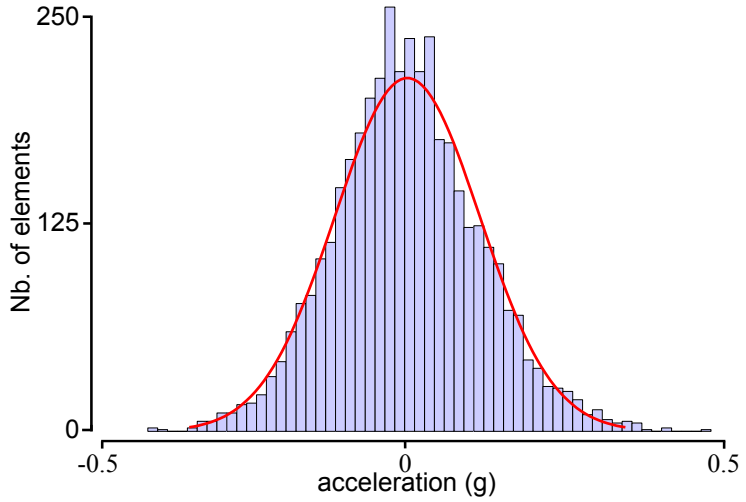

Figure 3.15: Histogram of measured acceleration on haptic handle while a Brownian motion is displayed from a microprobe. A Gaussian fitting, solid curve, has been added to highlight the Gaussian shape of the distribution.

perienced the haptic sensations of the different scenarios mentioned above. Their surveys confirm that operators perceived and enjoyed the display of real Brownian motion as well as contact forces from the microscopic world. The haptic sensations make interaction much more intuitive and help users better understand operation scenarios and microworld phenomena.

3.6 Conclusion

Due to the intrinsic cantilever property, conventional haptic interfaces have limited bandwidth which is far from matching human proprioceptive capacities. This paper presents a method to extend the frequency bandwidth of haptic interfaces from DC to 1 kHz. Furthermore, the method ensures that haptic signals within the bandwidth can be rendered in a uniform manner.

The method consists of setting up a parallel structure of a low-frequency and a high-frequency haptic devices by signal crossover. After identifying haptic devices, compensations can be designed to make the overall dual-stage haptic interface have uniform magnitude response in frequency domain. In the presented work, the low-frequency device is the Pantograph and the high-frequency device is the Haptuator: a vibration transducer. The dual-stage frequency bandwidth is extended up to 1 kHz, which can satisfy the frequency range of human haptic perception.

The dual-stage haptic interface is able to render both conventional force feedback as well as high dynamic impact forces. Through experiences, subjects reported that the manipulation is rendered more realistic. This confirms the importance of extending the bandwidth of a haptic interface. Through teleoperation, the microscopic dynamic vibrations can be rendered by the dual-stage interface, which makes

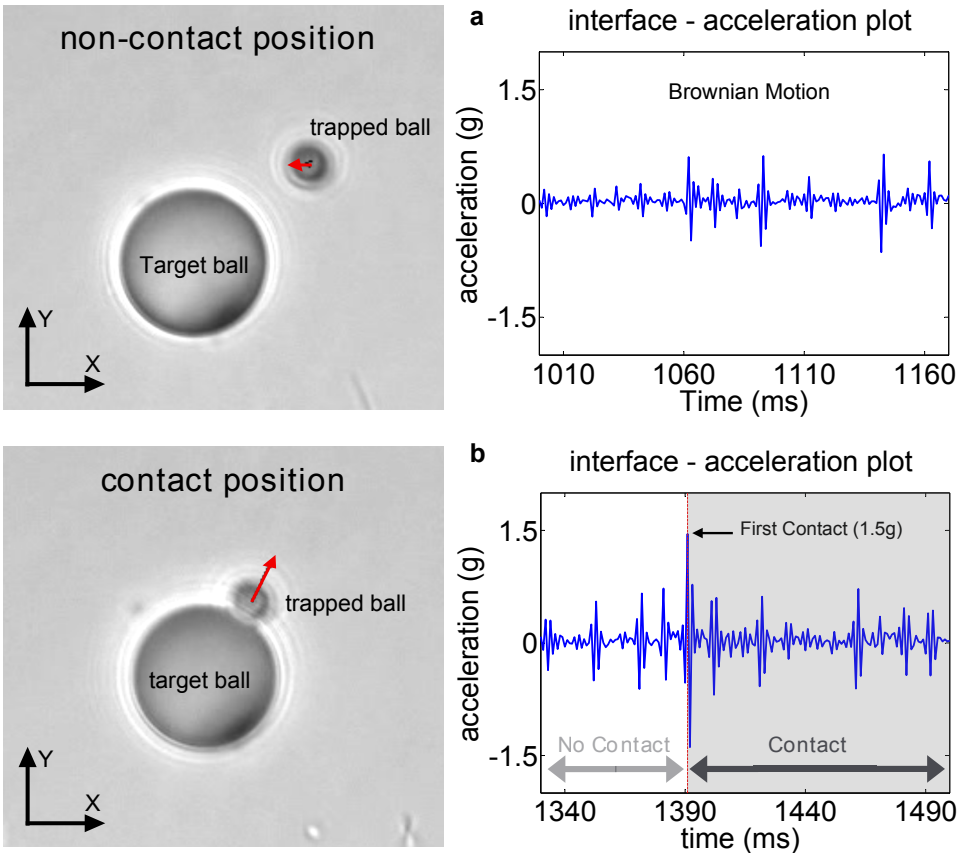

Figure 3.16: Second scenario. (a) Far from the obstacle, the operator only experiences Brownian motion. The small red flash indicates the instantaneous force vector. The right graph shows the y-axis acceleration profile. (b) When the contact occurs with an obstacle, the force marks a peak as shown by red arrow. The right graph shows the y-axis acceleration profile.

the manipulation more intuitive and reliable.

In future works, we will investigate issues due to the introduction of delays in the haptic loop. To improve closed loop performances, an advanced control design must be implemented which is not in the screen of this paper. From user point of view, user studies must be carried out to highlight the benefit using two-stage crossover haptic devices. A new design for haptic handles is under investigation in order to extend several commercial haptic devices mechanical bandwidth.

Chapter 4

Design of a Haptic Interface for Watchmakers

Contents

One important application domain of Chronogrip platform is high end watchmaking industry, but equipped general purposed use interface cannot lead to intuitive operation for watchmaking process and furthermore no haptic feedback is provided. This chapter is dedicated to a novel design of intuitive haptic interface for watchmakers. In this chapter, the specifications of this new design TéléTweez will be firstly studied. Then in the section of mechatronics design, several concepts of actuator system will be studied. After evaluation, the final design will be described as well as the first prototype. In section 5, the dynamics will be studied and a virtual environment application will be demonstrated.

4.1 Introduction

Watchmaking has long history. Prestigious watch brand has the tradition of handmade process and small batch production to express the art of precision and unique masterpiece. After industrial revolutions, automation prevails. It brought the challenges to the sector that the watches become more and more complex and accurate, but handmade process has saturated productivity and accuracy. From the aspect of manufacturing, high-end watchmaking can hardly be realized by automation for the reason that small batch production requires much more flexibility where automation can hardly achieve in a reasonable cost.

Under such circumstances, the Chronogrip cobotic platform was proposed to address this challenge for the prestigious watchmaking industry. The features such as high precision, large motion stroke, compact and modular designs are desirable for watchmaking process. However, one issue arises that the proficient watchmaking operators are not familiar with the user interface, the joystick or tablet. They are too different in operating principle compared to conventional watchmaking tools, the tweezers. Furthermore, no haptic feedback is provided in the current cobotic platform, which makes the operation nonintuitive. As a consequence, the operators must spend significant time in adapting to it and therefore productivity is decreased.

To address this issue, we propose a novel haptic interface design named TéléTweez and its first prototype in this chapter. It is the first realizable haptic tweezers that can also be used as a conventional tweezers, which ensures that the usage is familiar to watchmaking operators. Thanks to this versatility, it can also be used in other tweezers-involved applications.

This chapter is organized as follows: the next section will survey some most recent user interfaces or tweezers-based tool developed by research institutes or industrial companies. Tough no other haptic user interface design has been reported for watchmaking, the survey will discuss research/commercial products with similar specifications. Then we proceed to study the technical specifications of the TéléTweez interface. After comparison and evaluation several candidate solutions, a design concept is proposed and the first prototype is produced. Finally, an application is demonstrated and the subject is concluded.

4.2 State-of-the-Art

The da Vinci Surgical System is a sophisticated teleoperation robotic platform dedicated to minimally invasive surgery (MIS) [da Vinci-Surgery 2015]. It consists of an ergonomically designed user interface to facilitate surgeon's operation. It is constructed in a fashion that the experience of teleoperation is very similar to using a real tweezer. One thing to notice is that da Vinci Surgical System does not provide haptic display. The figure 4.1 demonstrates a typical example of operation scenario.

Servomedics company [SERVOMEDICS 2015] developed various models of electronic tweezers (not teleoperation interface) dedicated to medical, scientific and industrial applications. For the model that they developed for surgery applications:

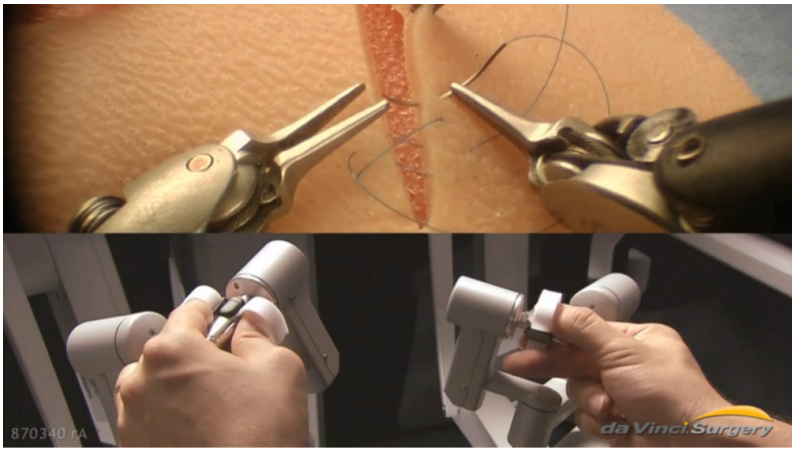

Figure 4.1: An operation scenario of da Vinci Surgical system [da Vinci-Surgery 2015]. Surgeon's hand movements are translated via the master device (shown in lower part) to the slave da Vinci instruments (shown in upper part) with magnitude scaled down.

the weight is 60 gram; the charge time is about 60 minutes to have a battery life of 2 hours; the operation resolution is 0.1 mm; the maximum motor torque output is between 2 and 2.5 mNm. The tweezers are made in stainless steel and are equipped with force control unit and sensors such as gyroscope, encoders and thermometer. In terms of manipulation, the tweezers are not manipulated by pinching, but by rotating a round button to control opening of two levers. Furthermore, haptic display is not provided. Figure 4.2 demonstrates some tweezers models and inner structure layout for a future design.

(a) (b)

Figure 4.2: Servomedics electronic tweezers [SERVOMEDICS 2015]: (a) The blue model (shown above) is a high precision tweezers for laboratory applications; the white model (shown below) is dedicated to surgery. (b) Anatomy of a future tweezers concept: it incorporates 5 servomotors with magnetic encoders, a 32 bits microprocessor and communication network.

The figure 4.3 demonstrates two haptic interfaces developed for training in vir-

	Haptics included	DOF	Operation principles	Applications
da Vinci surgical interface [da Vinci-Surgery 2015]	No	6 + 1 (gripping)	tweezers	MIS
Servomedics electronic tweezers [SERVOMEDICS 2015]	No	1 (gripping)	modified tweezers	scientific, industrial
Microsurgical tweezers [Payne 2015]	Yes	1 (gripping)	tweezers	microsurgery
Haptic tweezers interface [Burdet 2004]	Yes	6 + 1 (gripping)	tweezers	microsurgery training
Haptic scissors interface [Okamura 2003]	Yes	1 (trans.) + 1 (cutting)	scissors	VR
Haptic tweezers interface [Rizun 2006a]	Yes	1 (gripping)	tweezers	surgery

Table 4.1: Comparison of different types of smart materials.

tual environment. The figure 4.3 (a) consists of a tweezers with a rotational motor installed at the tip of the tweezers. The trainee can perceive the sense of touch provided by the motor during contact with a virtual object [Burdet 2004]. The interface is tweezers based. But since a motor is mounted at the tip, inertia is increased and it cannot no longer operate like a conventional tweezers. The figure 4.3 (b) is the design of a haptic scissors. The scissors can provide cutting (rotational) forces as well as translational forces [Okamura 2003].

The research work [Payne 2015] designed a force-feedback tweezers (not teleoperation interface) for micro-surgical applications, shown in the figure 4.4. The concept is intended to improve human perception of low-level grasping forces in milli Newton scale (0-300 mN) that is otherwise imperceptible to human touch. The particularity of the design is that the provided haptic feedback is not aligned in the grasping direction as the intuitive manner, but perpendicular to the grasping direction. In other words, it stimulates fingertip instead of finger pad in case of haptic display. The design could avoid problems such as closed loop stability and spacing constraint in grasping direction. However, operation intuitiveness must be examined since haptics is not supplied in conventional manner. Furthermore, the design imposes holding gesture to a predefined fashion, which can be incompatible with specific applications. For example, various gestures described in 4.3.1 for watchmaking process cannot be realized by this design.

Another design of haptic tweezers for robotic surgery is reported in [Rizun 2006a] [Rizun 2006b]. It is a modular and ergonomic single-DOF surgical master device

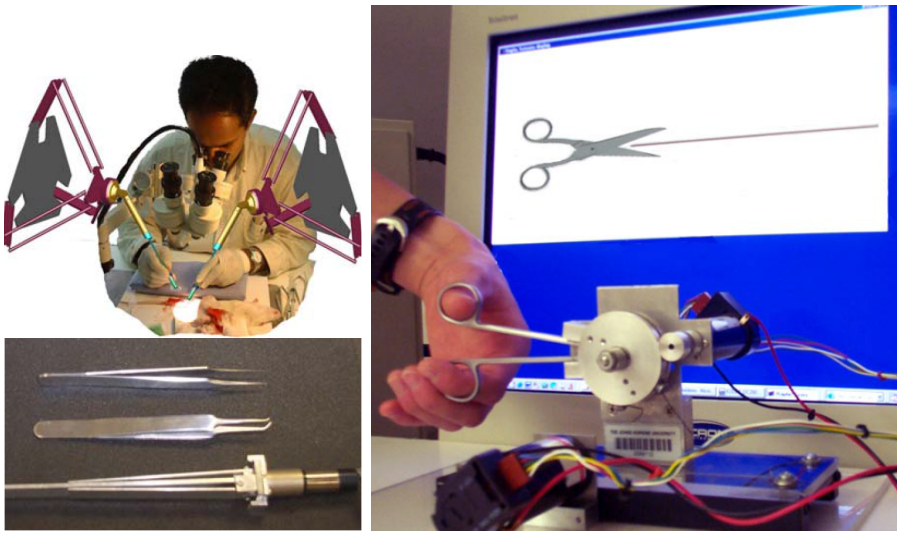

(a) (b)

Figure 4.3: The haptic user interfaces for training in virtual environment: (a) The microsurgery-training working scenario of the haptic tweezers and its comparison to real tweezers [Burdet 2004]. (b) The haptic scissors [Okamura 2003].

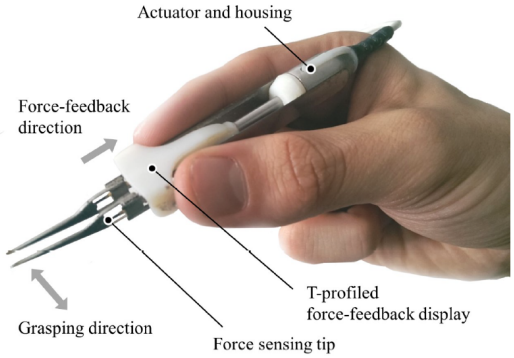

Figure 4.4: The haptic tweezers for micro-surgical applications [Payne 2015].

with all electronics embedded, as shown in the figure 4.5. The interface is comparable to a conventional tool in geometry and weight: the overall length is 153 mm and the total mass is 125 g. A voice coil actuator is embedded to provide haptic display in high bandwidth. It can provide maximum opening/closing force output up to 5N and cover the frequency spectrum of human touch. The interface can also operate as a conventional tool. This is the only interface design that we have found which can be served as a combination of haptic interface and conventional tweezers. Albeit the advantages, one potential issue arises from the voice coil actuator: it produces significant heat in short time and that can disturb users' operations or even endanger their safety. It could be the reason no report about prototype or commercialization

about this research work has been found.

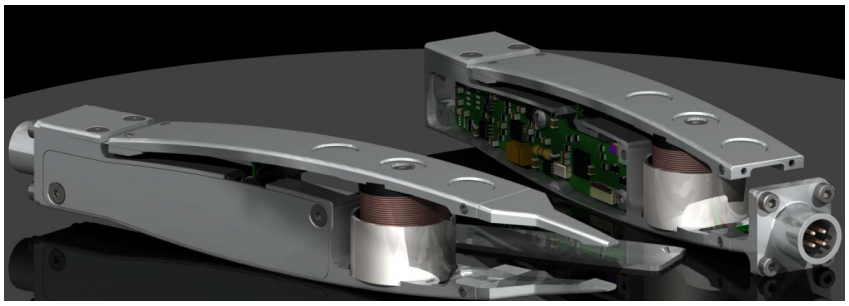

Figure 4.5: The haptic tweezers of the project NeuroArm for robotic surgery [Rizun 2006b].

The studies mentioned above are summarized in the table 4.1.

Among all design variance, one important issue is whether to provide haptics to users. Though no public report is accessible about why haptics is not provided for da Vinci or Servomedics, it can be derived that adding haptics can give rise to design difficulties. Firstly, haptics display needs to be realized by appropriate actuator system, which gives rise to design burden. Take the interface of da Vinci, as shown in the figure 4.1 as an example, providing haptics for the compact structure means being able to find actuator system which is small, has a minimum level of motion stroke, and can produce enough torque for haptic display. For most of commercially available actuators, small dimension, large motion stroke and high torque output are contradiction. Secondly, including haptics brings challenge to control loop stability. The research work [Mohand Ousaid 2014a] shows that a trade-off must be imposed between stability and transparency for micro-scale teleoperation with haptic feedback. With haptics added to the control loop, dedicated strategy must be carefully designed in order to ensure stability and haptic quality. Despite those difficulties presented in the aspect of system design and control, we believe the benefits are worth the challenges. In various studies [Hayward 2004] [Saddik 2007] [Coles 2011] [Shimoga 1993] [Burdea 1996] [Wagner 2002] [Tavakoli 2004], it is shown that haptics can promote intuitiveness, reduce force magnitude, energy consumption, as well as the task completion time and the error rate. It is based on those studies that we decide to include haptics in the TéléTweez. In the future, a set of rigorous tests of user experience must be carefully established to evaluate whether haptics is able to enable intuitive interaction between human and machine for watchmaking process.

In this section, some of user interfaces or tweezers based tools with relevant specifications are surveyed. They all bear one common characteristics: the designs are similar to conventional tools so that the interfaces are familiar to manipulate. This conforms to our most important design idea that the TéléTweez must be a tweezers to facilitate tweezers-like operations. The only comparable haptic tweezers [Rizun 2006b] is also designed to be an interface as well as a conventional tweezers, but the fast generation of heat from voice coil could prevent it from being commer-

cialized. In the next section, the technical specifications of the TéléTweez will be studied.

4.3 Technical Specifications of the TéléTweez

In this section, the geometric and mechanical characteristics of tweezers used in watchmaking process, as well as their conventional usage will be firstly studied. In the next step, the analysis of haptic tweezers will determine what electronic functionalities the TéléTweez should embed. At last, a conclusion can be derived to summarize the Technical Specifications of the TéléTweez.

4.3.1 Description of Tweezers in Watchmaking Industries

Tweezers are tools used to carry out operations like picking up and placing objects, where manipulations are usually subject to constrained conditions (small dimension, extreme temperature, toxic substances, etc.) that cannot be directly handled by human hands. Typical tweezers have two levers. When force is applied by fingers to pinch two levers to clamp target objects, operators can feel mechanical resistance from the tweezers. In this chapter, we will describe this spring-like resistance property as *mechanical stiffness*. Different tweezers vary in shapes, sizes, tips, materials and etc. Figure 4.6 demonstrates some different types of tweezers, designed and manufactured by Dumont company [Dumont 2015].

Figure 4.6: Different types of tweezers designed and manufactured by Dumont company [Dumont 2015].

In watchmaking industries, the most used tweezers have sturdy and long tips, with flat edges that can assist gripping with the side. A typical tweezers used in watchmaking process, 707 from Ideal-tek [ideal tek 2015], possesses characteristics as listed in the table 4.2.

The figure 4.7 illustrates several characteristics of the tweezers 707 from Ideal-tek.

The characteristics of the Ideal-tek 707 tweezers	
static opening width (tips):	4 mm
max. clamping stroke :	4 mm (per lever)
levers length:	115 mm (70 - 160 mm)
max. width:	11 mm
thickness :	11 mm
material :	Delrin, stainless steel
mass:	5 - 20 g
geometric form:	fine-pointed tip, wide flat handle
mechanical stiffness (clamping) at fingers:	250 N/m
finger contact position:	30 - 50 mm from tips
manipulation angle:	5 - 60 deg.

Table 4.2: The characteristics of the Ideal-tek 707 tweezers.

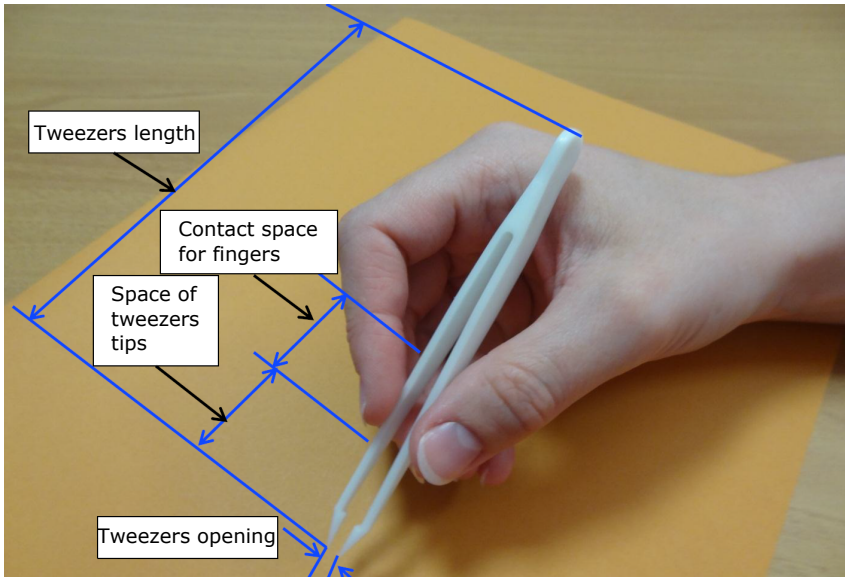

Figure 4.7: Several characteristics of the tweezers 707 from Ideal-tek.

The gesture of holding tweezers in conventional watchmaking process must be investigated before proceeding to design rationales. The manner to hold tweezers depends on the geometry of the object to manipulate, as well as the operation to realize. In any case, the thumb and index fingers are always involved to maintain and drive the two levers of tweezers, while the rest of hand helps support and guide tweezers to facilitate the manipulation. The manner to hold tweezers in watchmak-

ing process can be categorized by three types of gesture:

- The first typical gesture is analogous to holding a pencil. Two levers are controlled by the thumb and index fingers with the conjoining part of tweezers resting upon the webbing (perlicue) between the thumb and index fingers. According to the inclination angle between the tweezers and the working plane, the contact position between the tweezers and operator's hand can vary from the perlicue to the phalanx of the index finger, as shown in the figure 4.8. The middle finger can be used to support or guide the tweezers and the ring finger to locate and guide the hand towards manipulation.

Figure 4.8: The first typical gesture to use tweezers in watchmaking process.

- The second typical gesture consists in maintaining the opening of tweezers by using the thumb, index and middle fingers. The index and middle fingers are placed side-by-side so that reaction forces are distributed more evenly among fingers with respect to the first gesture. As a result, less force is required during manipulation, shaking and fatigue are reduced, and target can be manipulated more stably. The figure 4.9 illustrates the gesture.

Figure 4.9: The second typical gesture to use tweezers in watchmaking process.

- The third typical gesture takes place when the inclination angle between the working plane and the tweezers is imposed to be less than 30 degree. As for the second gesture, the tweezers is held by the thumb, index and middle fingers to distribute evenly the force during manipulation. This gesture is ideal for

manipulation along the axis which is perpendicular to the working plane. The figure 4.10 illustrates this gesture.

Figure 4.10: The third typical gesture to use tweezers in watchmaking process.

In this subsection, the mechanical and geometric characteristics of tweezers used in watchmaking industry, as well as their conventional usage have been described. It is a must to achieve an intuitive design because the added haptic display and teleoperation function must not be obtained through remarkable loss of conventional gesture. Otherwise, the design is not intuitive.

In the next subsection, we proceed to the description of haptic interface used in the watchmaking process.

4.3.2 Description of Haptic Tweezers

A haptic tweezers consists in a tool based on tweezers working principle through which operators can control slave devices to manipulate targets with haptic display. This is the basic definition of haptic tweezers and the functionalities it describes correspond to *Robotic Control Mode* in this chapter. In such a mode, the haptic tweezers does not physically come into contact with manipulation targets. If the design allows operators to use it as a conventional tweezers: clamping directly target objects, the functionalities can be extended to a further level. Typically, the force of clamping can be precisely adjusted and maintained by the mechatronic system of the haptic tweezers, instead of human hands. Such a mode is referred to as *Manual Control Mode* in this chapter. In the following text, the Robotic Control Mode and the Manual Control Mode will be described respectively.

4.3.2.1 Robotic Control Mode

In this mode, the first issue to address is to control the opening of the slave gripper via teleoperation. That means the pinching gesture of operators must be *copied*, via coupling computational system, to the slave device. Therefore, at least a motion sensor must be equipped to detect the opening status.

While operator pinches the haptic tweezers, like how he/she were manipulating conventional tweezers, the slave gripper receives motion command to adjust the opening of tips. Typically, the opening stroke of the slave gripper is scaled down

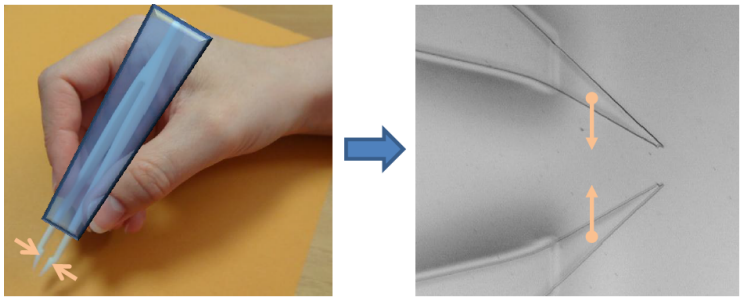

(a)

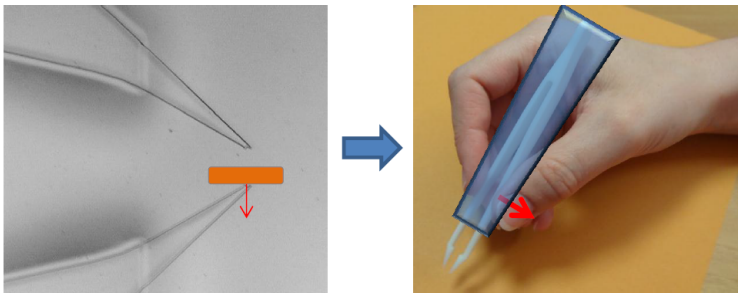

(b)

Figure 4.11: Robotic control mode by schematic diagrams of the haptic tweezers and slave gripper: (a) The opening of the haptic tweezers is copied to the slave gripper. (b) The haptic information is transferred from the slave gripper to the haptic tweezers.

proportionally from the opening stroke of the interface, linearly or nonlinearly depending on specific implemented motion control law, saturation condition, filter implementation and etc. The figure 4.11 (a) illustrates the pinching manipulation is copied from the haptic tweezers to the slave gripper.

On the side of slave gripper, when it encounters an obstacle during manipulation, a contact force arises. This information can be detected by image processing or a local force sensor. The second functionality the haptic tweezers must realize is to render haptic display, so that operators are able to feel force feedback when contact or collision occurs. From this condition, an actuator system must be designed to render haptic display.

The amplitude of generated force in micro-scale is typically of the order of micro Newton. Therefore the haptic display must be scaled into human sensing capability, linearly or nonlinearly depending on filter condition or other signal processing. The figure 4.11 (b) illustrates the haptic information is displayed to operators.

For the considerations of safety and energy consumption, maximum input voltage and current are 100 V and 2 A respectively.

4.3.2.2 Manual Control Mode

The requirement of being a tweezers imposes constraints on geometric and mechanical properties. With those properties more close to a conventional tweezers, more intuitiveness are promoted. Several specifications can be deduced:

- mechanical stiffness of clamping at fingers: 250 N/m;
- static opening width at lever tips: typically 7 mm (may subject to change according to specific applications and tips installed);
- static opening width at position of finger attachment: from 9 to 15 mm;
- length of levers: from 115 to 160 mm;
- width of levers: from 11 to 50 mm;
- total mass: from 5 to 70 gram;

The constraint of being a tweezers sounds trivial but actually excludes many design options. The haptic interface developed in [Burdet 2004] conforms to tweezers working principle. However, the actuator system installed at the tip is a direct obstruction of manual control mode. Likewise, the da Vinci surgical interface [da Vinci-Surgery 2015] cannot work in manual control mode by the same reason. The electronic tweezers designed by [SERVOMEDICS 2015] can work in manual control mode. However, the way to operate does not conform to conventional usage.

However, the benefits are worth the challenge. When target objects are held steady by the haptic tweezers, the holding force can be maintained and adjusted precisely by the mechatronic system of the interface, instead of operator's hand. This can directly reduce fatigue and enhance manipulation efficiency. Technically speaking, the actuator system must be able to generate a minimum level of force (at finger attachment position) in order to balance the mechanical stiffness, 250 N/m. In order to compute this minimum level of output force, the maximum clamping displacement at finger position must be considered. Based on geometry, this displacement is slightly (depending on specific model) smaller than the static opening at the tip. For design margin, this value can be set as the static opening: 7 mm. As a result, the effective force generated by the actuator system must be at least:

$$F_{act} = 250N/m \times 0.007 = 1.75N \tag{4.1}$$

The force generated by the actuator system must be at least 1.75 N.

4.3.3 Technical Specifications of the TéléTweez

The study on the mechanical characteristics of the tweezers used in watchmaking process and their usage provides critical basis for the design of the TéléTweez. The best way to achieve intuitiveness is to design the mechanical properties of the TéléTweez being similar to the tweezers used in conventional watchmaking process. In 4.3.2, two functioning modes are described: robotic control mode and manual

Technical Specifications of the TéléTweez	
Robotic Control Mode	sensor for opening status
	actuator sys. for haptic display
	max. input 100 V and 2 A
Manual Control Mode	tweezers based structure;
	mechanical clamping stiffness: 250 N/m ;
	static opening at tip: 7 mm
	static opening at finger pos. : 9 - 15 mm;
	length: 115 - 160 mm;
	width: 11 - 50 mm;
	mass: 5 - 70 g;
	min. output force: 1.75 N.

Table 4.3: Technical Specifications of the TéléTweez.

control mode. In the analysis of robotic control mode, several electronic specifications are described. In the analysis of manual control mode, more geometric and mechanical specifications are derived. By combining the studies of the two modes, the complete set of the technical specifications of the TéléTweez can be derived. They are summed up in the table 4.3.

In this section, the tweezers used in conventional watchmaking process is investigated and the functionalities of haptic tweezers are described. The technical specifications the TéléTweez are derived. In the next section, the mechatronic design of the TéléTweez will be presented.

4.4 Mechatronics Design

In the previous section, the specifications of the TéléTweez have been derived. Briefly, the TéléTweez must be a tweezers and its dimension must be close to the dimension of a conventional tweezers; besides, it must embed sensor and actuator address robotic and manual control modes. Central to the challenges of concept design lies in the choice of actuator and how to use it to render haptic display, given the limitations of dimension and power input. In this section, the design of actuator system will be firstly studied, followed by mechanical and electronic consideration.

4.4.1 Actuator System Design

The actuator system consists of an actuator and a transmission chain. It can convert electric energy to mechanical energy. The mission of the transmission chain is to realize the energy flow between the two levers and the actuator. Since space is

limited, the most effective layout of the actuator system is to take advantage of the length of the interface, as shown in the figure 4.12. The design of the transmission chain depends on the type of the specific actuator. Therefore, the currently available actuator technologies must be firstly surveyed.

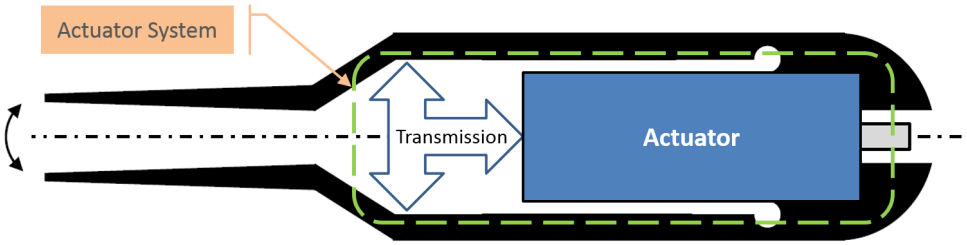

Figure 4.12: The schematic diagram of the actuator system.

Except conventional DC/AC actuators, many studied are dedicated to new actuators using various smart materials in recent years. However, smart materials are mostly in development phase, a few of them are mature for industrial production. Several popular smart materials are expected to be studied in order to see the possibility to fit into the TéléTweez design.

Electrorheological fluids (referred as ERF for the rest of the chapter) are liquids that respond mechanically to electric fields by changing their properties, such as viscosity and shear stress electroactively. In terms of the composition, they are suspensions of extremely fine microparticles in an electrically insulation fluid. They are sensitive to electric fields. The microparticles respond to the external field like electrical dipoles and in such a case they form cluster chains along field lines [Wen 2008] [Odenbach 2010]. The alignment of the particles along field lines causes the apparent increase of viscosity on a macroscopic scale, which can change reversibly by an order of up to hundred thousand in response to an electric field. For example, a typical ERF can go from the consistency of a liquid to that of a gel, and back, with response times on the order of milliseconds [Régnier 2008]. The increase in viscosity can be used for energy dissipation.

Magnetorheological fluids (referred as MRF for the rest of the chapter) are suspensions of micron-sized ferromagnetic particles (typically 1 to 10 micron meter) in a nonmagnetic host liquid (mineral oils, synthetic oils or water). They are rheological fluids alternative to ERF [Odenbach 2010]. The behavior and mode of operation between MRF and ERF are similar, except MRF responds to magnetic instead of electric field. Compared to ERF, typical MRF can generate rheological effect with voltage input below one hundred volts with maximum stress about 20 times greater than that of ERF [Régnier 2008]. Therefore, it has less constraints regarding power input compared to ERF.

Piezoelectric materials refer to the substance characterized the piezoelectric effect, which describes the reversible relation between the applied mechanical stress and the accumulated electric charge inside materials [Galassi 2012] [Polla 1998].

Smart Material Type	motion stroke	force	precision	bandwidth	dynamics
Piezoelectric material	limited	large	high	high	fast
MRF	passive	high		high	nonlinear
ERF	passive	medium		high	nonlinear
Shape memory alloy (e.g. NiTi)	high	high		low	nonlinear, hysteresis, thermal
Magnetostrictive alloy (e.g. Terfenol-D)	medium			high	
Electroactive polymers	high	low		medium	

	footprint	power req.	price	commercialization
Piezoelectric material	small	high	medium	high
MRF		low	low	low
ERF		high	low	low
Shape memory alloy (e.g. NiTi)		low		low
Magnetostrictive alloy (e.g. Terfenol-D)				
Electroactive polymers		high		

Table 4.4: Comparison of different types of smart materials.

They are non conductive materials and can be divided by two categories: crystals and ceramics. Such materials are applied in many industrial sectors. One application example is to embed piezoelectric materials inside cars' airbag system. The material detects the intensity of the shock and sends an electrical signals to trigger the airbag in case of considerable accident.

There are also other types of smart materials such as shape memory polymer, shape memory alloy, magnetostrictive alloy, electroactive polymer, etc. A brief

survey of all those smart materials is listed in the table 4.4.

In the following text, five design options will be studied and presented in the order from the least realizable to the most realizable. They are based on different actuators: electrorheological fluids, magnetorheological fluids, stack piezoelectric material and DC motor. The layout of all The design options is set to align with the length direction of the interface to optimize space occupation. The design of the transmission chain varies with respect to the choice of actuator.

4.4.1.1 Option 1: Electrorheological Fluids

This concept mainly consists of a sealed piston filled with ERF and a moving core inside the piston. Through the transmission chain, the opening of the TéléTweez is converted to the linear motion of the core inside the piston. The schematic diagram is shown in the figure 4.13. Under a given density of electric fields, ERF inside the piston can change state from liquid to solid, which produces motion resistance or complete block effect. Since the piston can only impede movement, this design option aims to work as a brake system. The moving core of inside the piston can be designed to have multiple layers to increase resistance from ERF effect.

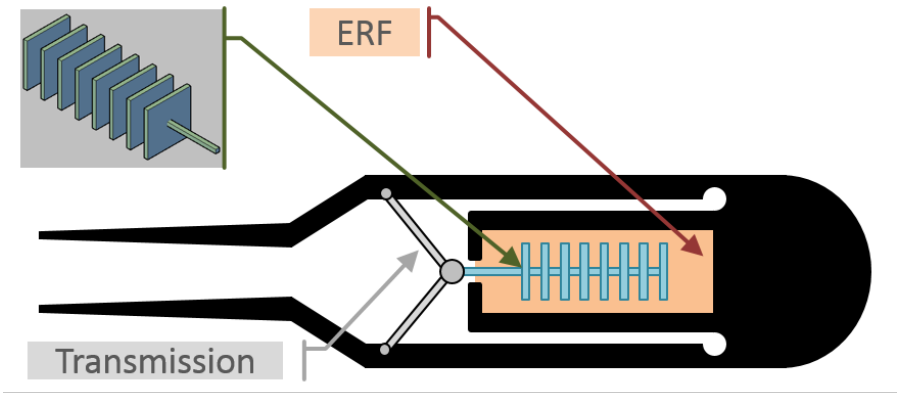

Figure 4.13: The actuator system concept with piston filled with ERF.

After survey of ERF product from laboratories and industries, the available ERF cannot give rise to significant electrorheological effect if the applied electric field strength is lower than 1 kV/mm, as explained in [Yongliang 2010]. Recall that the input voltage cannot be greater than 100 V. As a consequence, this design option is not compatible with our technical specifications.

4.4.1.2 Option 2: Magnetorheological Fluids

The concept principle is analogous to the option 1 : providing resistance by increasing the viscosity of fluids inside the piston. The design differs in the fluid solution, MRF instead of ERF. Furthermore, there are two configurations to generate magnetic field. The configuration 1 is to wind copper coil directly around the piston.

In this situation, the magnetic field is along the axis of the piston. The configuration 2 is to take advantage of ferromagnetic materials to enhance magnetic field. The figure 4.14 illustrates two configurations respectively. In the second option, four commercial electromagnet are employed and set up perpendicularly to the piston. Each electromagnet contains a ferromagnet cylinder inside in order to enhance magnetic field.

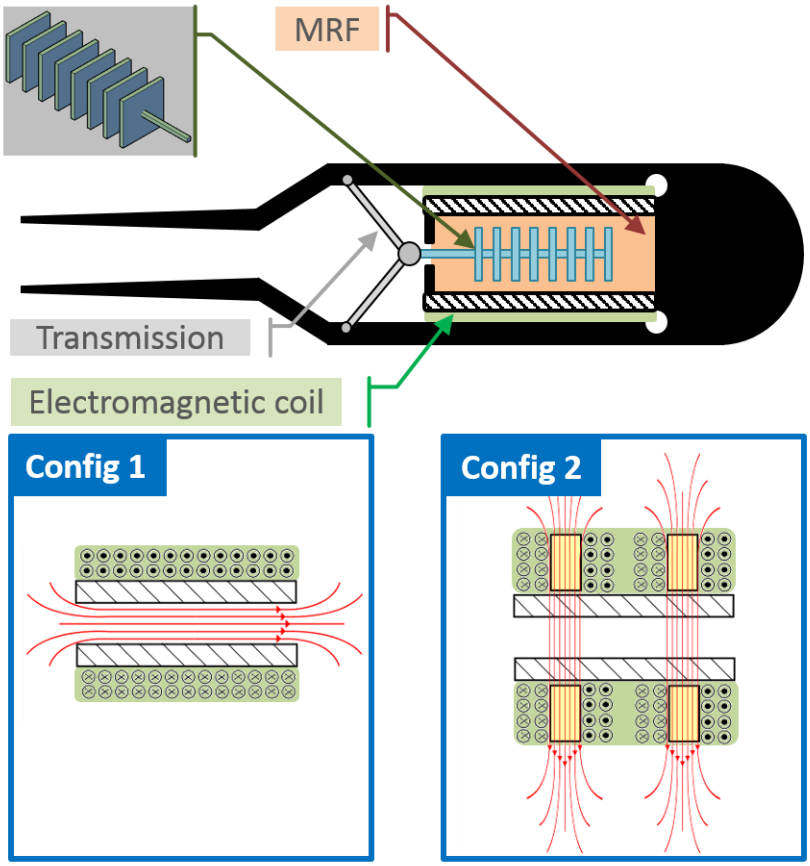

Figure 4.14: Two MRF piston configurations. Config 1: the piston is wound by copper coil. The magnetic field is along the axis of the piston. Config 2: four small electromagnet are set up perpendicularly to the axis of the piston. Each electromagnet has a cylinder ferromagnetic material inside to enhance the magnetic field.

Several experiments are conducted to test maximum force output with limited power input according to technical specifications. As a consequence, neither of the two options meets the minimum requirement of force output.

4.4.1.3 Option 3.1: Stack Piezoelectric Materials

Similar to the previous two design options, the concept consists of a piston for providing resistance. Inside the piston, the moving part is a cylinder of stack piezoelectric material with a shell wrapped around, as shown in the schematic diagram 4.15. With power applied to the piezoelectric material, it deforms along the axis of cylinder. This deformation must be transformed to the perpendicular direction provide friction resistance. In the following text, the perpendicular transformation is referred to as *transverse expansion*. The purpose of the shell wrapped around is to convert the deformation in axial direction to a maximum level of transverse expansion. This shell will be referred to as *mechanical amplifier*.

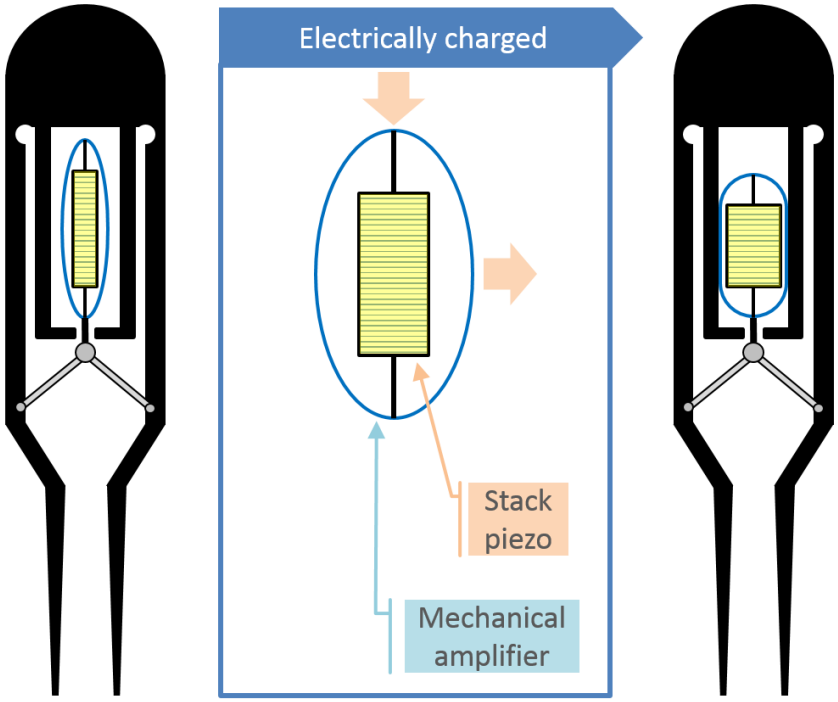

Figure 4.15: The actuator system concept using stack piezoelectric material. The left part of image zooms into the detail of the piston. This part is wrapped by a mechanical amplifier which converts the direction of the transformation of piezoelectric effect.

Considering the small deformation range of piezoelectric materials and the limited dimension of the cylinder, the amplifier must be compact, simple and efficient. Given the deformation along the cylinder axis, the geometry of the mechanical amplifier must be optimized to maximize the transverse expansion. The appendix A shows details about the geometric optimization of the mechanical amplifier.

After obtaining the optimized geometry of the mechanical amplifier (see the appendix A), a survey about commercial piezoelectric materials is carried out in

Piezoelectric cylinder	Length L (mm)	δL (μm)	Radius (mm)	e (mm)	a (mm)	Trans. exp. $2\delta a$ (mm)	Ratio $2\delta a/\delta L$
PI P-007.40	54	60	3.5	5	3.5+2	0.34	5.7
PI P-010.80	107	120	5	5	5+2	0.97	8
PI P-010.40P	58	60	5	5	5+2	0.29	4.8
PI P-010.80P	111	120	5	5	5+2	1.0	8.3

Table 4.5: Comparison of different types of PI piezoelectric products. The column $2\delta a$ denotes the transverse expansion. Refer to the appendix A for details about the description of each parameter.

order to list potential products which can match the design. Several candidates from the supply Physik Instrumente (PI) are listed in the table 4.5. From the table, it can be seen the best transverse elongation can be obtained up to 1.0 mm, with PI P-010.80P.

From the analysis above, the maximum transverse expansion is about 1 mm. From zero to 1 mm as transverse expansion, the piston must have precise geometry to make a difference between fluent passage and brake effect. Furthermore, the mechanical amplifier must be realized with thin and rigid material to satisfy the hysteresis. To sum up, this concept is theoretically realizable but demands high fabrication precision and expensive material.

4.4.1.4 Option 3.2: Stack Piezoelectric Materials

The previous concept requires high precision in piston geometry and rigid material for mechanical amplifier, which gives rise to difficulties in realization and therefore high cost. In this part, an alternative concept based on stack piezoelectric materials is presented.

Being analogous to brake mechanism of bicycle, in this concept, the resistance force is provided by applying friction to relative motion, and the friction is obtained by imposing surface contact. The figure 4.16 illustrates the brake mechanism which provides resistance. The red thin plate together with the black part are attached to one lever of the TéléTweez; while the yellow shell with a gray piezoelectric material are attached to the other lever. When no resistance is needed, the red plate can go freely through the gap between two yellow parts. If resistance is needed, the piezoelectric material elongates and results pressure induced friction. Since the range of deformation of the piezoelectric material is limited, the gap between two yellow parts must be precisely set up according to the thickness of the red plate and the deformation capability of the piezoelectric material. In order to avoid frication complexity due to precision requirement, four fine screws are used to allow adjust the gap manually. They are represented by four red long shafts in the image.

In order to evaluate the design, a concrete piezoelectric material must be selected.

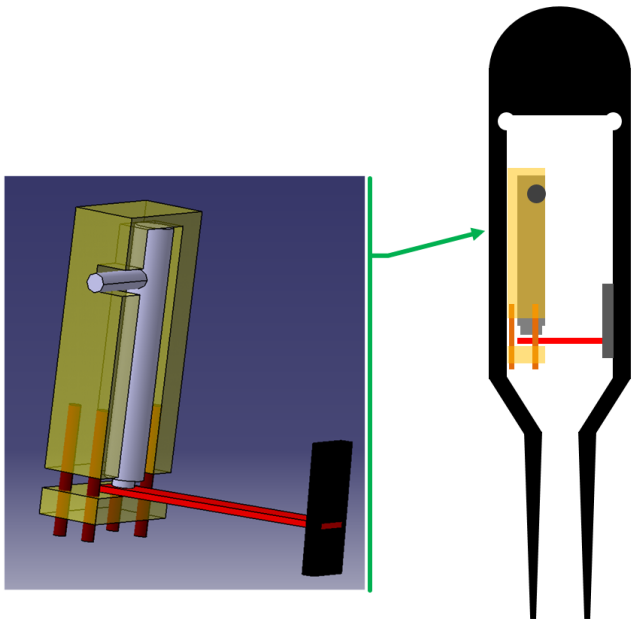

Figure 4.16: The pressure subsystem of the TéléTweez concept. The four red shafts stand for four screws to adjust distance between the cap and the piezoelectric cylinder.

After investigation of candidate products available in the market, the PI stack piezo actuator P-830.20 is chosen for this concept. Its maximum required power supply is 100 V. The maximum travel range is 30 micron meter and its maximum push force is 1 kN. The mass of this actuator is only 16 g and its length is about 4 cm. Assume in a normal working situation, the system is configured so that the actuator has to contribute its 85% travel range to fully press the thin plate. Since more deformation the actuator performs, less push force it will behave. A safe assumption is made that the push force would be reduced by the same ratio as that of deformation. Therefore, the maximum push force it can perform is:

$$F_{push} = 1000N \times (1 - 0.85) = 150N \tag{4.2}$$

Assume the friction coefficient between the thin plate and the piezoelectric actuator is only 0.1 and the geometry coefficient is 0.5 (the ratio to convert the friction to the force that acts between the two tips of tweezers). With all the assumptions and physical parameters stated above, the maximum resistance force that acts between the two levers can be derived as:

$$F_{block} = F_{push} \times 0.1 \times 0.5 = 7.5N > F_{act} = 1.75N \tag{4.3}$$

The resulting resistant force is much higher than the value indicated in the technical specifications, therefore, this design option for the actuator system can be

considered realizable.

4.4.1.5 Option 4: DC Motor with Ball Screw

All the previous design options for the actuator system have one common characteristics: they can only provide passive resistance. A new actuator system is presented here, which consists of a DC motor and a ball screw. The main difference between this design with respect to all other previous options lies in the fact that it can also provide active force output.

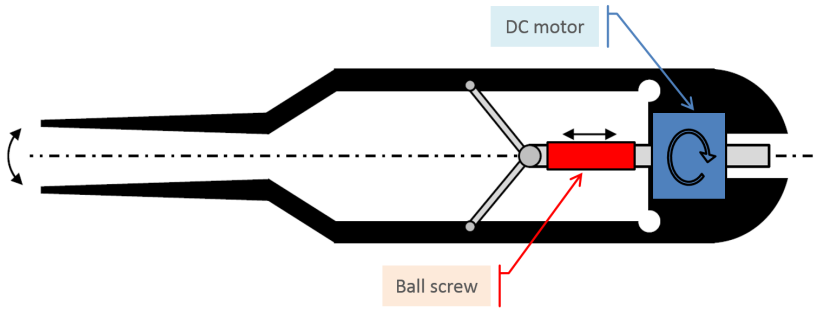

Figure 4.17: The schematic diagram of the concept based on DC motor and ball screw. In this section view, the blue rectangle represents the DC motor; the red bloc stands for the ball screw.

The figure 4.17 illustrates the working principle. Through the ball screw, the rotation of the motor can be converted to linear motion. The linear motion can then be transformed to the change of opening via the two rod-pivot structure. For robotic and manual control mode, the ball screw must be reversible. If rotation leads to translation (haptic display), it will be referred to as *forward transmission* in the following for the ball screw; if translation gives rise to rotation, it will be referred to as *backward transmission*. For each case, the transmission efficiency is a function of ball screw angle θ (see the figure 4.18) and friction coefficient. They are summarized in the figure 4.19. Refer to the appendix B for detail.

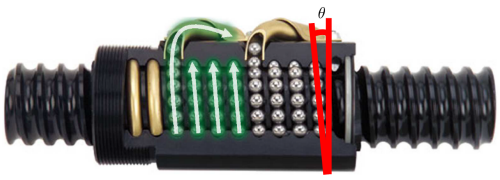

Figure 4.18: Rockford ball screw [Rockford 2016].

From the figure 4.19, it can be seen that the smaller the friction coefficient, the higher the transmission efficiency for both cases. Depending on the choice of μ, a range of θ can also be found to favor both cases. A list of commercial products can

Supplier	Ref.	Dia. (mm)	Lead (mm)	Forw. eff.	Backw. eff.	Price (euro)
Eichenberger	Carry ZYI	4.0	1.0	0.89	0.87	633
HIPP	KGT-Z1-03-01	3.0	1.0	0.91	0.90	1013
Steinmeyer	1214/1.3.76.90	3.0	1.0	0.91	0.90	796

Table 4.6: Commercial ball screw ball candidates.

be found with compatible size, but most suppliers do not provide the property of friction coefficient. In order to proceed the choice of ball screw, it is considered as $\mu = 0.01$, which is often found in the literature. Three options are shown in the table 4.6. Eichenberger Carry ZYI is finally chosen because of its comprise between price and efficiency.

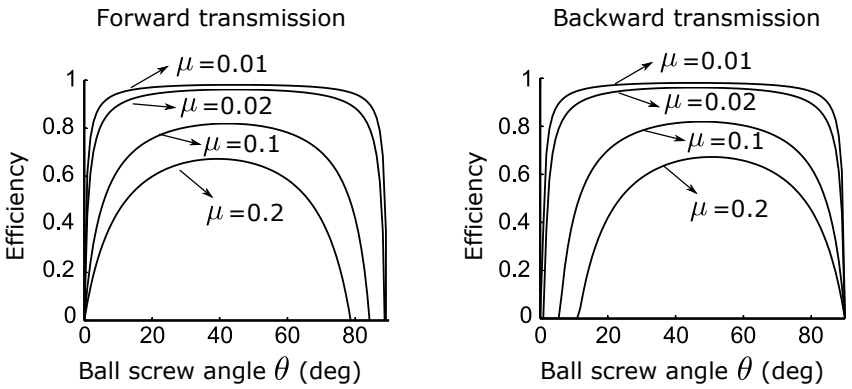

Figure 4.19: Ball screw transmission efficiency. Refer to the appendix B for detail.

In terms of the criterion for choose the motor, the size, weight, required power and output torque (continuous) must be considered to match the required specifications. Furthermore, the inertia and resistance must be as low as possible so as to promote haptic fidelity and ease of usage. Based on those considerations, a customized Maxon DC coreless motor is chosen. The dimension is 28 mm long and 10 mm as diameter. The mass is only 13 g and the rotor inertia is 0.151 gcm^2. The nominal required voltage is 4.5 V and the maximum continuous current is 0.64 A. The maximum continuous output torque is 2.2 mNm. From the equation B.2 in the appendix B, the output translation force can be computed with torque of motor:

$$F_a = \frac{2\pi\eta_f C}{p} = 12.3N \tag{4.4}$$

Though the overall geometry or transmission is not yet fixed, the scheme 4.17 can lead to a rough estimation of output force acted at finger position. By optimizing the simple geometry, the force reduction factor (from output translation force to force

Actuator system options	Power supply	Minimum force output	Active/passive force rendering	Realization difficulty
Option 1 (ERF)	$>$ 100 V	$<$ 1.75 N	Passive	High
Option 2 (MRF)	$<$ 100 V	$<$ 1.75 N	Passive	High
Option 3.1 (PM)	$<$ 100 V	$>$ 1.75 N	Passive	High
Option 3.2 (PM)	$<$ 100 V	$>$ 1.75 N	Passive	Low
Option 4 (Motor + ball screw)	$<$ 100 V	$>$ 1.75 N	Passive and Active	Low

Table 4.7: Evaluation of the Actuator system options.

sensed by finger) can be controlled within a reasonable level so that the specification of minimum output force of 1.75 N can be fulfilled.

4.4.1.6 Evaluation of the Actuator System Options

In the previous text, five design options are presented for actuator system. Studies are carried out to analyze the pro and con for each option. A table 4.7 is established below to summarize essential properties of each option.

From the table, it can be determined that the option 4 (motor and ball screw) meets the power supply and minimum force output requirement, and it is not difficult to realize. Furthermore, it is the only design option which can realize active force rendering. Therefore, this option is chosen as the actuator system for the TéléTweez.

4.4.2 Mechatronic Design of the TéléTweez

Transmission must be designed so that the output from motor and ball screw can be converted to tweezers state change and haptic display. Classical solution such as what is illustrated in the figure 4.17 leads to an issue that the transmission ratio depends on the state of the opening or the angle of the pivot, which means the ratio is not constant during operation. In order to deal with this problem, a contact mechanism is proposed, as shown in the figure 4.20. It is composed of a roller and a arc-surface track (green curve in the figure 4.20). The roller is attached to the slider (driven by ball screw) and the arc-surface track is part of lever geometry. The arc-surface can satisfy the condition that whatever the opening state, the normal direction of the contact surface must always form the same angle with respect to the axial direction.

According to the transmission structure, the force ratio is:

$$\frac{F_Y}{F_X} = \frac{\eta_t}{\tan\alpha} \tag{4.5}$$

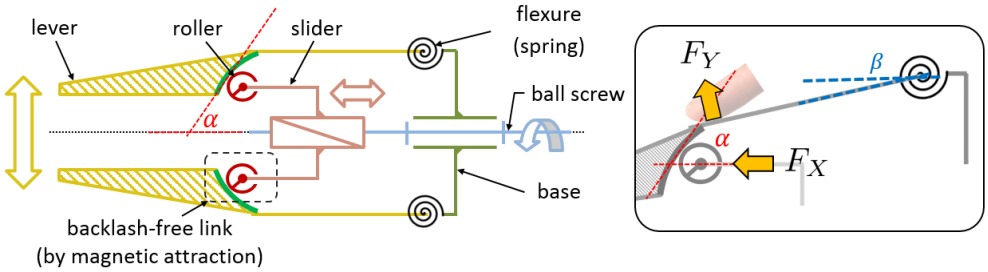

Figure 4.20: Scheme of transmission. The right part of the figure illustrates that the force transmission ratio depends only on α, but not the opening state β.

where α is the angle between the tangent of contact and the axial direction. Since α is designed to be constant, the force ratio is constant. The term η_t is the transmission efficiency when friction is considered, and it can be computed the same way as presented in the appendix B. With the available roller options such as ball bearings, a high value can be obtained for η_t. The force F_X is half of the translation force provided by ball screw (consider two levers are symmetric), and F_Y is the haptic feedback to user. The angle α must be designed based on the technical specification of minimum output force (1.75 N) and the maximum translation force (equation 4.4) provided by actuator system. It is chosen as $\alpha = 63°$ so that the maximum haptic force F_Y can be from 2 to 3 N. Note that the force ratio is a tangent function which is steep around 63°. In other words, the force ratio is sensitive to the variation of α. Therefore, keeping α constant can promote haptic fidelity.

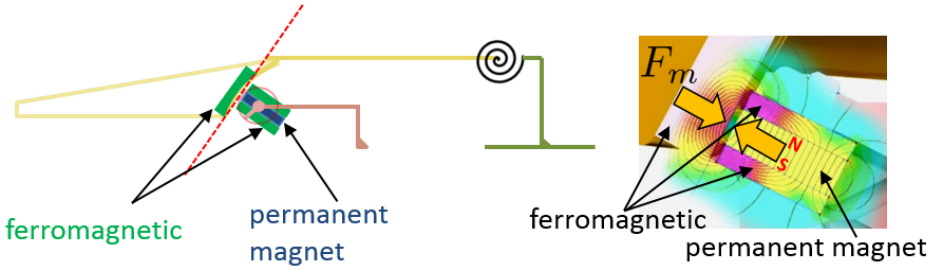

Figure 4.21: Backlash-free link by magnetic attraction. The right part of the figure shows the attraction force and the flux flow.

The transmission mechanism described above cannot handle the situation when closing of tweezers must be driven by motor. To deal with this problem, attraction preload between the lever and slider near the roller position can be implemented to ensure permanent contact between roller and arc-surface track. As illustrated by the figure 4.21, the attraction is realized by one permanent magnet and a ferromagnetic circuit fixed respectively on the side of slider and lever. High magnetic permeability

material is used to maximize flux flow in limited space. The magnet and ferromagnetic materials must be in very near proximity, but not in touch in order to prevent sliding friction during relative motion. Considering the force F_Y during closing is 1.75 N and the angle as $\alpha = 63°$ defined above, the minimum attraction force must be greater than 3.9 N to ensure contact between roller and lever track. Commercial magnets with compact size are already available to meet this requirement. Another advantage of the preload attraction is to avoid backlash. This can both favor the aspects of control and haptics.

The mechanical stiffness is realized with flexure (thin metallic sheet) as indicated by the figure 4.20. This choice can also help reduce backlash.

In terms of electronics, motor driver and amplification circuits are embedded into the TéléTweez. For position sensing, strain gauges are glued on the flexure for each lever; an infrared sensor is installed to measure the translation of slider; a magnetic rotary encoder is mounted on the rear shaft of the motor to measure the rotation. An accelerometer of 3 axes is mounted on the base. For force sensing, a resistive polymer is installed at the finger pressing position, and force can also be estimated from current of motor. The total power requirement is dominated by motor, the maximum power input is 4.5 V and 1.3 A.

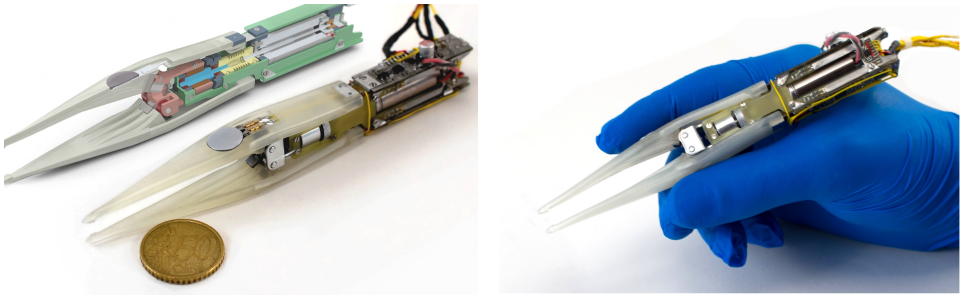

Figure 4.22: TéléTweez CAD and prototype.

The final CAD and the first prototype is shown in the figure 4.22. The table 4.8 summarized the comparison between the technical specifications and real performance of the prototype. It is important to mention that the real mechanical stiffness is less than expected. This is mainly due to the limited material choice used in 3D printing for levers. This can be solved by using stronger flexure and stiffer material for levers (if by other process than 3D printing). Static opening is slightly different, that might not influence operation intuitiveness. If so, it can be easily corrected in fabrication process. Apart from those, it can be seen that the prototype of TéléTweez meets the requirement from specifications.

	Technical Specifications	TéléTweez prototype
Robotic Control Mode	sensor for opening status	pos. (strain gauge, infrared, magnetic rotary encoder, accelerometer) + force (resistive polymer)
	actuator sys. for haptic display	reversible ball screw + DC coreless motor
	max. input 100 V and 2 A	4.5 V and 1.3 A
Manual Control Mode	tweezers based structure	compatible
	mechanical clamping stiffness at finger: 250 N/m	190 N/m
	static opening at tip: 7 mm	10 mm
	static opening at finger pos. : 9 - 15 mm	22 mm
	length: 115 - 160 mm	144 mm
	width: 11 - 50 mm	14.5 mm
	mass: 5 - 70 g	39 g
	min. output force: 1.75 N	2.2 N

Table 4.8: Comparison between desired technical Specifications and the performance of the TéléTweez prototype.

4.5 Dynamics Analysis and Virtual Environment Application

In the previous section, various options about actuator system are studied and the final complete design as well as the prototype are presented. In this section, the linear dynamic model of the TéléTweez will be firstly developed. Then the haptic bandwidth will be identified. At last, a virtual environment application will be demonstrated. Those studies allow for a better understanding of the system dynamics and pave the way for future sophisticated control strategies.

4.5.1 Dynamic Modeling

The dynamic modeling to develop corresponds to the working scenario that haptic signal, which is represented by input motor torque, is sent to the TéléTweez and the overall interface responds with two fingers holding each lever. In this preliminary study, we focus on the establishment of the dynamic modes, which will be essential for future haptic control applications. Before proceed to dynamic modeling, several assumptions and conditions are made:

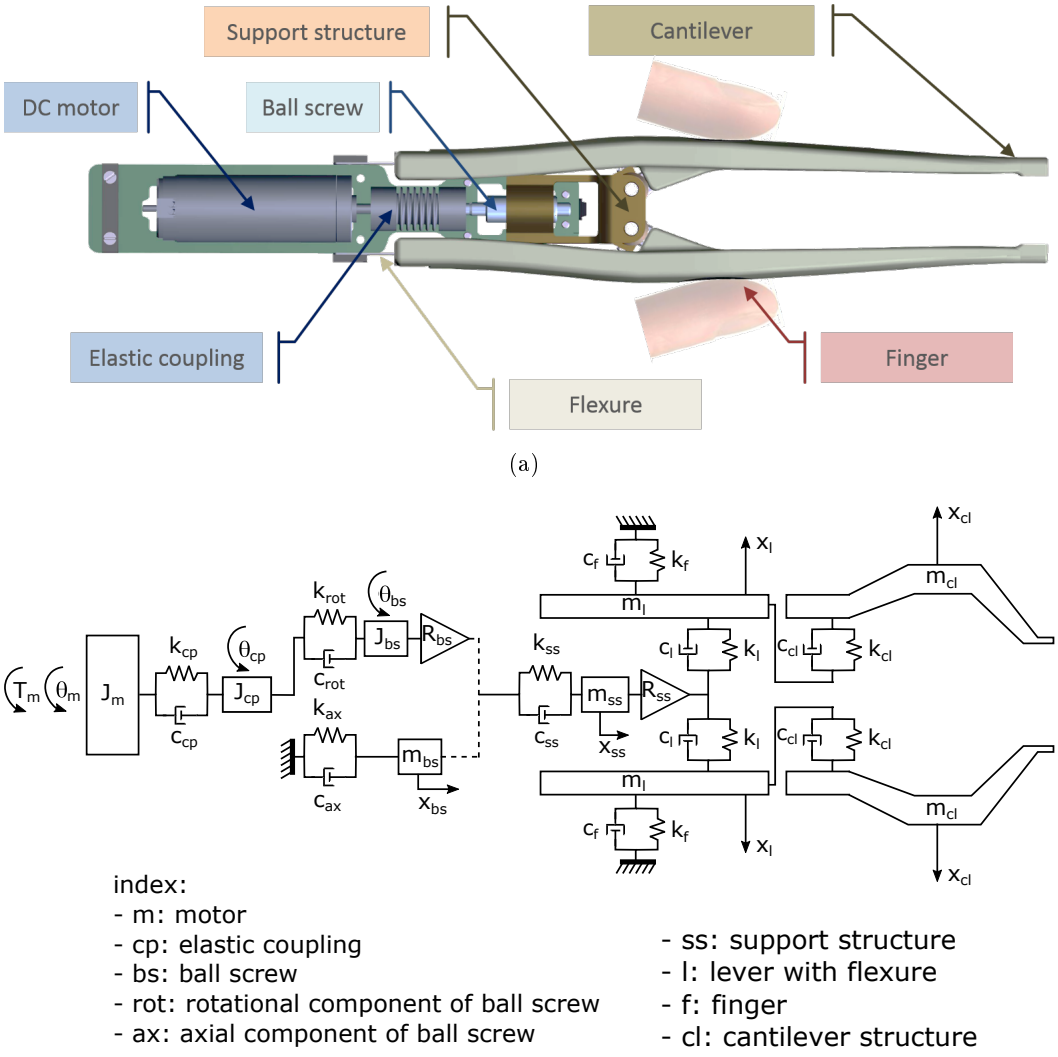

Figure 4.23: Dynamic modeling of the TéléTweez. (a) Flexible components of the TéléTweez, which give rise to dominant dynamic modes. (b) Bloc diagram of the TéléTweez.

- only considering linear time invariant model, nonlinear components such as friction or hysteresis are not considered;
- the TéléTweez is symmetrically held by two fingers at each lever;
- the dynamics of the two levers are considered identical;
- the dynamics of the two fingers are considered identical;
- the finger can be modeled as a second order spring-damping system [Wiertlewski 2012];
- the gravity is not considered.

The TéléTweez is a complex and highly coupled system. The dominants dynamic modes result from flexible structures. As shown from the figure 4.23 (a), the components we consider in this study are the DC motor; the elastic coupling between the DC motor and the ball screw; the ball screw; the support structure fixed with the nut of the ball screw; the fingers of operator; the flexure which generates the mechanical stiffness of the levers; and the long stretched-out cantilever structure (tip of the TéléTweez). Except the ball screw, all other flexible components can be modeled as a second order spring-damping system. As for the ball screw, generally it can be characterized as a system with three dynamic modes: axial, rotational and flexural. Typically the first axial and rotational mode dominate the ball screw dynamics [Frey 2012] [Henke 2014]. Therefore, a discrete model of the ball screw with the first axial and rotational mode is established in our study.

The figure 4.23 (b) illustrates the bloc diagram. The parameter J_m denotes rotary inertia of the DC motor, θ_m and T_m are respectively the rotation angle and the torque of the motor. The J_{cp}, k_{cp} and c_{cp} stand for the rotary inertia, stiffness and damping of the elastic coupling component. The axial and rotational mode of the ball screw are considered separated. The parameters J_{bs} and m_{bs} represent the rotary inertia and mass of the ball screw. The parameters k_{rot} and c_{rot} stand for the dynamics of the first rotational mode; while k_{ax} and c_{ax} are for the first axial mode. The parameter R_{bs} is the rotation-translation ratio ($R_{bs} = lead/2\pi$) of the ball screw. The parameters m_{ss}, k_{ss} and c_{ss} represent the dynamics of the support structure. R_{ss} is the transmission ratio between the axial motion and the opening of levers. For each lever, m_l represents the mass which is rigidly attached to the flexure, while k_l and c_l are stiffness and damping parameters of the flexure. The out stretched cantilever structure can be considered as a rigid mass m_{cl} connected to the rest of the lever with stiffness k_{cl} and damping c_{cl}. At last, finger dynamics can be represented by stiffness k_f and damping c_f.

The general matrix form of the linear dynamic model can be written as

$$\mathbf{M}\ddot{\mathbf{X}} + \mathbf{C}\dot{\mathbf{X}} + \mathbf{K}\mathbf{X} = \mathbf{F} \tag{4.6}$$

For the TéléTweez, each term is expressed below:

$$\mathbf{X} = \begin{bmatrix} \theta_m & \theta_{cp} & \theta_{bs} & x_{bs} & x_{ss} & x_l & x_{cl} \end{bmatrix}^T$$

$$\mathbf{M} = diag(J_m \quad J_{cp} \quad J_{bs} \quad m_{bs} \quad m_{ss} \quad m_l \quad m_{cl})$$

$$\mathbf{F} = \begin{bmatrix} T_m & 0 & 0 & 0 & 0 & 0 & 0 \end{bmatrix}^T$$

$$\mathbf{C} = \begin{bmatrix} c_{cp} & -c_{cp} & 0 & 0 & 0 & 0 & 0 \\ -c_{cp} & c_{cp}+c_{rot} & -c_{rot} & 0 & 0 & 0 & 0 \\ 0 & -c_{rot} & c_{rot} & 0 & 0 & 0 & 0 \\ 0 & 0 & 0 & c_{ax}+c_{ss} & -c_{ss} & 0 & 0 \\ 0 & 0 & 0 & -c_{ss} & c_{ss}+2c_l & -\frac{2c_l}{R_{ss}} & 0 \\ 0 & 0 & 0 & 0 & 0 & c_f & 0 \\ 0 & 0 & 0 & 0 & 0 & -c_{cl} & c_{cl} \end{bmatrix}$$

$$\mathbf{K} = \begin{bmatrix} k_{cp} & -k_{cp} & 0 & 0 & 0 & 0 & 0 \\ -k_{cp} & k_{cp}+k_{rot} & -k_{rot} & 0 & 0 & 0 & 0 \\ 0 & -k_{rot} & k_{rot} & 0 & 0 & 0 & 0 \\ 0 & 0 & 0 & k_{ax}+k_{ss} & -k_{ss} & 0 & 0 \\ 0 & 0 & 0 & -k_{ss} & k_{ss}+2k_l & -\frac{2k_l}{R_{ss}} & 0 \\ 0 & 0 & 0 & 0 & 0 & k_f & 0 \\ 0 & 0 & 0 & 0 & 0 & -k_{cl} & k_{cl} \end{bmatrix}$$

The linear model above described dominant dynamic modes of the TéléTweez in analytical form. It can help understand the overall dynamics, and is essential for developing sophisticated control strategies for future haptic applications. Since the parameters of the model are not known, it cannot be determined which flexible structure results the most dominant dynamic mode or what is the frequency information about the dominant dynamic modes. Instead of identifying the dynamics of each flexible component, in the next subsection, we aim to examine the overall frequency of the TéléTweez. That will help determine the frequency bandwidth within which the haptic display is uniform in magnitude.

4.5.2 Frequency Bandwidth Identification

The purpose of this subsection is to define the frequency bandwidth for haptic application. The input is the haptic signal, which is realized by the torque or current of the DC motor. The output is the acceleration produced at the contact position between the two levers and fingers. The acquired acceleration is considered as the perception of the haptic signals for human operator. In order to realize this signal acquisition, an 3-axis accelerator is attached at the position of finger contact, as shown in the figure 4.24. The acceleration signal that we are interested in is which aligns with the opening direction.

The input signal for identification must spread its energy evenly in frequency domain. For this purpose, the pseudo random binary sequence (PRBS) is taken as input signal. An analytical signal generator algorithm is directly implemented in the embedded controller so as to avoid memory restriction to store large precomputed

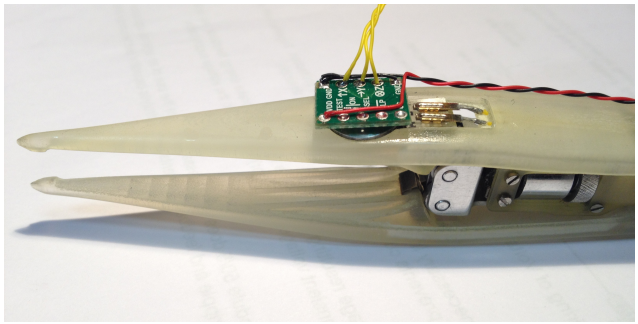

Figure 4.24: Accelerator setup to measure the bandwidth of the TéléTweez.

PRBS data. The sample frequency is set to be 10 kHz, so the range of inspection is from DC to 5 kHz.

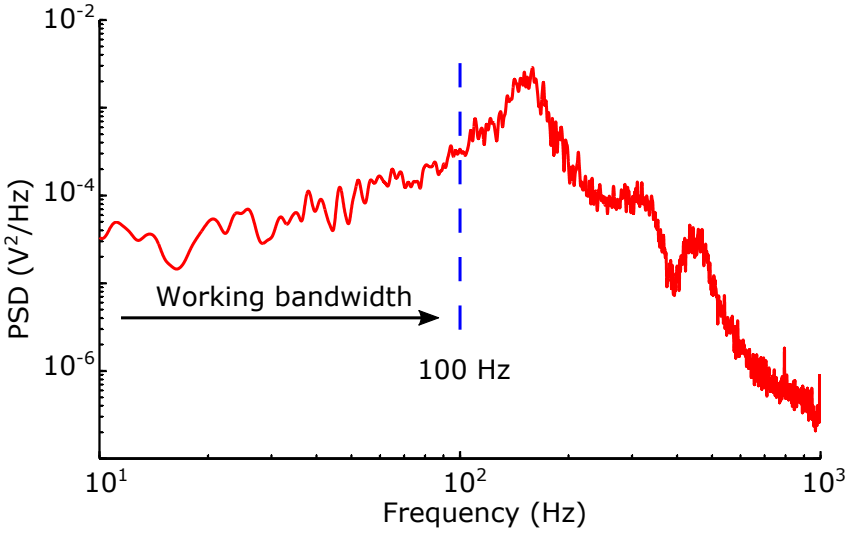

Figure 4.25: Frequency bandwidth of the TéléTweez: 100 Hz.

Same as the working scenario of dynamic modeling, one operator holds steady the TéléTweez with index and thumb fingers. During identification, PRBS is sent to the motor from the embedded real-time controller, and the acceleration signal is measured by AI channel of the NI DAQ card in 10 kHz. The result power spectrum density (PSD) against frequency is shown in the figure 4.25. From the figure, it can be observed that the most dominant dynamic mode is located at about 150 Hz, an anti-resonance occurs at around 390 Hz. The frequency bandwidth can be determined as 100 Hz, within which the haptic rendering has almost flat magnitude.

4.5.3 Virtual Environment Application

A virtual environment application is realized in order to demonstrate the haptic display of the TéléTweez. The electronic setup is illustrated by the figure 4.26.

A control card with microcontroller PIC 32 integrated is used to realize real-time application algorithms. An external battery box is connected to the TéléTweez to provide power for the motor and sensors.

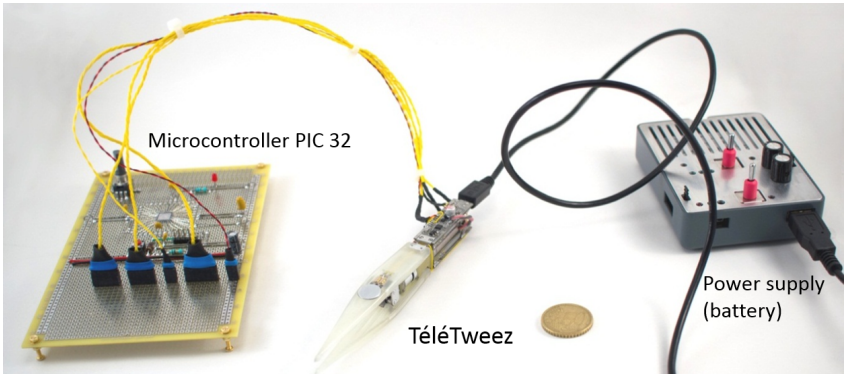

Figure 4.26: Microcontroller PIC 32, external power supply and TéléTweez.

In the application, a virtual cube is configured in the middle between two lever tips (with width smaller than static opening). Operator holds the TéléTweez and starts to pinch. When levers start to penetrate inside the virtual cube, a haptic force is feedback to user in order to oppose the action (see the figure 4.28(a) and (b)). The force employed in the application is based on a spring force model as a function of penetration distance.

Categorized as the classical virtual wall issue, implementing high stiffness can lead to chatter (instability). That is because in sample data implementation zero-order-hold operator is inevitable, which effectively introduces loop delays. The other factor is the possible asynchrony of wall threshold crossings with sampling times [Gillespie 1996]. Those two factors give rise to the instability issue in discrete virtual environment implementation.

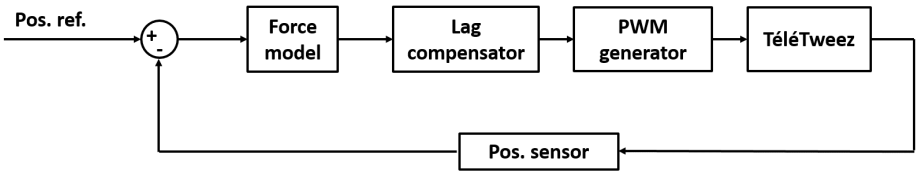

Figure 4.27: Block diagram for virtual environment application (in case of penetration inside virtual object).

To avoid the chatter issue in our application, a lag compensator is introduced (see the figure 4.27) in the closed loop. The idea is to reduce the amplitude of high frequency band (where chatter occurs) without introducing delay in that band. Frequency bandwidth identification indicates resonance occurs beyond 100 Hz (see the figure 4.25). Therefore, the corresponding frequency interval introduced by

compensator's pole and zero must be designed to be within 100 Hz so that high frequency signals are reduced in amplitude but without phase decrease.

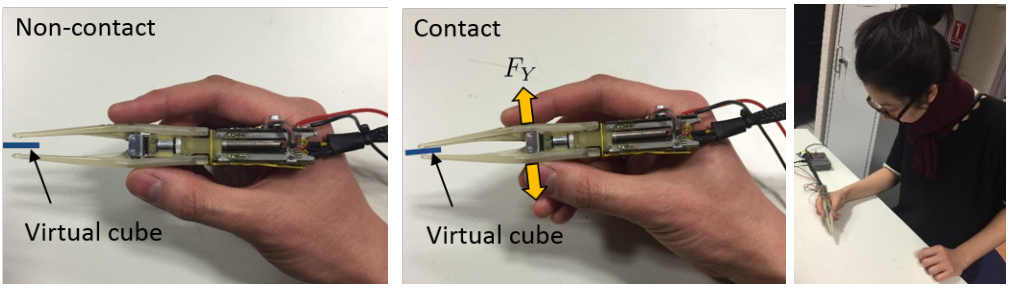

(a) (b) (c)

Figure 4.28: Virtual environment application: (a) when levers and virtual cube are not in contact, no haptic force is produced; (b) in case of contact, haptic feedback is provided to user. The force model is a spring model as a function of penetration depth; (c) people experience the virtual environment application.

With the spring force model, the virtual cube geometry and lag compensation implemented in the microcontroller, several people are invited to test the virtual environment application. Position and force data cannot be extracted to be plotted here in the current development phase because the microcontroller has too limited memory resource to store large data set and online communication of data will consume too much processing time to cause closed loop unstable. From the survey, it is reported that the usage is very similar to manipulating with conventional tweezers, in other words, it is intuitive to use. Besides, they are able to feel a stiff object between the tips and the interface is stable during haptic display (see the figure 4.28(c)).

4.6 Conclusion

In this chapter, a novel haptic interface concept, the TéléTweez, is designed and prototyped in order to achieve intuitive cobotic manipulation for watchmaking industries. The TéléTweez is compact and is equipped with electronic driver circuits and multiple sensors. The generation of haptic signal relies on a reversible actuator system which consists of a DC motor and a ball screw transmission structure. Frequency analysis suggests that the haptic bandwidth is from DC to 100 Hz. From the virtual environment application, it is reported that the TéléTweez is very intuitive to use and they are able to feel a stiff object between tips from haptic display. From the aspect of functionality, the TéléTweez is able to combine haptic interface and conventional tweezers. With this combination satisfied, the TéléTweez is believed to the first concept which can be commercialized.

In the next step, we aim to evaluate the TéléTweez by setting up rigorous tests of user experience in a watchmaking scenario. In particular, it is important to

investigate whether haptic display of the TéléTweez can help enhance watchmaking productivity and effectiveness. The TéléTweez will be implemented in the cobotic platform Chronogrip for tweezers based manipulation.

In the future, identification for each flexible component can be conducted to identify the source of the most dominant dynamic mode. That can be used to enhance the mechanical design and furthermore improve the frequency bandwidth. Based on the dynamic model, sophisticated control strategies will be studied and implemented to achieve versatile watchmaking applications. Though the TéléTweez is designed for watchmaking process, it can be potentially applied for a great variety of applications since the design is based upon a general purpose tweezers.

Conclusions and Future Works

Nowadays, there is a market window between large-batch automation and small batch handmade production for microsystems. The need for flexible micro-manipulation solutions is urgently demanded particularly par small- and medium-sized enterprises. For this purpose, microrobotic company Percipio Robotics has proposed a pioneer semi-automatic cobotic platform Chronogrip to address this need. However, the solution is not yet complete. Much efforts are needed to handle critical challenges in terms of trajectory tracking and haptic feedback. The objective of this thesis is thus not to design and realize a brand new cobotic platform, but to handle these challenges for the existing platform Chronogrip, which are concluded as follows:

Research 1: As the elementary positioning unit of Chronogrip, piezoelectric stick-slip actuator is a promising choice and widely applied for micro-manipulation for its high precision and speed, compact size, high energy/weight ratio, ease of integration, relative low cost, etc. But today the lack of fundamental study on its dynamics delays the development of trajectory tracking strategies. Commercial products and research results provide limited options for control aspect, which significantly constrains the development of microrobotic applications. The modeling of this kind of actuators is complex because: the system is coupled and involves nonlinearity (dynamics of the piezoelectric material, the friction dynamics and the dynamics of the moving slider); there is no systematic methodology for parameters identification; and existing friction models are often limited due to the complexity of the presliding motion. The consequence is that existing models are quite accurate for a limited working range, which is not sufficient when the microrobotic systems are involved for hybrid displacements (from micro- to milli-meter range). Chapter 2 proposes an extended dynamic model for microrobotic systems using piezoelectric stick-slip actuators. In the study, it is underlined that the modeling of hysteresis results from the coupled behavior between piezoelectric element and friction. Thus it cannot be dealt with by traditional identification method. The friction model is based on single-state elasto-plastic friction model. However, from the result of frequency analysis of piezoelectric element and the coupled actuator, we proposed two asperities to match the observed dynamics. At the same time, some conditions are emphasized in the friction modeling when different motion directions must be considered. Moreover, we show for the first time how the break-away displacement can evolve with the amplitude and the frequency of an input sawtooth signal. Results of ongoing research show that this dependence relies more on amplitude rather than frequency, and is not the same when the actuator is moving in a forward direction and in a backward direction. Finally, we managed to obtain a complete coupled nonlinear model being able to describe the dynamics of stick-slip type actuators for both scanning mode and stepping mode in the time and the frequency domains and for backward and forward directions of the motion. The model agrees with

experimental data and the validation of stick-slip actuator model in these operating conditions has never been demonstrated in the literature. At the end of the chapter, a velocity control strategy for large motion distance is demonstrated by using partial dynamic model. Results of this chapter open new perspectives for cinematic and dynamic models of robotic systems intended to do tasks at the micro scales. At the moment of writing, the identification for complete model is still on the way, when it is finished, results can be used for the development of dedicated trajectory tracking strategies (e.g. velocity and/or position control).

Research 2: The human sense of touch is exquisitely sensitive to vibrations, and this is over a significant band of frequencies reaching one kilohertz in healthy adult individuals. Although the displacement detection threshold is function of numerous factors, people remain through their lives extraordinarily sensitive to small oscillatory and transient mechanical perturbations, especially when applied to the hand. Human evolves to rely on wide range of sense of touch to make decisions and conduct intuitive operations. In the microworld, due to the complex physics, the motion and force in this environment are characterized by high dynamics in frequency domain. As a result, haptic interfaces applied to micro-manipulation cobotic platform ought to be able to transmit high frequency signals from DC to kilohertz range to a user's hand, lest the information that these signals contain be lost or tainted. Nowadays, available haptic interfaces have limited bandwidth much lower than kilohertz, which obstructs the development and implementation of microrobotic applications. The fundamental problem behind is by including cantilevered segments to achieve mobility, bandwidth is reduced. Hardly can any haptic interface option have its first dynamic mode higher than 1 kHz, unless a comprise must be made to reduce workspace. To overcome this problem, in Chapter 3, we describe a method for a dual-stage haptic interface design that can achieve a flat frequency response in the whole tactile range. Low frequency movements are transmitted by a parallel mechanism the Pantograph up to its first resonant mode 200 Hz. Since above a few hundred Hertz vibratory amplitudes become small, higher frequency oscillations are reproduced by an inertia-based, ungrounded actuator the Haptuator at the tip operating on the basis of conservation of momentum. Using a crossover technique borrowed from audio engineering combined with dynamic modeling, identification, and frequency compensation, a first haptic interface with an overall flat response over 1 kHz was achieved. The interface is applied in the experiment of haptic optical tweezers replay. It is reported that users can feel low frequency contact force as well as high frequency Brownian motion. A key advantage of this approach is to enable to use of conventional force feedback devices for applications were high bandwidth response is desired. Furthermore, it is the first kilohertz haptic interface with large working space and it opens new perspectives that with this method high dynamic phenomena in the microworld can be faithfully transmitted in order to enhance understanding of physics and conduct intuitive and effective operations. In the next step, the method is expected to be implemented in closed loop (motion control plus haptic feedback) in the cobotic platform, and sophisticated control strategy would be developed to maintain stability.

Research 3: High end watchmaking industry is featured by small batch handmade production of complex microsystems. However, handmade process has saturated accuracy and productivity, which makes the watchmakers more and more difficult to conquer their place in global competition. To handle this issue, Chronogrip is proposed for flexible and accurate watchmaking process. However, a significant problem is that the general purposed interfaces (joystick and tablet installed in Chronogrip) are not intuitive to use for watchmaking, because operators are trained for years with tweezers and therefore any other unfamiliar operating principle will not give rise to the same production criterion. Except the difference in operating principle, Chronogrip does not provide haptic display. It is shown in the literature that with haptic feedback, teleoperated tasks can be conducted with lower average force, more precision, smaller error rate and thus high productivity. Survey of available haptic interface options suggest there is no one that can satisfy the specifications of a haptic tweezers applied to intuitive watchmaking process. To handle this challenge, in Chapter 4, we aim to design and realize a haptic tweezers, TéléTweez, to meet the needs of intuitive tweezers based operations. Conventional tweezers are light and compact tools, hence intuitiveness imposes constraints on design criteria such as dimension, weight and form. Implementing haptics with limited conditions is challenging. Several actuator options are evaluated and the design based on DC coreless motor with reversible ball screw is chosen for its capability of output active/passive force, lower threshold of realization, low level of power requirement, etc. In terms of transmission, a link based on magnetic attraction is designed to ensure constant force reduction ratio and remove backlash. The first prototype was produced and evaluation shows that major design criteria are met. A virtual environment application is demonstrated and it is reported that people are able to operate intuitively as with a conventional tweezers. Moreover, with compensation implemented, they are able to feel hard virtual objects without chatter issue reported. Though designed for watchmaking process, the tweezers based principle determines that TéléTweez can be used in a wide range of applications where haptic tweezers principle is required.

To sum up, the three research programs are dedicated to handling critical challenges arising in the design and realization of micro-manipulation cobotic platform. In the near future, current research results are expected to implement in Chronogrip system to enhance micro-manipulation. In the long run, with the complete set of piezoelectric stick-slip actuator dynamic model and trajectory tracking strategies, desired complex trajectories can be realized; with haptic-bandwidth-extending method and necessary control algorithms for closed loop implementation, high dynamics microrobotic applications can be realized with enhanced understanding of physics and promoted operation intuitiveness; with a further optimization of TéléTweez, tweezers based micro-manipulation can be realized in the most natural way. With all combined, flexible micro-manipulation will be achieved.

Appendix A

Geometric Optimization of Mechanical Amplifier

This chapter studies the geometric optimization of mechanical amplifier discussed in the text 4.4.1.3. The figure A.1 illustrates geometric parameters. A hypothesis is made before further analysis: during deformation, the line segment c remains the same length. This condition must hold to ensure the deformation along the axis direction can be converted to the transverse expansion.

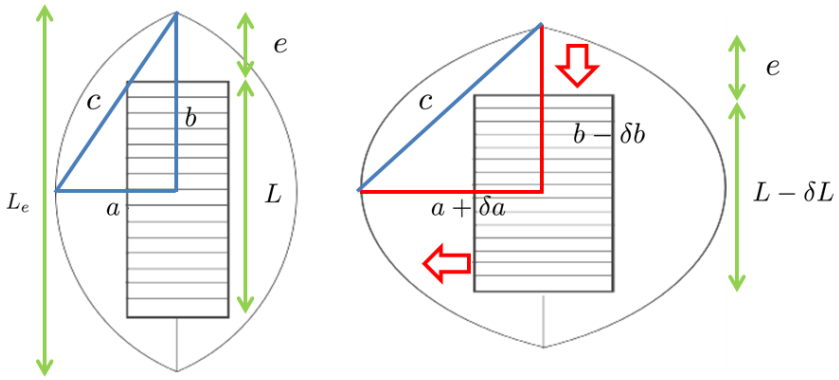

Figure A.1: Geometry of the concept of mechanical amplifier. δL denotes the longitudinal contraction due to the piezoelectric effect; two times of δa stands for the expected transverse expansion. Study the model analytically in order to maximize the ratio $\delta L/\delta a$.

In the figure, L_e and L denotes the length of the amplifier and piezoelectric material respectively without electrical charges applied; e the length of connection between the poles of the amplifier and piezoelectric material; δL the contraction; a, b and c the characteristic length of the triangle without deformation; δa and δb the elongation and contraction respectively when deformation occurs. Then, the analytical expression of the transverse expansion will be derived as a function of all geometry parameters:

$$\delta a = F(L, L_e, e, \delta L, a, b, c, \delta b) \tag{A.1}$$

For the triangle:

$$(a+\delta a)^2+(b-\delta b)^2=c^2 \tag{A.2}$$
$$a^2+b^2=c^2 \tag{A.3}$$

By combing those two equations above:

$$\delta a=\sqrt{a^2+2b\delta b-\delta b^2}-a \tag{A.4}$$

Consider geometric constraints:

$$b=\frac{L}{2}+e \tag{A.5}$$
$$\delta b=\frac{\delta L}{2} \tag{A.6}$$
$$L_e=L+2e \tag{A.7}$$

it can be deduced the resulting analytical form of the transverse expansion using independent variables:

$$\delta a=\sqrt{a^2+\frac{L_e\delta L}{2}-\frac{\delta L^2}{4}}-a \tag{A.8}$$

In order to optimize the transverse expansion δa, the geometry parameters a, δL and L_e are examined:

$$\frac{\partial(\delta a)}{\partial a}=\frac{1}{\sqrt{1+\frac{\delta L(2L_e-\delta L)}{4a^2}}}-1<0 \tag{A.9}$$
$$\frac{\partial(\delta a)}{\partial(\delta L)}=\frac{L_e-\delta L}{4\sqrt{a^2+\frac{L_e\delta L}{2}-\frac{\delta L^2}{4}}}>0 \tag{A.10}$$
$$\frac{\partial(\delta a)}{\partial L_e}=\frac{\delta L}{4\sqrt{a^2+\frac{L_e\delta L}{2}-\frac{\delta L^2}{4}}}>0 \tag{A.11}$$

From the results above, it can be determined that δa is proportional to δL and L_e, but inversely proportional to a. This indicates that a long and thin geometry is the optimized form. Combined with the hypothesis mentioned before, a schematic diagram of the mechanical amplifier can be shown in the figure A.2. The four orange parts constitute the skeleton of the amplifier and are connected by revolve joints. They must be rigid to satisfy the hypothesis. As stated above, the structure should be long and thin (but it must abide by geometry constraints) to provide optimized deformation conversion.

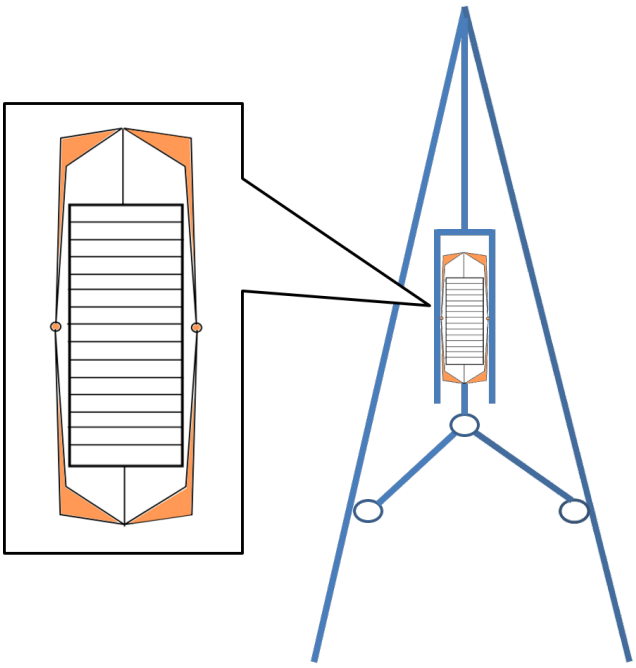

Figure A.2: The schematic diagram of the optimized mechanical amplifier.

Appendix B

Static Analysis of Ball Screw

This chapter aims to analyze statically the transmission efficiency of forward and backward transmission for ball screw.

As shown in the zoomed part of the figure B.1, the nut can be represented as an inertia, and the shaft in contact is the triangle characterized by the angle θ. The triangle is actually the 3D shaft unfolded on a plane. Therefore, the hight is period times of πd and the bottom side is period times of lead (For simplicity, we take 1 period).

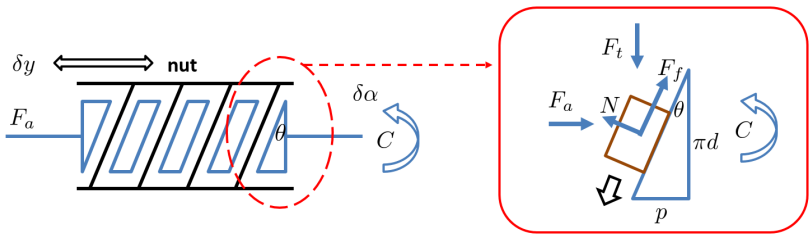

Figure B.1: Analysis of ball screw mechanics for forward transmission.

The figure B.1 illustrates the analysis of direction transmission. The friction force is a function of the normal force: $F_f = \mu N$. We define the efficiency of forward transmission as η_f, and it can be expressed as:

$$\eta_f = \frac{F_a \Delta y}{C \Delta \alpha} \tag{B.1}$$

where $\Delta\alpha$ and Δy are motor rotation angle and output translation respectively. The ratio $\Delta y/\Delta\alpha$ can be derived from the geometry of the triangle shown above, and is equal to $p/2\pi$. Regarding the input torque C, it is equal to $F_t d/2$ from the balance condition. Therefore, the forward efficiency can be derived as:

$$\eta_f = \frac{F_a \Delta y}{C \Delta \alpha} = \frac{P F_a}{\pi d F_t} = \tan\theta \frac{F_a}{F_t} \tag{B.2}$$

The force F_a and F_t are the loads in axial and perpendicular direction respectively. They can be expressed:

$$F_t = \mu N cos\theta + N sin\theta \tag{B.3}$$

$$F_a = -\mu N sin\theta + N cos\theta \tag{B.4}$$

replace those two expressions into the equation of η_f:

$$\eta_f = \tan\theta \frac{1 - \mu \tan\theta}{\mu + \tan\theta} \tag{B.5}$$

the friction coefficient can usually be modeled as the tangent value inside a friction cone $\mu = \tan\phi$. Therefore, the equation of η_f can be expressed as:

$$\eta_f = \frac{\tan\theta}{\tan(\theta + \phi)} \tag{B.6}$$

In case of backward transmission, the friction force and F_t changes their direction. Accordingly,

$$F_t = \mu N cos\theta - N sin\theta \tag{B.7}$$
$$F_a = \mu N sin\theta + N cos\theta \tag{B.8}$$

By following the same analysis, the efficiency of backward transmission η_b can be derived as:

$$\eta_b = \frac{C\Delta\alpha}{F_a \Delta y} = \frac{\tan(\phi - \theta)}{\tan\theta} \tag{B.9}$$

As shown above, the forward and backward transmission efficiency is a function of the friction coefficient and ball screw angle θ. They can be illustrated by the figure B.2.

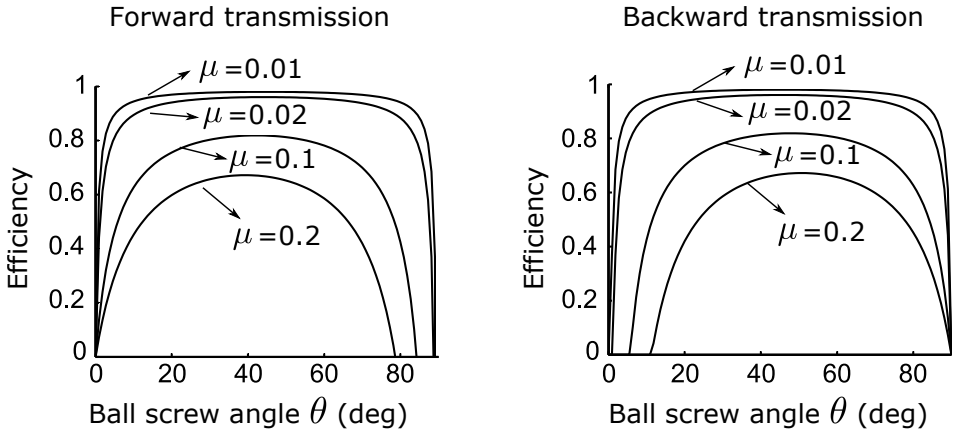

Figure B.2: Ball screw transmission efficiency.

Appendix C

Publication List

Published:

T. Lu, M. Boudaoud, D. Heriban, S. Regnier, "Nonlinear modeling for a class of nano-robotic systems using piezoelectric stick-slip actuators," in Intelligent Robots and Systems (IROS), 2015 IEEE/RSJ International Conference on , vol., no., pp.6020-6025, Sept. 28 2015-Oct. 2 2015

T. Lu, A.M. Ousaid, C.Pacoret, S.Régnier, V. Hayward, "Dual Stage Options for Interface Designs Suitable for Haptic Interaction at the Micro-Nano Scales," in International Symposium on Experimental Robotics (ISER), pp. 105-114, 2014

Pending:

T.Lu, C.Pacoret, D.Hériban, A. Mohand-Ousaid, S.Régnier, and V. Hayward, "KiloHertz Bandwidth, Dual-Channel Haptic Device" (Journal)

T. Lu, M. Boudaoud, D. Heriban, S. Regnier, "A New Voltage/Frequency Rate Dependent Modeling for Nano-Robotic System" (Journal)

Bibliography

[AmScope 2015] AmScope. *http://www.amscope.com/*, 2015. (Cited on pages 8 and 9.)

[Anis 2006] Y.H. Anis, J.K. Mills and W.L. Cleghorn. *Visual measurement of MEMS microassembly forces using template matching.* In Robotics and Automation, 2006. ICRA 2006. Proceedings 2006 IEEE International Conference on, pages 275–280, May 2006. (Cited on page 10.)

[Bassous 1977] E Bassous, HH Taub and L Kuhn. *Ink jet printing nozzle arrays etched in silicon.* Applied Physics Letters, vol. 31, no. 2, pages 135–137, 1977. (Cited on page 21.)

[Bellouard 2002] Yves Bellouard. *Microrobotics, Microdevices Based on Shape-Memory Alloys.* Encyclopedia of Smart Materials, 2002. (Cited on pages 22 and 24.)

[Belly 2012] Christian Belly and Willy Charon. *Benefits of amplification in an inertial stepping motor.* Mechatronics, vol. 22, no. 2, pages 177–183, 2012. (Cited on page 37.)

[Bergander 2003] A. Bergander and J.-M. Breguet. *Performance improvements for stick-slip positioners.* In Micromechatronics and Human Science, 2003. MHS 2003. Proceedings of 2003 International Symposium on, pages 59–66, Oct 2003. (Cited on page 38.)

[Berkelman 1997] Peter Berkelman and Ralph L. Hollis. *Dynamic performance of a magnetic levitation haptic device.* In Matthew R. Stein, editeur, Intelligent Systems & Advanced Manufacturing, pages 140–149. International Society for Optics and Photonics, December 1997. (Cited on pages 66 and 67.)

[Beyeler 2007] Felix Beyeler, Adrian Neild, Stefano Oberti, Dominik J Bell, Yu Sun, Jürg Dual and Bradley J Nelson. *Monolithically fabricated microgripper with integrated force sensor for manipulating microobjects and biological cells aligned in an ultrasonic field.* Microelectromechanical Systems, Journal of, vol. 16, no. 1, pages 7–15, 2007. (Cited on page 21.)

[Bolopion 2013] Aude Bolopion and Stéphane Régnier. *A review of haptic feedback teleoperation systems for micromanipulation and microassembly.* Automation Science and Engineering, IEEE Transactions on, vol. 10, no. 3, pages 496–502, 2013. (Cited on page 24.)

[Breguet 1998] J. M Breguet and R. Clavel. *Stick and slip actuators: design, control, performances and applications*. In Micromechatronics and Human Science, 1998. MHS '98. Proceedings of the 1998 International Symposium on, pages 89–95, Nov 1998. (Cited on page 38.)

[Breguet 2007] Jean-Marc Breguet, Walter Driesen, Fabian Kaegi and Thomas Cimprich. *Applications of piezo-actuated micro-robots in micro-biology and material science*. In Mechatronics and Automation, 2007. ICMA 2007. International Conference on, pages 57–62. IEEE, 2007. (Cited on page 36.)

[Buechner 2012] Steffen Buechner, Stephan Zschaeck, Arvid Amthor, Christoph Ament and Mike Eichhorn. *Dynamic friction modeling and identification for high precision mechatronic systems*. In IECON 2012-38th Annual Conference on IEEE Industrial Electronics Society, pages 2263–2268. IEEE, 2012. (Cited on page 40.)

[Burdea 1996] Grigore C Burdea, Grigore C Burdea and Cristian Burdea. Force and touch feedback for virtual reality. Wiley New York, 1996. (Cited on page 90.)

[Burdet 2004] Etienne Burdet, Roger Gassert, Frederic Mani, Fei Wang, CL Teo and Hannes Bleuler. *Design of a haptic forceps for microsurgery training*. In Proceedings of Eurohaptics, numéro LSRO-CONF-2007-025, 2004. (Cited on pages 88, 89 and 96.)

[Butt 1991] Hans-Jüurgen Butt. *Electrostatic interaction in atomic force microscopy*. Biophysical journal, vol. 60, no. 4, page 777, 1991. (Cited on page 7.)

[Cambridge 2003] Engineering Department Cambridge University. Materials data book. 2003. (Cited on page 64.)

[Campion 2005a] G. Campion and V. Hayward. *Fundamental limits in the rendering of virtual haptic textures*. In Eurohaptics Conference, 2005 and Symposium on Haptic Interfaces for Virtual Environment and Teleoperator Systems, 2005. World Haptics 2005. First Joint, pages 263–270, March 2005. (Cited on pages 63 and 76.)

[Campion 2005b] G. Campion, Qi Wang and V. Hayward. *The Pantograph Mk-II: a haptic instrument*. In Intelligent Robots and Systems, 2005. (IROS 2005). 2005 IEEE/RSJ International Conference on, pages 193–198, 2005. (Cited on pages 27, 64, 67 and 68.)

[Cedrat 2015] Technologies Cedrat. *http://www.cedrat-technologies.com/*, 2015. (Cited on page 36.)

[Chang 2009] Ren-Jung Chang and Chih-Yi Cheng. *Vision-based compliant-joint polymer force sensor integrated with microgripper for measuring gripping force.* In Advanced Intelligent Mechatronics, 2009. AIM 2009. IEEE/ASME International Conference on, pages 18–23, July 2009. (Cited on page 10.)

[Chanphat 2006] S. Chanphat and W. Wannasuphoprasit. *A Novel Transformable Cobot.* In Robotics, Automation and Mechatronics, 2006 IEEE Conference on, pages 1–6, Dec 2006. (Cited on page 1.)

[Coles 2011] Timothy Coles, Dwight Meglan and Nigel W John. *The role of haptics in medical training simulators: a survey of the state of the art.* Haptics, IEEE Transactions on, vol. 4, no. 1, pages 51–66, 2011. (Cited on page 90.)

[da Vinci-Surgery 2015] da Vinci-Surgery. *http://www.davincisurgery.com/*, 2015. (Cited on pages 86, 87 and 96.)

[Dahl 1968] PR Dahl. *A solid friction model.* Rapport technique, DTIC Document, 1968. (Cited on page 39.)

[De Wit 1993] C.C. De Wit, H. Olsson, K.J. Astrom and P. Lischinsky. *Dynamic Friction Models and Control Design.* In American Control Conference, 1993, pages 1920–1926, June 1993. (Cited on page 39.)

[De Wit 1995] C Canudas De Wit, Hans Olsson, Karl Johan Astrom and Pablo Lischinsky. *A new model for control of systems with friction.* Automatic Control, IEEE Transactions on, vol. 40, no. 3, pages 419–425, 1995. (Cited on pages 39 and 55.)

[Diolaiti 2006] Nicola Diolaiti, Günter Niemeyer, Federico Barbag and J Kenneth Salisbury Jr. *Stability of haptic rendering: Discretization, quantization, time delay, and coulomb effects.* Robotics, IEEE Transactions on, vol. 22, no. 2, pages 256–268, 2006. (Cited on page 25.)

[Dumont 2015] Dumont. *http://www.outils-dumont.ch/*, 2015. (Cited on page 91.)

[Dupont 2002] Pierre Dupont, Vincent Hayward, Brian Armstrong and Friedhelm Altpeter. *Single state elastoplastic friction models.* Automatic Control, IEEE Transactions on, vol. 47, no. 5, pages 787–792, 2002. (Cited on pages 39, 40, 43, 44 and 45.)

[Enikov 2000] ET Enikov and BJ Nelson. *Three-dimensional microfabrication for a multi-degree-of-freedom capacitive force sensor using fibre-chip coupling.* Journal of Micromechanics and Microengineering, vol. 10, no. 4, page 492, 2000. (Cited on page 13.)

[FEI 2015] FEI. *http://www.fei.com/*, 2015. (Cited on pages 9 and 10.)

[FemtoTools 2016] FemtoTools. *http://www.femtotools.com/*, 2016. (Cited on page 14.)

[Finio 2011] B.M. Finio, K.C. Galloway and R.J. Wood. *An ultra-high precision, high bandwidth torque sensor for microrobotics applications.* In Intelligent Robots and Systems (IROS), 2011 IEEE/RSJ International Conference on, pages 31–38, 2011. (Cited on page 63.)

[Florens 2004] Jean-Loup Florens, Annie Luciani, Claude Cadoz and Nicolas Castagné. *ERGOS: A multi-degrees of freedom and versatile force-feedback panoply.* In Proceedings of EuroHaptics, pages 356–360, 2004. (Cited on pages 66 and 67.)

[ForceDimension 2016] ForceDimension. *http://www.forcedimension.com/*, 2016. (Cited on page 27.)

[Frey 2012] Siegfried Frey, Alexandru Dadalau and Alexander Verl. *Expedient modeling of ball screw feed drives.* Production Engineering, vol. 6, no. 2, pages 205–211, 2012. (Cited on page 112.)

[Fung 2008] Rong-Fong Fung, Chang-Fu Han and Jer-Rong Chang. *Dynamic modeling of a high-precision self-moving stage with various frictional models.* Applied Mathematical Modelling, vol. 32, no. 9, pages 1769–1780, 2008. (Cited on page 37.)

[Galassi 2012] Carmen Galassi, Maria Dinescu, Kenji Uchino and Michael Sayer. Piezoelectric materials: advances in science, technology and applications, volume 76. Springer Science & Business Media, 2012. (Cited on page 98.)

[Gescheider 1988] G. A. Gescheider, R. T. Verillo and C. M. Checkosky. *Four channels mediate the mechanical aspects of touch.* 1988. (Cited on page 64.)

[Gillespie 1996] Brent R. Gillespie and Mark R. Cutkosky. *Stable User-Specific Haptic Rendering Of The Virtual Wall.* In ASME International Mechanical Engineering Conference and Exposition, 1996. (Cited on page 115.)

[Gillespie 2001] R.B. Gillespie, J.E. Colgate and M.A. Peshkin. *A general framework for cobot control.* Robotics and Automation, IEEE Transactions on, vol. 17, no. 4, pages 391–401, Aug 2001. (Cited on page 1.)

[Goldfarb 1997] M. Goldfarb and N. Celanovic. *Modeling piezoelectric stack actuators for control of micromanipulation.* Control Systems, IEEE, vol. 17, no. 3, pages 69–79, Jun 1997. (Cited on page 11.)

[Greminger 2004] M.A. Greminger and B.J. Nelson. *Vision-based force measurement.* Pattern Analysis and Machine Intelligence, IEEE Transactions on, vol. 26, no. 3, pages 290–298, March 2004. (Cited on page 10.)

[Gu 2014] G.-Y. Gu, L.-M. Zhu, C.-Y. Su, H. Ding and S. Fatikow. *Modeling and Control of Piezo-Actuated Nanopositioning Stages: A Survey.* Automation Science and Engineering, IEEE Transactions on, vol. PP, no. 99, pages 1–20, 2014. (Cited on page 42.)

[Han 2011] SI Han and Jang M Lee. *Friction and uncertainty compensation of robot manipulator using optimal recurrent cerebellar model articulation controller and elasto-plastic friction observer.* IET control theory & applications, vol. 5, no. 18, pages 2120–2141, 2011. (Cited on page 40.)

[Haption 2015] Haption. *http://www.haption.com/*, 2015. (Cited on page 25.)

[Harris 2013] Fred Harris, Elettra Venosa, Xiaofei Chen, Prafulla Muthyala and Chris Dick. *An extension of the Linkwitz-Riley crossover filters for audio systems and their sampled data implementation.* In Systems, Signals and Image Processing (IWSSIP), 2013 20th International Conference on, pages 175–178, 2013. (Cited on pages 69 and 71.)

[Hayward 1994] Vincent Hayward, Jehangir Choksi, Gonzalo Lanvin and Christophe Ramstein. *Design and multi-objective optimization of a linkage for a haptic interface. in Advances in Robot Kinematics.* In Preprints of the ISER-4, International Symposium on Experimental Robotics, pages 352–359, 1994. (Cited on page 68.)

[Hayward 2000] Vincent Hayward and Brian Armstrong. *A new computational model of friction applied to haptic rendering.* In Experimental Robotics VI, pages 403–412. Springer, 2000. (Cited on page 39.)

[Hayward 2004] Vincent Hayward, Oliver R. Astley, Manuel Cruz?Hernandez, Danny Grant and Gabriel Robles?De?La?Torre. *Haptic interfaces and devices.* Sensor Review, vol. 24, no. 1, pages 16–29, 2004. (Cited on pages 65 and 90.)

[Hayward 2007] V. Hayward and K.E. MacLean. *Do it yourself haptics: part I.* Robotics Automation Magazine, IEEE, vol. 14, no. 4, pages 88–104, Dec 2007. (Cited on page 66.)

[Henke 2014] Benjamin Henke, Oliver Sawodny and Robert Neumann. *Distributed Parameter Modeling of Flexible Ball Screw Drives Using Ritz Series Discretization.* 2014. (Cited on page 112.)

[Houston 2007] Keith Houston, Clements Eder, Arne Sieber, Arianna Menciassi, Maria Chiara Carrozza and Paolo Dario. *Polymer sensorised*

microgrippers using SMA actuation. In Robotics and Automation, 2007 IEEE International Conference on, pages 820–825. IEEE, 2007. (Cited on page 22.)

[ideal tek 2015] ideal tek. *http://www.ideal-tek.com/*, 2015. (Cited on page 91.)

[Israelachvili 2011] Jacob N Israelachvili. Intermolecular and surface forces: revised third edition. Academic press, 2011. (Cited on page 7.)

[J.-G. S. Demers 1998] I P W Sinclair J.-G. S. Demers J.M.A. Boelen. *Freedom 6S Force Feedback Hand Controller.* Proceedings of SPRO'98 1st IFAC Workshop on SpaceRobotics, 1998. (Cited on page 67.)

[Kanda 2006] Takefumi Kanda, Akira Makino, Tomohisa Ono, Koichi Suzumori, Takeshi Morita and Minoru Kuribayashi Kurosawa. *A micro ultrasonic motor using a micro-machined cylindrical bulk PZT transducer.* Sensors and Actuators A: physical, vol. 127, no. 1, pages 131–138, 2006. (Cited on page 36.)

[Karnopp 1985] Dean Karnopp. *Computer simulation of stick-slip friction in mechanical dynamic systems.* Journal of dynamic systems, measurement, and control, vol. 107, no. 1, pages 100–103, 1985. (Cited on page 39.)

[Kim 2002] Jaehwan Kim, Hyang-Ki Kim and Seung-Bok Choi. *A hybrid inchworm linear motor.* Mechatronics, vol. 12, no. 4, pages 525–542, 2002. (Cited on page 36.)

[Kristian 2005] M Kristian, Ole Hansen*et al. Electro-thermally actuated microgrippers with integrated force-feedback.* Journal of Micromechanics and Microengineering, vol. 15, no. 6, page 1265, 2005. (Cited on page 12.)

[Lampaert 2002] Vincent Lampaert, Jan Swevers and Farid Al-Bender. *Modification of the Leuven integrated friction model structure.* Automatic Control, IEEE Transactions on, vol. 47, no. 4, pages 683–687, 2002. (Cited on page 39.)

[Lampaert 2003] Vincent Lampaert, Farid Al-Bender and Jan Swevers. *A generalized Maxwell-slip friction model appropriate for control purposes.* In Physics and Control, 2003. Proceedings. 2003 International Conference, volume 4, pages 1170–1177. IEEE, 2003. (Cited on page 39.)

[Landolsi 2009] Fakhreddine Landolsi, Fathi H Ghorbel, Jun Lou, Hao Lu and Yuekai Sun. *Nanoscale friction dynamic modeling.* Journal of dynamic

systems, measurement, and control, vol. 131, no. 6, page 061102, 2009. (Cited on page 43.)

[Landragin 1996] A Landragin, J-Y Courtois, G Labeyrie, N Vansteenkiste, CI Westbrook and A Aspect. *Measurement of the van der Waals force in an atomic mirror.* Physical review letters, vol. 77, no. 8, page 1464, 1996. (Cited on page 7.)

[Laycock 2003] S. D. Laycock and A. M. Day. *Recent Developments and Applications of Haptic Devices.* Computer Graphics Forum, vol. 22, no. 2, pages 117–132, 2003. (Cited on page 66.)

[Lee 1991] Lieng-Huang Lee. *The chemistry and physics of solid adhesion.* In Fundamentals of Adhesion, pages 1–86. Springer, 1991. (Cited on page 8.)

[Lee 2005] Sangki Lee, Hoon Cheol Park and Kwang Jin Kim. *Equivalent modeling for ionic polymer-metal composite actuators based on beam theories.* Smart Materials and Structures, vol. 14, no. 6, page 1363, 2005. (Cited on page 11.)

[Li 2013] Jianping Li, Hongwei Zhao, Han Qu, Tao Cui, Lu Fu, Hu Huang, Luquan Ren and Zunqiang Fan. *A piezoelectric-driven rotary actuator by means of inchworm motion.* Sensors and Actuators A: Physical, vol. 194, pages 269–276, 2013. (Cited on page 36.)

[Linkwitz 1978] Siegfried H. Linkwitz. *Passive Crossover Networks for Noncoincident Drivers.* JAES, vol. 26 Issue 3, pages 149–150, March 1978. (Cited on page 71.)

[López 2012] Javier López, Jose Breñosa, Ignacio Galiana, Manuel Ferre, Antonio Giménez and Jorge Barrio. *Mechanical design optimization for multi-finger haptic devices applied to virtual grasping manipulation.* Strojniski Vestnik/Journal of Mechanical Engineering, vol. 58, no. 7-8, pages 431–443, 2012. (Cited on page 67.)

[Lu 2009] Haiwei Lu, Jianguo Zhu, Zhiwei Lin and Youguang Guo. *An inchworm mobile robot using electromagnetic linear actuator.* Mechatronics, vol. 19, no. 7, pages 1116–1125, 2009. (Cited on page 36.)

[McJunkin 2005] S.T. McJunkin, M.K. O'Malley and J.E. Speich. *Transparency of a Phantom premium haptic interface for active and passive human interaction.* In American Control Conference, 2005. Proceedings of the 2005, pages 3060–3065 vol. 5, June 2005. (Cited on page 66.)

[Mohand-Ousaid 2012] Abdenbi Mohand-Ousaid, Guillaume Millet, Stéphane Régnier, Sinan Haliyo and Vincent Hayward. *Haptic interface transparency achieved through viscous coupling.* The International Journal of Robotics Research, vol. Vol 31 No 3, pages Pages 319–329, 2012. (Cited on pages 26 and 66.)

[Mohand Ousaid 2014a] A. Mohand Ousaid, A. Bolopion, S. Haliyo, S. Regnier and V. Hayward. *Stability and transparency analysis of a teleoperation chain for microscale interaction.* In Robotics and Automation (ICRA), 2014 IEEE International Conference on, pages 5946–5951, May 2014. (Cited on page 90.)

[Mohand-Ousaid 2014b] Abdenbi Mohand-Ousaid, Tianming Lu, Cécile Pacoret, Stéphane Régnier and Vincent Hayward. *Dual Stage Options for Interface Designs Suitable for Haptic Interaction at the Micro-Nano Scales.* In ISER 2014, International Symposium on Experimental Robotics, 2014. (Cited on page 66.)

[Moon 2006] Chanwoo Moon, Sungho Lee and JK Chung. *A new fast inchworm type actuator with the robust I/Q heterodyne interferometer feedback.* Mechatronics, vol. 16, no. 2, pages 105–110, 2006. (Cited on page 36.)

[Morita 2000] Takeshi Morita, Minoru K Kurosawa and Toshiro Higuchi. *A cylindrical micro-ultrasonic motor (stator transducer size: 1.4 mm in diameter and 5.0 mm long).* Ultrasonics, vol. 38, no. 1, pages 33–36, 2000. (Cited on page 36.)

[Nature-Education 2010] Nature-Education. *http://www.nature.com/scitable/topicpage/what-is-a-cell-14023083*, 2010. (Cited on page 6.)

[Neuman 2004] Keir C. Neuman and Steven M. Block. *Optical trapping.* Review of Scientific Instruments, vol. 75, no. 9, pages 2787–2809, 2004. (Cited on page 64.)

[Ni 2011] Z. Ni, C. Pacoret, R. Benosman, S. Ieng and S. Régnier. *Asynchronous Event Based High Speed Vision for Micro-particles Tracking.* Journal of microscopy, 2011. (Cited on pages 14 and 81.)

[Ni 2013a] Z. Ni, C. Pacoret, R. Benosman and S. Régnier. *2D High Speed Force Feedback Teleoperation of Optical Tweezers.* In IEEE International Conference on Robotics and Automation, 2013. (Cited on pages 14, 64 and 80.)

[Ni 2013b] Zhenjiang Ni. *Asynchronous Event Based Vision: Algorithms and Applications to Microrobotics.* PhD thesis, Université Pierre et Marie Curie-Paris VI, 2013. (Cited on pages 64, 66 and 68.)

[NI 2014] *http://www.ni.com/*, 2014. (Cited on page 69.)

[Odenbach 2010] Stefan Odenbach and Dmitry Borin. *Electrorheological fluids and magnetorheological suspensions.* Journal of Physics: Condensed Matter, vol. 22, no. 32, page 320301, 2010. (Cited on page 98.)

[Okamura 2003] Allison M Okamura, Robert J Webster III, Jason T Nolin, KW Johnson and H Jafry. *The haptic scissors: Cutting in virtual environments.* In Robotics and Automation, 2003. Proceedings. ICRA'03. IEEE International Conference on, volume 1, pages 828–833. IEEE, 2003. (Cited on pages 88 and 89.)

[Pacoret 2009] Cécile Pacoret, Richard Bowman, Graham Gibson, Sinan Haliyo, David Carberry, Arvid Bergander, Stéphane Régnier and Miles Padgett. *Touching the microworld with force-feedback optical tweezers.* Optics Express, vol. 17, no. 12, pages 10259–10264, 2009. (Cited on page 80.)

[Pacoret 2013] Cecile Pacoret and Stephane Regnier. *Invited Article: A review of haptic optical tweezers for an interactive microworld exploration.* Review of Scientific Instruments, vol. 84, no. 8, page 081301, 2013. (Cited on page 80.)

[Payne 2015] Christopher James Payne. *Ungrounded haptic-feedback for handheld surgical robots.* PhD thesis, Imperial College London, 2015. (Cited on pages 88 and 89.)

[Peng 2011] J.Y. Peng and X.B. Chen. *Modeling of Piezoelectric-Driven Stick-Slip Actuators.* Mechatronics, IEEE/ASME Transactions on, vol. 16, no. 2, pages 394–399, April 2011. (Cited on pages 38 and 40.)

[Peshkin 2001] M.A. Peshkin, J.E. Colgate, W. Wannasuphoprasit, C.A. Moore, R.B. Gillespie and P. Akella. *Cobot architecture.* Robotics and Automation, IEEE Transactions on, vol. 17, no. 4, pages 377–390, Aug 2001. (Cited on page 1.)

[PI 2016] PI. *http://www.physikinstrumente.com/*, 2016. (Cited on pages 19, 20, 21, 23 and 35.)

[Polla 1998] Dennis L Polla and Lorraine F Francis. *Processing and characterization of piezoelectric materials and integration into microelectromechanical systems.* Annual review of materials science, vol. 28, no. 1, pages 563–597, 1998. (Cited on page 98.)

[Rakotondrabe M 2009] Lutz P. Rakotondrabe M Haddab Y. *Quadrilateral Modelling and Robust Control of a Nonlinear Piezoelectric Cantilever.*

Control Systems Technology, IEEE Transactions on, vol. 17, pages 528 – 539, 2009. (Cited on pages 38 and 42.)

[Rakotondrabe 2009] M. Rakotondrabe, Yassine Haddab and P. Lutz. *Development, Modeling, and Control of a Micro-/Nanopositioning 2-DOF Stick-Slip Device*. Mechatronics, IEEE/ASME Transactions on, vol. 14, no. 6, pages 733–745, Dec 2009. (Cited on pages 38 and 40.)

[Rakotondrabe 2010] M. Rakotondrabe, C. Clevy and P. Lutz. *Complete Open Loop Control of Hysteretic, Creeped, and Oscillating Piezoelectric Cantilevers*. Automation Science and Engineering, IEEE Transactions on, vol. 7, no. 3, pages 440–450, July 2010. (Cited on pages 42 and 50.)

[Régnier 2008] Stéphane Régnier and Nicolas Chaillet. La microrobotique : Applications *à* la micromanipulation. Hermes Science Publications, 2008. (Cited on pages 1, 6, 9, 19 and 98.)

[Régnier 2010] S. Régnier and M. Gauthier. Robotic microassembly. Wiley-IEEE press, 2010. (Cited on pages 6 and 11.)

[Rizun 2006a] P Rizun, D Gunn, B Cox and G Sutherland. *Mechatronic design of haptic forceps for robotic surgery*. The International Journal of Medical Robotics and Computer Assisted Surgery, vol. 2, no. 4, pages 341–349, 2006. (Cited on page 88.)

[Rizun 2006b] Peter R Rizun, Dylan C Gunn, Brian L Cox and Garnette R Sutherland. *Mechanical design of haptic forceps for robotic surgery*. In Haptic Interfaces for Virtual Environment and Teleoperator Systems, 2006 14th Symposium on, pages 331–335. IEEE, 2006. (Cited on pages 88 and 90.)

[Rockford 2016] Rockford. *http://www.rockfordballscrew.com/*, 2016. (Cited on page 105.)

[Romano 2012] J.M. Romano and K.J. Kuchenbecker. *Creating Realistic Virtual Textures from Contact Acceleration Data*. Haptics, IEEE Transactions on, vol. 5, no. 2, pages 109–119, 2012. (Cited on pages 1 and 63.)

[Saddik 2007] El Saddik. *The Potential of Haptics Technologies*. Instrumentation Measurement Magazine, IEEE, vol. 10, no. 1, pages 10–17, Feb 2007. (Cited on page 90.)

[Sato 1997] M. Sato, Y. Hirata and H. Kawarada. *Space Interface Device for Artificial Reality -SPIDAR*. Journal of Robotics and Mechatronics, pages 177 – 184, 1997. (Cited on page 28.)

[Serafin 2003] Stefania Serafin, Federico Avanzini and Davide Rocchesso. *Bowed string simulation using an elasto-plastic friction model.* In Proc. Stockholm Music Acoustics Conf.(SMAC 2003), pages 95–98, 2003. (Cited on page 40.)

[SERVOMEDICS 2015] SERVOMEDICS. *http://www.servocad.com/*, 2015. (Cited on pages 86, 87 and 96.)

[Shi 2012] Liwei Shi, Shuxiang Guo and K. Asaka. *Modeling and position control of IPMC actuators for the underwater biomimetic microrobot.* In Mechatronics and Automation (ICMA), 2012 International Conference on, pages 1698–1703, Aug 2012. (Cited on page 11.)

[Shimoga 1993] Karun B Shimoga. *A survey of perceptual feedback issues in dexterous telemanipulation: I. Finger force feedback.* In Virtual Reality Annual International Symposium, 1993., 1993 IEEE, pages 271–279. IEEE, 1993. (Cited on page 90.)

[Sitti 1998] M. Sitti and H. Hashimoto. *Tele-nanorobotics using atomic force microscope.* In Intelligent Robots and Systems, 1998. Proceedings., 1998 IEEE/RSJ International Conference on, volume 3, pages 1739–1746 vol.3, 1998. (Cited on page 1.)

[Sitti 2004] M. Sitti. *Micro- and nano-scale robotics.* In American Control Conference, 2004. Proceedings of the 2004, volume 1, pages 1–8 vol.1, 2004. (Cited on page 63.)

[SmarAct 2016] SmarAct. *http://www.smaract.de/*, 2016. (Cited on pages 23 and 35.)

[Špiller 2011] Martin Špiller and Zdeněk Hurák. *Hybrid charge control for stick–slip piezoelectric actuators.* Mechatronics, vol. 21, no. 1, pages 100–108, 2011. (Cited on page 37.)

[Stocco 1996] L Stocco and S E Salcudean. *A Coarse-Fine Approach to Force-Reflecting Hand Controller Design.* Electrical Engineering, no. April, 1996. (Cited on page 66.)

[Sun 2002] Yu Sun and Bradley J Nelson. *Biological Cell Injection Using an Autonomous MicroRobotic System.* The International Journal of Robotics Research, vol. 21, pages 861–868, October 1, 2002. (Cited on page 1.)

[Sun 2004] Yu Sun, Michael Greminger, Bradley J Nelson*et al. Investigating protein structure with a microrobotic system.* In Robotics and Automation, 2004. Proceedings. ICRA'04. 2004 IEEE International Conference on, volume 3, pages 2854–2859. IEEE, 2004. (Cited on page 13.)

[Sun 2005] Yu Sun, Chauncey F Graetzel, Steven N Fry and Bradley J Nelson. *A MEMS micro force sensor for drosophila flight characterization.* In Robotics and Biomimetics (ROBIO). 2005 IEEE International Conference on, pages 505–510. IEEE, 2005. (Cited on page 13.)

[Swevers 2000] J. Swevers, F. Al-Bender, C.G. Ganseman and T. Projogo. *An integrated friction model structure with improved presliding behavior for accurate friction compensation.* Automatic Control, IEEE Transactions on, vol. 45, no. 4, pages 675–686, Apr 2000. (Cited on page 39.)

[Tavakoli 2004] M. Tavakoli, R.V. PateI and M. Moallem. *Design issues in a haptics-based master-slave system for minimally invasive surgery.* In Robotics and Automation, 2004. Proceedings. ICRA '04. 2004 IEEE International Conference on, volume 1, pages 371–376 Vol.1, April 2004. (Cited on page 90.)

[Threlfall 1978] DC Threlfall. *The inclusion of coulomb friction in mechanisms programs with particular reference to dram au programme dram.* Mechanism and Machine Theory, vol. 13, no. 4, pages 475–483, 1978. (Cited on page 39.)

[Vasiljev 2007] P Vasiljev, D Mazeika and G Kulvietis. *Modelling and analysis of omni-directional piezoelectric actuator.* Journal of Sound and Vibration, vol. 308, no. 3, pages 867–878, 2007. (Cited on page 36.)

[Vinci-Energies 2014] Vinci-Energies. *http://www.vinci-energies.com/*, 2014. (Cited on page 1.)

[Wagner 2002] Christopher R Wagner, Robert D Howe and Nicholas Stylopoulos. *The role of force feedback in surgery: analysis of blunt dissection.* In haptics, page 73. IEEE, 2002. (Cited on page 90.)

[Wall 2001] Steven A Wall and William Harwin. *A high bandwidth interface for haptic human computer interaction.* Mechatronics, vol. 11, no. 4, pages 371–387, June 2001. (Cited on page 66.)

[Wang 2001] Xiaoye Wang, GK Ananthasuresh and James P Ostrowski. *Vision-based sensing of forces in elastic objects.* Sensors and Actuators A: Physical, vol. 94, no. 3, pages 142–156, 2001. (Cited on page 10.)

[Wang 2007] W.H. Wang, X.Y. Liu and Y. Sun. *Autonomous Zebrafish Embryo Injection Using a Microrobotic System.* In Automation Science and Engineering, 2007. CASE 2007. IEEE International Conference on, pages 363–368, 2007. (Cited on page 1.)

[Wen 2008] Weijia Wen, Xianxiang Huang and Ping Sheng. *Electrorheological fluids: structures and mechanisms.* Soft Matter, vol. 4, no. 2, pages 200–210, 2008. (Cited on page 98.)

[Wiertlewski 2012] M Wiertlewski and V Hayward. *Mechanical behavior of the fingertip in the range of frequencies and displacements relevant to touch.* Journal of biomechanics, vol. 45, pages 1869–1874, 2012. (Cited on pages 75 and 111.)

[Xiao 2000] Xudong Xiao and Linmao Qian. *Investigation of humidity-dependent capillary force.* Langmuir, vol. 16, no. 21, pages 8153–8158, 2000. (Cited on page 7.)

[Xie 2011] Hui Xie and S. Régnier. *Development of a Flexible Robotic System for Multiscale Applications of Micro/Nanoscale Manipulation and Assembly.* Mechatronics, IEEE/ASME Transactions on, vol. 16, no. 2, pages 266–276, April 2011. (Cited on page 14.)

[Yang 2011] Chia-Feng Yang, Shyr-Long Jeng and Wei-Hua Chieng. *Motion behavior of triangular waveform excitation input in an operating impact drive mechanism.* Sensors and Actuators A: Physical, vol. 166, no. 1, pages 66–77, 2011. (Cited on page 37.)

[Yao 2010] Hsin-Yun Yao and Vincent Hayward. *Design and analysis of a recoil-type vibrotactile transducer.* The Journal of the Acoustical Society of America, vol. 128, no. 2, pages 619–627, 2010. (Cited on page 68.)

[Yongliang 2010] Zhang Yongliang, Lin Rui, Yu Junyi and Zhang Shouqin. *The mechanical properties of polyaniline Electrorheological fluid.* In Mechanic Automation and Control Engineering (MACE), 2010 International Conference on, pages 6274–6278, June 2010. (Cited on page 100.)

[Zhong 2011] Bowen Zhong, Lining Sun, Liguo Chen and Zhenhua Wang. *The dynamics study of the stick-slip driving system based on LuGre dynamic friction model.* In Mechatronics and Automation (ICMA), 2011 International Conference on, pages 584–589, Aug 2011. (Cited on page 39.)